Trinity College Dublin
Coláiste na Tríonóide, Baile Átha Cliath
The University of Dublin

Identifying the therapeutic potential of novel compounds in the treatment of Glioblastoma Multiforme.

Masters by Research Thesis
June 2023
Submitted to Trinity College Dublin in fulfilment of the thesis requirements for masters:

Emily Keenan
17331173

Supervisor:
Dr. Melissa Conroy

Neuroscience
Department of Physiology
School of Medicine
Trinity College Dublin

Declaration of Integrity

I declare that this thesis has not been submitted as an exercise for a degree at this or any other university and it is entirely my own work.

I agree to deposit this thesis in the University's open access institutional repository or allow the Library to do so on my behalf, subject to Irish Copyright Legislation and Trinity College Library conditions of use and acknowledgement.

I consent to the examiner retaining a copy of the thesis beyond the examining period, should they so wish (EU GDPR May 2018).

Name: Emily Keenan

Date: 31/08/2022

Table of Contents

Abstract

Glioblastoma multiforme (GBM) is the most common and aggressive brain cancer in adults with a dismal 5-year survival rate of <5%. Despite advanced diagnostic and multimodal treatments including surgery, followed by radiotherapy and chemotherapy (CRT), treatment resistance is a major clinical challenge and the survival rates for GBM are not improving. Therefore, innovative therapeutic approaches are urgently needed for GBM patients. (*E)-2-(2-(Pyrazin-2-yl)vinyl)phenol,* Pyrazinib (P3) a small molecule pyrazine compound has shown significant therapeutic potential as a radiosensitiser in oesophageal cancer and here we assess its therapeutic potential in GBM. *(E)-2-(2-quinolin-2-yl-vinyl)-benzene-1,4-diol HCl*, 1,4 dihydroxy quininib (Q8), an antagonist of the cysteinyl leukotriene receptor-1 has shown potential as novel anti-angiogenic in colorectal cancer models and here we assess its therapeutic utility in GBM. Natural killer (NK) cells are potent anti-tumour immune cells and are gaining momentum as cell-based immunotherapies. This study investigates Pyrazinib (P3), 1,4 dihydroxy quininib (Q8) and a P3 prodrug called P3 Phosphate for their potential to sensitise GBM tumours to current standard-of-care chemotherapy and for their utility in combination with NK cell therapies.

Acknowledgments

I would like to start by thanking my supervisor Dr. Melissa Conroy for her support and patience throughout this year. I can honestly say that without her guidance, motivation, understanding and encouragement during my research, this project would not have been possible. You have donated your time and experience to help me evolve as a scientist and for that I am truly grateful.

Special thanks to members of the Neuroscience, Department of Physiology namely Marianna Mekhaeil for her fantastic project management and support in overseeing this project from start to finish. To Eimear Mylod, Evie Papakyriakopoulou, Caroline Marion and everyone in the department of surgery in Trinity Translational Medicine Institute for their encouragement and joy they brought to the lab, who were always willing to lend a helping hand and provide me with instruction and advice during my time with the group. I would like to thank Dr. Niamh O' Boyle and the department of Pharmacy and Pharmaceutical Science, Trinity College Dublin for allowing me to pursue my interest in chemistry and enable me to synthesise a novel drug. I would like to extend my gratitude to everyone in the Trinity Biomedical Sciences Institute that I worked with who made me feel extremely welcome and part of the team here at in Trinity. Thank you to Professor Jacintha O'Sullivan for gifting P3 for use in this study.

I am grateful to my family, especially my parents David and Nicola, who have been there to support me through any challenges I faced and when I felt like giving up! Your tremendous support has meant the world to me.

Abbreviations

ACN	Acetonitrile
ADCC	Antibody dependent cell mediated cytotoxicity
APCs	Antigen-presenting cells
BBB	Blood-Brain Barrier barrier
^{13}C	Carbon 13
CAR	Chimeric antigen receptor
CNS	Central Nervous System
cGy	Centi-gray
CSCs	Circulating stem cells
CRC	Colorectal Cancer
CysLT1	Cysteinyl leukotriene receptors 1
CysLT2	Cysteinyl leukotriene receptors 2
CRS	Cytokine release syndrome
CRT	Chemotherapy and radiotherapy
DCM	Dichloromethane
DCs	Dendritic cells
DIPEA	Diisopropylethylamine
DMAP	4-Dimethylaminopyridine
DMSO	Dimethyl sulfoxide
ECM	Extra cellular matrix
ELISA	Enzyme linked immunoabsorbant assay
FT-IR	Fourier-transform infrared
FOXP3	Forkhead box P3
FcyR III	The Fc fragment of the IgG low affinity III receptor
GAMs	Glioma associated microglia/macrophages
GBM	Glioblastoma multiforme
GSCs	Glioma stem cell
GVHD	Graft versus-host disease

^{1}H	Proton
HPLC	High performance liquid chromatography
Hz	Hertz
ICIs	Immune checkpoint inhibitors
ILCs	Group I Innate Lymphocytes
IDO	Indoleamine 2, 3-dioxygense
KIRs	Killer immunoglobulin-like receptors
LILRs	Leukocyte immunoglobulin-like receptors
MHC-I	Major histocompatibility class-I molecules
MS	Mass spectrometry
MFI	Mean fluorescence intensity
MP	Mobile phase
MDSCs	Myeloid-derived suppressor cells
MGMT	O-6-methylguanine methyltransferase
NK Cells	Natural killer cells
NKG2D	Natural killer group 2 member D
NMR	Nuclear Magnetic Resonance
OAC	Oesophageal adenocarcinoma
OXPHOS	Oxidative phosphorylation
PD-1	Programmed cell death protein 1
PD-L1	Programmed death ligand 1
PBS	Phosphate buffered saline
PBMC	Peripheral blood mononuclear cells
P3	Pyrazinib
P3 Phosphate	(E)-2-(2-(pyrazin-2-yl)vinyl)phenyl dihydrogen phosphate
Q8	1,4-dihydroxy Quininib
Rf	Retention factor
RT	Room temperature
SM	Starting material

TAMs	Tumour-associated macrophages
TILs	Tumour infiltration lymphocytes
TMZ	Temozolomide
TLC	Thin layer chromatography
Tregs	T regulatory lymphocytes
TGF-β	Transforming growth factor-β
TME	Tumour microenvironment
TMS	Tetramethyl silane
VC	Vehicle control
VEGF	Vascular endothelial growth factor
WHO	World Health Organisation

1. Introduction

1.1 The clinical challenge of Glioblastoma multiforme

Glioblastoma multiforme (GBM) is the most common and aggressive primary tumour of the central nervous system (CNS) [1]. The National Cancer Registry (Ireland) recorded 124 patients were diagnosed with GBM between 1994-2013, making it the most common of brain tumours (43%). The five-year net survival (NS) for adult GBM was 3.8 % which is the lowest survival rate of malignant brain cancers [2]. Classified by world health organisation (WHO), GBM is a grade IV glioma of astrocytic lineage [3]. GBM is most commonly identified in malignant brain tumours, with histological studies showing extreme cell heterogeneity amongst these tumours. GBM tumours can be characterized by cellular pleomorphism, diffuse growth patterns and mitotic activity variability [4]. Genetic abnormalities in glioblastoma include mutations in cell receptors, resulting in the dysfunction of signalling pathways. Hence, pharmacological management of these pathway abnormalities could lead to possible therapies for GBM by targeting interactions with selective inhibitors [5]. Glioblastoma multiforme is characterized by high proliferative activity [6] and its ability to infiltrate normal surrounding tissue making complete tumour resection impossible and radiotherapy less efficient [7]. The optimal end result of anti-cancer treatment should be tumour regression, allowing for the longest possible disease-free survival [8]. Maximal surgical resection, followed by chemotherapy and radiotherapy, is the standard treatment for GBM [9]. The best results are achieved when radiotherapy is performed after surgery, with a dose of 5000–6000 centi-gray (cGy). Radiation over 6000 cGy was shown to increase toxicity with no survival benefit [6].The standard chemotherapeutic treatment protocols for glioblastoma include Temozolomide. Temozolomide (TMZ) confers a higher median survival time in patients in comparison to other chemotherapy agents [10] as well as minimal additional toxicity [11]. A study by Hegi *et al.* showed patients treated with a combination of TMZ and radiotherapy had a median survival of 21.7 months (95 percent confidence interval, 17.4 to 30.4), whereas those who received radiotherapy alone had a 15.3 month median survival (95 percent confidence interval, 13.0 to 20.9) [12]. Overall, the prognosis of GBM still remains poor even with standard treatment and novel therapeutic options are urgently needed.

1.1.1 Temozolomide resistance in GBM

Temozolomide (TMZ) (*Figure 1*) (brand names: Temodar, Temodal) is an Imidazotetrazine lipophilic prodrug, capable of crossing the blood brain barrier. It can be administered orally however, due to low solubility in physiological media and shorter plasma half-life (1.8h), TMZ requires continuous intravenous administration [13]. High doses of TMZ may have positive outcomes due to extensive tumour killing, however toxic side effects do not allow for a continued increase in dosage. High doses can result in haematological toxicity, pneumocystis pneumonia, acute cardiomyopathy, hepatotoxicity and oral ulceration with subsequent discontinuation of therapy [13]. Therapy with TMZ increases survival after diagnosis from 12 to 14.4 months making the development of combination therapies with TMZ a desirable concept [14].

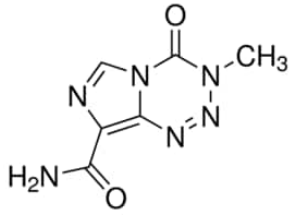

Figure 1: Structure of Temozolomide. TMZ is an imidazotetrazine lipophilic prodrug capable of crossing the blood brain barrier and is used for the standard treatment of Glioblastoma multiforme

The development of TMZ resistance is mediated by the DNA repair enzyme, O-6-methylguanine methyltransferase (MGMT), as it can reverse the methylation damage induced by alkylating agents [15],[16]. TMZ resistant GBM cell lines are treated with a combination of drugs, the most commonly used are O6-methylguainine-DNA (MGMT) inhibitors [17],[18].

MGMT is an endogenous DNA repair enzyme that can help maintain genomic stability *via* mismatch repair. Under conditions of TMZ treatment, MGMT can remove the methyl group in O6-methylguanine thereby neutralizing the drug-induced DNA damage and reducing the overall efficacy of TMZ (*Figure 2)* [18]. Therefore, MGMT expression, which is determined by CpG methylation status of the *MGMT* gene promoter region, is an important factor in TMZ treatment response. Hypermethylation of the *MGMT* promoter results in decreased expression of the MGMT protein and has been shown to correlate with prolonged survival in GBM patients [18]. In contrast, unmethylated tumours (with increased MGMT activity) commonly exhibit resistance to TMZ. Therefore, the epigenetic status of *MGMT* has been established as a

surrogate marker of intrinsic resistance to TMZ [19],[20]. While several studies have shown that a deficiency of MGMT can increase the sensitivity of high-grade glioma to alkylating agents, such as TMZ, many tumours with low levels of MGMT are nevertheless chemo resistant. This suggests that other mechanisms are also involved in the formation of resistance to chemotherapy [16]. Mechanisms of intracellular and extracellular catabolic enzymes such as MGMT contribute to the Blood-Brain Barrier barrier defences within both the endothelium and astrocytes. Therefore, a new generation of therapy agents must be able to traverse the BBB, circumvent the anatomical barrier, avoid efflux transport, and evade enzymatic conversion to an inactive metabolite to be successful [21].

Recent studies have shown that treatment of TMZ-resistant tumours with TMZ and either O6-benzylguanine or IFN-β make the cells more sensitive to TMZ in comparison to treatment with TMZ alone [17]. IFN-β exerts anti-tumour effects as well as activating the p53 pathway. This cytokine has immunomodulatory, cell differentiation, anti-angiogenic, and anti-proliferative effects thus IFN-β could help in the treatment of TMZ resistant GBM tumours [17].

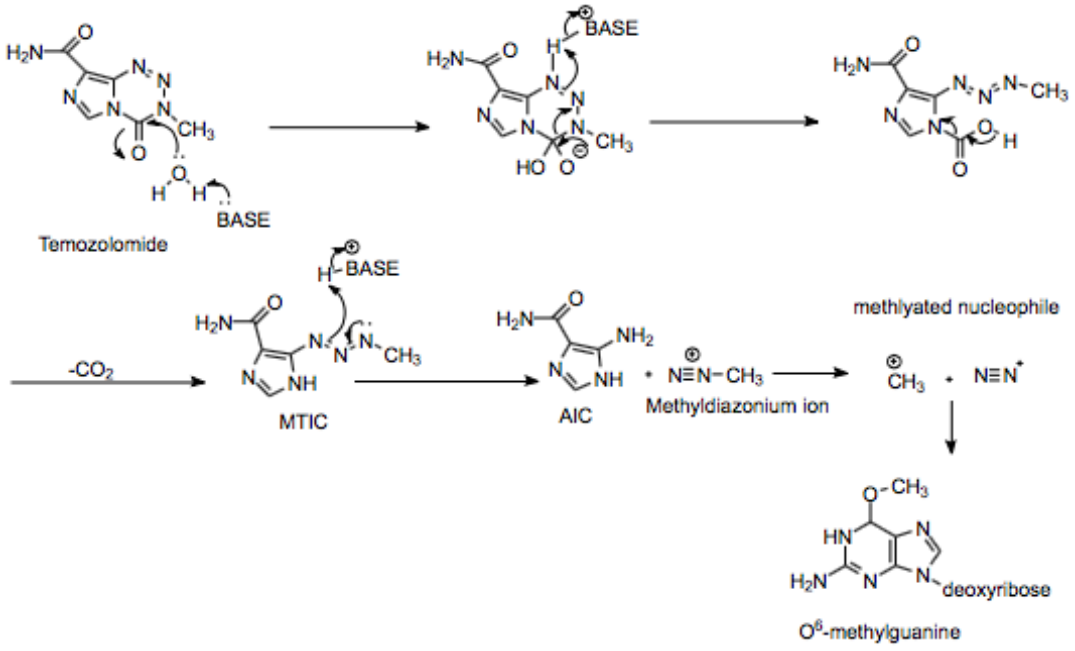

Figure 2: Metabolism of Temozolomide to active form, adapted from [22]**.** A methyldiazonium ion is formed due to the breakdown of MTIC, primarily resulting in the methylation of the guanine residues present in DNA molecules. As a result, O6 - and N7 -methylguanine is formed and is predominantly responsible for the cytotoxic effects of TMZ. DNA mismatch repair enzymes cause the generation of single and double strand breaks as a consequence of attempting to excise O-methylguanine. This leads to the activation of apoptotic pathways.

1.1.2 Bypassing the Blood Brain Barrier (BBB) in GBM treatment

The blood brain barrier (BBB) constitutes the boundary between the brain parenchyma and its vascular supply vessels. This barrier safeguards against foreign substances that are trying to gain entry to the CNS, as well as maintaining CNS homeostasis, including ionic and fluid balances. The BBB shields CNS neurons from circulating hormones, waste products, inflammatory mediators and toxic compounds, as well as strongly fluctuating ionic concentrations [23]. The BBB also prevents the unwanted emergence of CNS neuropeptides and neurotransmitters into general circulation [23]. This system functions to ensure the separation of CNS and systemic fluid contents through an intricate regulatory process.

Most molecules larger than ~500 Da are blocked by the BBB, restricting drug accessibility to various regions where they would be effective and limiting the clinical application of many anti-cancer drugs for treating brain tumours [1] This biomechanical barrier provides cellular resistance to pharmaceutical extravasation as well as the exposure of the parenchymal tissues of the CNS to chemotherapy agents [21]. Reduction in effective drug delivery can also be as a result of the abnormal and leaky tumor vasculature of GBM which causes high hydrostatic pressure in the tumour [24] increasing the permeability of immune cells to the damaged area [25]. Although different anti-cancer agents show varying permeability for BBB, the relationship of its permeability to therapeutic efficacy is not yet clear [26],[27]. The extracellular matrix (ECM) also acts as a physical barrier, limiting the delivery of therapeutics, nutrients, and immune cells to the tumours which contributes to poor prognosis.

1.2 The anti-tumour immune response in GBM

GBM solid tumours induce a higher expression of extra cellular matrix (ECM) molecules such as collagens, proteoglycans, hyaluronic acid and laminins. As a consequence of the increased ECM expression, the tumour becomes complex and disordered, altering their characteristics. The invasive nature of GBM results in the infiltration of healthy tissues in tandem with the generation of a diverse network of blood vessels, aiding tumour mass development, maintenance, and proliferation [28]. The GBM tumour microenvironment can suppress immune detection and limit elimination of cancer cells, by means of a wide range of mechanisms including the secretion of a diverse number of factors that interact with immune cells blocking their action [29].

The GBM tumour microenvironment (TME) is comprised of several different cell types including astrocytes, endothelial cells, circulating stem cells (CSCs), as well as a broad range of immune cells *(Figure 3).* In the GBM TME, glioma associated microglia/macrophages (GAMs), myeloid-derived suppressor cells (MDSCs), $CD4^+$ and $CD8^+$ T lymphocytes, T regulatory lymphocytes (Tregs), dendritic cells (DCs), and natural killer cells (NKs) have been identified *(Figure 3).* These cells and notably GAMs stimulate the local secretion of cytokines and chemokines initiating the reprogramming of immune cells to largely favour cancer growth and metastasis [30].

In addition to TAMs, GBM cells recruit Treg cells ($CD4^+$ $CD25^+$ $FoxP3^+$) *via* the CCL2 and CCL22 pathways [31]. Higher frequencies of Treg cells in GBM patients, suppress the function of antigen-presenting cells (APCs) and inhibit the proliferation of anti-tumour Th1 and $CD8^+$ T cells, thereby, contributing to immunosuppression [32],[33]. Forkhead box P3 (FOXP3) is the main transcription factor which controls the expression of cytokine genes, including IL-10 and transforming growth factor-β (TGF-β), and regulates the immune-suppressive activity of Tregs [32].

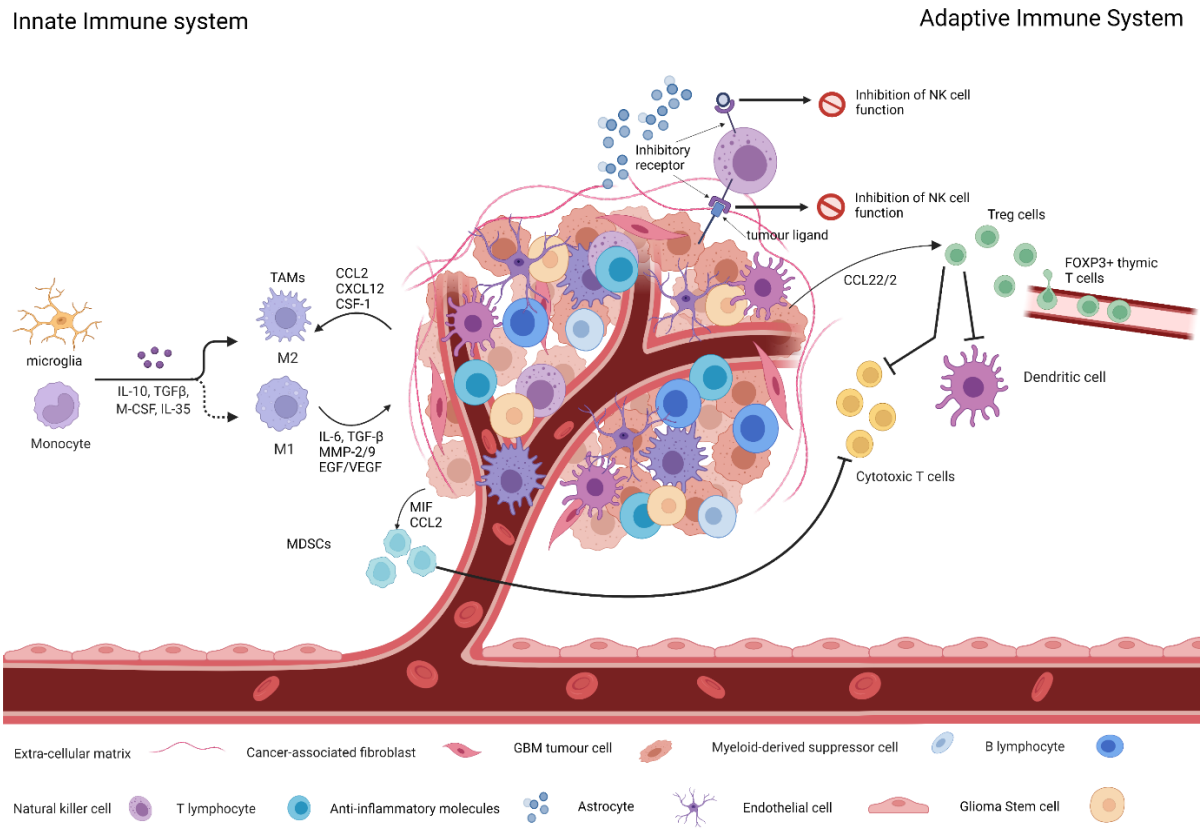

Figure 3: Illustration of the interplay of innate and adaptive immune components within the glioblastoma microenvironment including the cell types and factors involved in glioblastoma and tumour microenvironment (TME) crosstalk. Glioma cells secrete various chemoattractants to recruit different cell populations in TME including glioma associated microglia/macrophages (GAMs), myeloid-derived suppressor cells (MDSCs), $CD4^+$ and $CD8^+$ T lymphocytes, T regulatory lymphocytes (Tregs), dendritic cells (DCs), and natural killer cells (NKs) which play a crucial role in GBM proliferation, invasion, and resistance to treatment. On the side of the innate immune system, tumour-associated macrophages (TAMs), mainly comprised of microglia and peripheral monocytes, are attracted by tumour cells, which release pro-inflammatory cytokines, matrix remodelling protein, and growth factors to aid tumourigenesis. The adaptive immune system, on the other hand, is largely suppressed in its function through the recruitment of regulatory T cells (Treg). These inhibit the action of cytotoxic T cells and dendritic cells, disturbing a competent anti-tumour response. Therapeutically, this tumour-immune crosstalk can be targeted by inhibiting chemoattractants of pro-tumour immune cells. Adapted from Dapash M. *et al.* (2021) [46].

1.2.1 Natural Killers (NK) cells in GBM

Natural Killer (NK) cells are classified as group I innate lymphoid cells (ILCs) that are $CD3^-$, $CD56^+$ and respond quickly to a wide variety of pathological challenges [34]. NK cells develop in the bone marrow microenvironment under the influence of IL-2, IL-15, and surrounding bone marrow stromal cells [35]. Natural killer cell stimulation and effector function depends

on the integration of signals coming from two distinct types, activating and inhibitory receptors present on the NK cell surface. Activating receptors recognise molecules that are expressed on the surface of cancer cells and infected cells, thereby, 'switching on' the NK cell (*Figure 4*). However, for the complete activation of an NK cell, the interaction of at least two different activating receptors with their respective ligands is necessary [36]. The activation can be enhanced with the addition of different cytokines such as IL-2, IL-12, IL-15, IL-18 and IL-21 (*Figure 4*)[37].

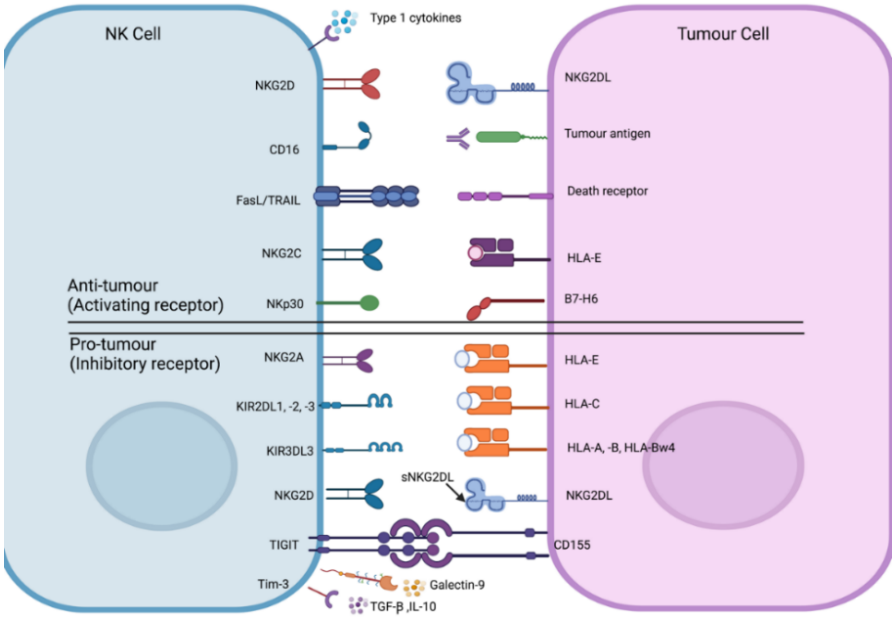

Figure 4: Anti-tumour and pro-tumour receptors present on NK cells. Schematic showing the activating and inhibitory receptors expressed on NK cells and function to regulate their activation.

NK cell killing is regulated by inhibitory receptors to ensure responses against healthy tissues is limited (*Figure 4*). This regulation of activity occurs *via* inhibitory receptor expression (*Figure 5A*) [38]. These germ-line encoded receptors can be split into 3 different groups: 1. Killer immunoglobulin-like receptors (KIRs); 2. C-type lectin, NKG2A/CD94 and 3. Leukocyte immunoglobulin-like receptors (LILRs) [39]. NK cell inhibitory receptors bind to major histocompatibility class-I molecules (MHC-I) which is ubiquitously expressed by healthy cells causing an NK cell inhibitory signal to be induced, preventing NK cell activation. Transformed cells downregulate MHC-1 to evade immune recognition by T cells but in doing so this "missing-self" danger signals earmarks these tumour cells for recognition by NK cells. [40](*Figure 5B*).

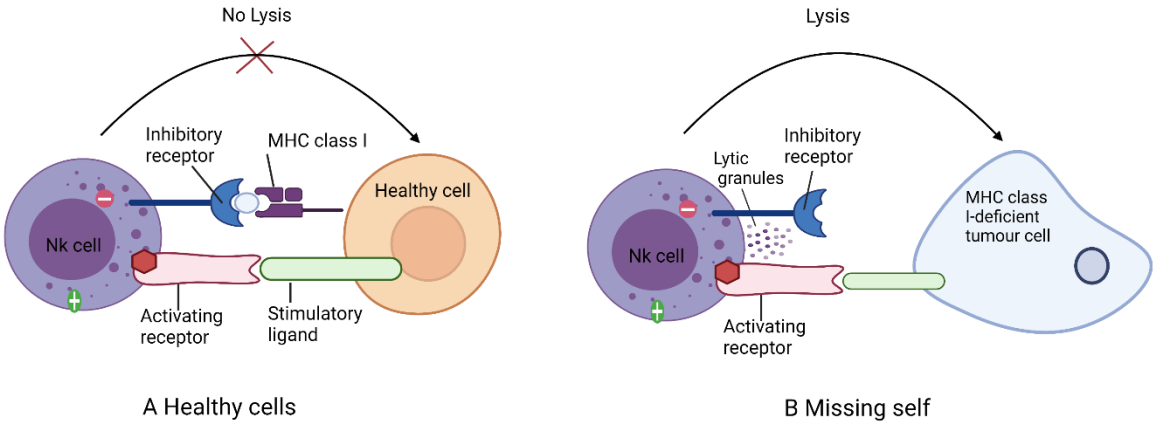

Figure 5: The regulation of NK cells *via* "missing self". Schematic illustrating the NK cell recognition of and response to **A)** healthy cells or **B)** viral infected/tumour cells. Adapted from (Morvan and Lanier, 2015) [40].

1.2.2 Targeted cell killing

Virus-infected cells or tumour cells loose surface MHC class I expression, leading to lower inhibitory signals in NK cells (*Figure 5B*). Cellular stress that is associated with viral infection or tumour development including DNA damage response, senescence programming or tumour suppressor genes, upregulate ligands for activating receptors in NK cells. As a result, the signal from activating receptors in NK cell shifts the balance toward NK cell activation and elimination (lysis) of target cells *(Figure 5B)* [36]. The ligation of NK cells results in the granule-based killing pathway being activated. NK cells release perforin, a pore-forming protein that pierces the plasmatic membrane on the target cell and allows the influx of serine proteases, called granzymes into the cytosol *(Figure 5B)* [35]. If the target cell cannot neutralize this harmful effect on its membrane, it will activate its own cell death by necrosis. If the target cell can restore the integrity of its membrane, granzyme can induce cell death through caspase activation and subsequent apoptosis [41].

1.2.3 Modulation of Natural Killer Cells in Cancer and GBM

There are numerous lines of attack by the tumour for direct evasion from NK cells *(Figure 6)*. Tumours have been shown to reduce expression or shed their ligands for important NK cell receptors. Alternatively, tumour cells can increase MHC class I, soluble MICA and FasL expression in order to increase NK cell inhibitory signalling, thereby, suppressing their

functions [42],[43],[44],[45]. For indirect NK cell evasion strategies, tumour cells utilize various immune cells *(Figure 6)*. Such mechanisms can disrupt receptor ligand interactions between NK and tumour cells thereby, releasing immune-suppressive cytokines into the microenvironment [36]. In GBM, a major way in which anti-tumour NK cell function is suppressed is *via* cellular contact with glioma cells [46]. The adaptive immune system can be suppressed by exhibiting significantly less anti-tumour capacity as a result of the secretion of soluble factors such as IL-10, TGF-β and indoleamine 2, 3-dioxygense (IDO) [47]. NK cell cytotoxic activity is downregulated as a result of these immunomodulatory molecules. An increase in TGF-β levels produced by glioma cells have been shown to downregulate the natural killer group 2 member D (NKG2D) receptor on the surface of NK cells [48] and facilitate immune escape [49],[50]. The levels of IFN-γ have shown to be regulated by NK cells within the TME, consequently promoting glioma stem cell (GSCs) differentiation [51]. Furthermore, this change allows GSCs to become more resistant to NK cell cytotoxicity [52].

Natural killer cell response

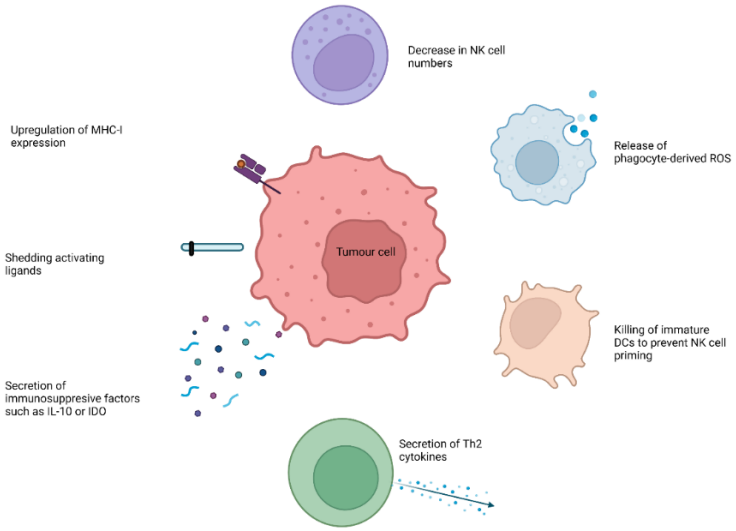

Figure 6: Tumour evasion and modulation of NK cells. Tumour cells use direct and indirect mechanisms to evade NK cell attack. Direct mechanisms include upregulation of MHC class 1 expression, shedding of soluble ligands for NK cell activation receptors and release of inhibitory cytokines. Indirect mechanisms include activation of inhibitory regulatory T cells, killing of immature dendritic cells to prevent NK cell priming, release of phagocyte-derived inhibitory cytokines and reducing the number of NK progenitor cells to lower NK cell counts. NK: natural killer cell; DC: dendritic cell, IL-10: interleukin 10; IDO: indoleamine 2,3-dioxygenase; MHC: major histocompatibility complex; ROS: reactive oxygen species: Th2: T helper cell type 2 [47].

1.2.4 Immune-suppressive effects of Transforming Growth Factor (TGF-β) in GBM

Transforming Growth Factor (TGF-β) is a multifunctional cytokine with many physiological and immunological effects [53]. In most human cells, the TGF-ß receptor and its ligand are expressed, producing three isoforms (TGF-β1, TGF-β2 and TGF-β3 and their respective receptors) all eliciting a similar biological effect on cells [54]. One of the functions of this cytokine is maintaining homeostasis and regulating the growth of cellular lineages. It has been shown that isoform TGF-β2 is overexpressed in glioma cell lines *in vitro* and *in vivo* [55]. It is thought that changes in the cell microenvironment induces TGF-β as well as triggering its own transcription [54].This growth factor supresses tumour cell growth in its initial stages of cancer and inflammation [53],[54]. Due to TGF-βs immune-suppressive and oncogenic capabilities, its dysregulation is linked to tumour progression [53]. As the cancer progresses, oncogenesis is triggered by TGF-β overexpression. TGF-β has immune-suppressive capabilities such as being able to inhibit the activity and proliferation of anti-tumour NK and T cells while increasing their apoptosis and synthesis of TGF-β. MHC class II antigen expression in microglial cells is negatively regulated by TGF-β growth factor resulting in a decrease in antigen presentation and dampening the adaptive anti-tumour immune response [56]. Therefore, this cytokine has the potential to be a therapeutic target to limit tumour progression in GBM and various clinical studies are investigating this [53],[54],[57]. Given the complex relationship between immune cells and the GBM TME, further research is crucial to uncover novel immunotherapeutic targets in this disease space [31].

1.3 Immunotherapies for GBM

1.3.1 Checkpoint inhibitors, targeted therapies for GBM

Immune checkpoint inhibitors (ICIs) signify some of the most proficient immunotherapeutic approaches currently used to treat cancer as they allow the immune system to attack the foreign cells while leaving the healthy cells alone [57]. ICIs are an example of a T cell-based therapy and have recently emerged as an NK cell-based therapy. This approach utilises monoclonal antibodies that bind to inhibitory molecules on the surface of lymphocytes or their ligands on the surface of tumour cells preventing ligation *(Figure 7)*. These checkpoint blockades prevent the interaction of immune cells inhibitory receptors with their cancer cell ligands causing the suppression of signals dampening immune cell activation.

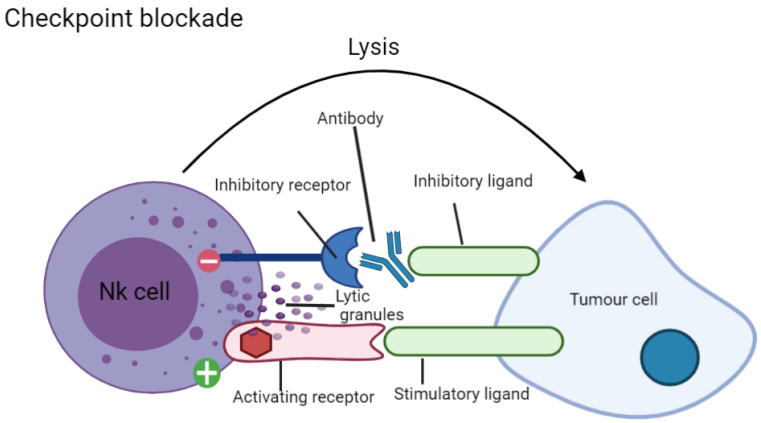

Figure 7: The regulation of NK cells *via* "checkpoint blockade". Schematic showing how monoclonal antibodies can prevent the interaction of natural killer (NK) cell inhibitory receptors with their ligands, thus alleviating NK cell suppression using the mechanism of "checkpoint blockade". Adapted from [40].

Programmed cell death protein 1 (PD-1) is a checkpoint protein on *T cells*, acting as a type of "off switch" that helps keep the T cells from attacking other cells in the body. It regulates T cell activity through ligation with its ligand, programmed death ligand 1 (PD-L1), which is expressed on some immune cells such as macrophages and dendritic cells and is upregulated on many cancer cells. Monoclonal antibodies that target either PD-1 or PD-L1 can block this binding and boost the immune response against cancer cells. Nivolumab (Opdivo) is anti-PD-1 drug that has potential efficacy in recurrent GBM and is currently being investigated in a

phase II trial as monotherapy or in combination with ipilimumab versus bevacizumab (NCT02017717) [58]. Anti-PD-1 and anti-PD-L1 inhibitors have also been shown to enhance NK cell-mediated cytotoxicity [59],[60].

Other immunotherapeutic strategies under clinical development for glioma treatment include anti TGF-β compounds (NCT01472731, Phase II completed) [61]. Importantly, the combination of TGF-β signalling inhibitors with U.S. FDA-approved immune checkpoint blockade agents, such as anti-PD1 and anti-PD-L1 antibodies, could improve clinical outcomes over targeting a single pathway, especially as these antibodies have recently been shown to have efficacy in murine models of glioma [62],[63]. Increasing the passage of monoclonal antibodies through the BBB is a unique challenge for these cancers and different approaches such as ultrasound, omental transplants and nasal delivery are also under investigation.

1.3.2 NK Cell Immunotherapy

Harnessing NK cells with therapeutic intent is an attractive option as NK cell immunotherapy offers several advantages [1]. Firstly, use of NK cells will bypass antigen-specificity requirements. Secondly, NK cells can directly kill tumour cells as well as rapidly secrete pro-inflammatory cytokines that can induce an adaptive immune response [64] NK cells are easy to isolate, manipulate and have a relatively short lifespan. Therefore, the risk of overexpansion of transferred NK cells in the recipient's body is reduced. The source of NK cells for adoptive immunotherapy can be autologous (the patient's own cells) or allogeneic (from healthy donors), offering less logistical challenges than T cells and removing the reliance on heavily pre-treated and possibly dysfunctional patient-derived immune cells [36].

1.3.3 Non-self: small molecule inhibitors

Killer immunoglobulin-like receptors (KIRs) are a superfamily of immunoglobulins that are present on the NK cell surface, which have an Ig-like domain that can bind to HLA class I molecules, helping them to differentiate between "self" and "non-self" (*Figure 8A*). During NK cell maturation, KIRs are involved in their education and selection [65],[66],[67]. The body's autoimmune response is shaped around the interaction between HLA class-I molecules that are expressed on healthy cells and inhibitory KIRs on the NK cell surface. A tumour immune response against a cancer cell is elicited due to the loss or less presence of HLA class-

I molecules as they are recognized as "non-self" by NK cells *(Figure 8A)* [68],[69]. However, some tumours can escape immune detection by expressing HLA class I molecules just like healthy cells, thereby evading NK cell killing, leading to continued tumour development [70]. Studies showed that patients with malignant tumours that had high expression of KIRs on NK cells and tumour infiltration lymphocytes (TILs) responded better to therapy when there was a loss or lower expression of these inhibitory receptors [71],[72], [73]. By blocking inhibitory KIRs, the immune response may be activated and enhanced leading to the reversal of tumour immune escape, making it a promising immunotherapy strategy.

A) **B)**

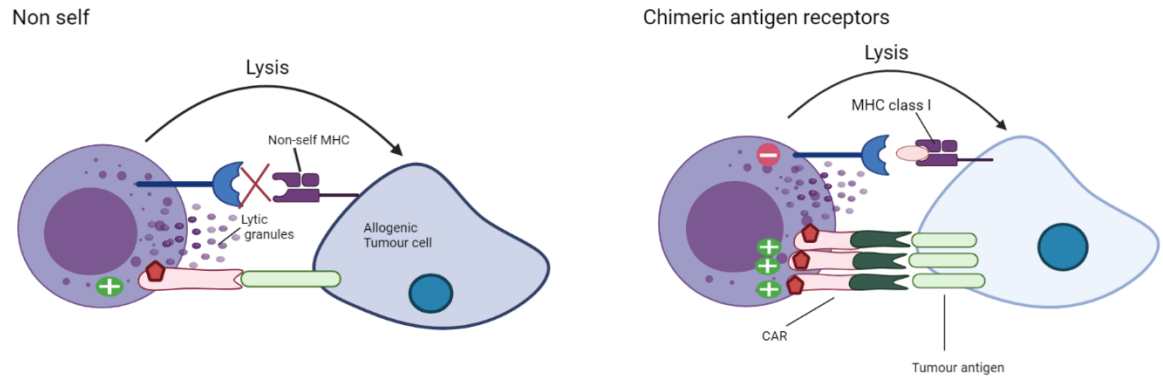

Figure 8: The regulation of NK cells *via* non-self MHC or Chimeric antigen receptors (CARs). Schematic diagrams showing **A)** NK cells can be transduced with activating chimeric antigen receptors (CARs) that specifically bind to antigens overexpressed by tumour cells **B)** Killer cell immunoglobulin like receptors (KIRs) and major histocompatibility complex (MHC) class I mismatch between donor and recipient, Adapted from [40].

1.3.4 Adoptive NK Cell Therapy (CAR-NK cells)

NK cells have several advantages over T cells for chimeric antigen receptors (CAR) therapy, with 17 CAR-NK cell trials currently being conducted worldwide [74]. To elicit antibody dependent cell mediated cytotoxicity (ADCC), the Fc fragment of the IgG low affinity III receptor (FcyR III) expressed by NK cells binds to the Fc fragment of antibodies (*Figure 8B*). This unique feature of NK cells allows for the combination of 2 targeted therapies that recognize different, or the same, tumor associated antigens, for example a chimeric antigen receptor (CAR) expressing NK cells and tumour-associated antigen-specific monoclonal antibodies. NK cells also recognize various ligands through a variety of activating receptors, including natural cytotoxicity receptors allowing for the spontaneous killing of tumour cells

(*Figure 8B).* CAR NK cells also have the potential to be safer than CAR T cells as they have less of a propensity to elicit cytokine storms, called cytokine release syndrome (CRS), a common and serious side effect of CAR T cells [75],[76],[77].

1.3.5 Limitations to NK Therapy for GBM

Many clinical trials investigating NK cell-based immunotherapy in solid tumours (including adoptive transfer of autologous, allogeneic NK cells, NK cell lines or CAR NK cells, cytokine-based therapy, anti-cancer inhibitors, or agonist of activating receptors) have achieved low efficacy [36]. The two major restrictions for NK cell activity in GBM are the immune-suppressive tumour microenvironment (TME) and the successful homing to and infiltration of tumours across the Blood-Brain Barrier barrier (BBB)[78]. NK cells are faced with immunosuppressive factors such as TGF-β in the TME while their metabolism is also impaired as a result of nutrient and oxygen deprivation, causing NK cell effector functions to be limited [78],[79]. Impacting the metabolic restrictions could represent a potential target to improve the efficacy of NK cell-based therapies against solid tumors. TGF-β inhibitors could alleviate immunomodulation and novel delivery could help to overcome challenges presented by the BBB [80].

1.4 Novel anti-cancer compounds for GBM

1.4.1 The anti-cancer utility of *(E)-2-(2-quinolin-2-yl-vinyl)-benzene-1,4-diol HCl* (Q8)

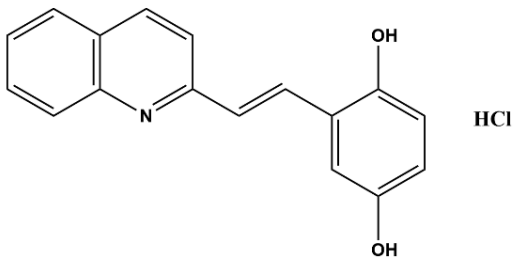

Figure 9: Structure of *(E)-2-(2-quinolin-2-yl-vinyl)-benzene-1,4-diol HCl (Q8)*

(E)- 2-(2-quinolin-2-yl-vinyl)-benzene-1,4-diol HCl (Q8) is a Quininib analogue and a small molecule antagonist of cysteinyl leukotriene receptors 1 and 2 (CysLT1 and CysLT2). Q8 was chosen for its anti-angiogenic efficacy across different cancer models [81]. Tumours express CysLT receptors with enhanced expression of CysLT1 in colorectal cancer showing a negative

correlation with patient survival [82]. Turtay et al., 2010 showed that antagonism of CysLT1 significantly reduces angiogenesis in rodent models, therefore anti-angiogenic therapies could be an alternative target for treating CRC [81].

Murphy et al., (2016) showed that treatment with 10μM Q8 resulted in significant reduction in secretions of important angiogenic mediators IL-6 (37.8%), VEGF (47.3%) and IL-8 (13.2%) [83]. This study also should that aside from pericardial edema, another recognised anti-angiogenic effect, larvae treated with Q8 did not demonstrate any additional behavioral or morphological deficits, signifying that Q8 is non-toxic. This study indicated that the 1–4 dihydroxy quininib, a CysLT1 antagonist, showed significant anti-cancer properties in CRC based on *in vitro, ex vivo* and *in vivo* assessment of this drug. The VEGF independent activity alongside additional anti-angiogenic response has proven that in combination with bevacizumab, Q8 offers a different therapeutic strategy to current anti-VEGF therapies [81].

Bevacizumab has been shown to work alone or in combination with cytotoxic chemotherapy in patients with good performance status at the at the time of GBM recurrence. However, the survival benefit is limited to 4 months and comes with numerous significant side-effects [84]. Therefore, Q8 may represent an alternative GBM treatment pathway as the expression of CysLT1 and CysLT2 is upregulated in glioma cells. By targeting these proteins that are linked to glioma cell proliferation the receptor antagonist Q8, may lead to an alternative GBM treatments. [85]. Overall, Q8 acts non-redundant to the VEGF pathway, and may represent an alternative strategy to counteract anti-VEGF resistance in GBM [86]. Due to the anti-angiogenic and antagonistic properties of Q8, this drug could have potential in the therapeutic arsenal against GBM. Here, we assess the potential of Q8 as an anti-proliferative agent and as combination therapy with standard of care chemotherapy or NK cell therapy in GBM.

1.4.2 The anti-cancer utility of *(E)-2-(2-(Pyrazin-2-yl)vinyl)phenol (P3)*

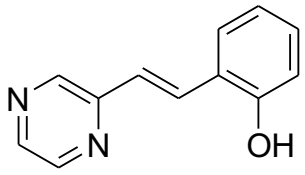

Figure 10: Structure of *(E)-2-(2-(Pyrazin-2-yl)vinyl)phenol (P3)*

(E)-2-(2-(Pyrazin-2-yl)vinyl)phenol (Pyrazinib, P3) is a pyrazine compound that targets oxidative phosphorylation and has shown to enhance radiosensitivity *in vitro* in an isogenic

radioresistance model of OAC [87]. Due to the anti-metabolic and anti-inflammatory activity of P3, its effect on immune cells such as dendritic cells have been investigated. As dendritic cells play a critical role in conducting anti-tumour immune responses through T cell activation, Pyrazinib (P3) was researched to see if it altered the expression of dendritic cell maturation markers. Pyrazinib (P3) did not directly alter the expression of maturation markers on $CD11c^+$ dendritic cells and does not negatively affect dendritic cell function or T cell viability or activation marker expression. However, Pyrazinib (P3) demonstrated significant inhibition of IL-1β secretion and increased IL-3 and IL-17ß secretion from treatment-naïve biopsies from OAC patients. The ability of Pyrazinib (P3) to inhibit both oxidative phosphorylation and glycolysis is a critical finding, which shows even in OAC tumours that have the ability to adapt their metabolism to hypoxic conditions [88]. Here, we assess the potential of P3 as an anti-proliferative and anti-inflammatory agent and as combination therapy with standard of care chemotherapy or NK cell therapy in GBM. This study also screens P3 for any potential adverse immunomodulatory effects on NK cells.

1.4.3 *(E)-2-(2-(pyrazin-2-yl)vinyl)phenyl dihydrogen phosphate (P3 Phosphate)*

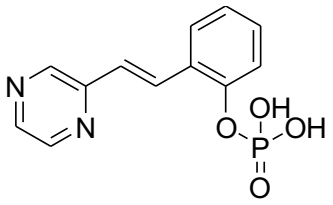

Figure 11: Structure of *(E)-2-(2-(pyrazin-2-yl)vinyl)phenyl dihydrogen phosphate (P3 Phosphate)*

(E)-2-(2-(pyrazin-2-yl) vinyl)phenyl dihydrogen phosphate (P3 Phosphate) is a prodrug of Pyrazinib. Due to the poor solubility of P3 an alternative version with better solubility is required for translation of the *in vitro* studies into in vivo models and eventually human use. P3 phosphate is formed using phosphate esters to give better solubility (McLoughlin et al, unpublished). P3 phosphate is dissolved in 6:4 ethanol: water making it more soluble than P3 which is dissolved in DMSO. The synthesis of this prodrug is described in section 2.7. The target and mechanism of action of this drug is unknown. Here, we assessed whether P3 Phosphate had equivalent or superior potential to P3 as an anti-proliferative and anti-inflammatory agent and as combination therapy with standard of care chemotherapy or NK cell therapy in GBM. In this study, we also assessed *(E)-2-(2-(Pyrazin-2-yl) vinyl)phenyl acetate* (P3 Acetate), the intermediate of P3 for its anti-cancer potential in GBM.

1.5 Hypothesis

P3, P3 phosphate and Q8 have anti-cancer potential in GBM alone and/or in combination with current standard of care chemotherapy, TMZ or in combination with NK cell therapies.

1.6 Study Aims

Aim 1: Elucidate whether P3 and Q8 have anti-proliferative potential alone and/or can sensitise the glioblastoma tumour cells to temozolomide, using the glioblastoma cell line model, T98G .

Aim 2: Examine whether P3 and Q8 can sensitise the glioblastoma cell line T98G to NK cell-mediated responses.

Aim 3: Assess whether P3 and Q8 can enhance NK cell responses in the GBM tumour microenvironment.

Aim 4: Developing and testing more soluble candidates of P3 for subsequent clinical application.

2.0 Materials and Methods

2.1 Patient Samples and Ethical approval

Fresh healthy donor derived blood was taken from consenting healthy donors or prepared from buffy coat packs that were obtained from the Irish Blood Transfusion Service in St. James's Hospital, Dublin. The work was performed in accordance with The Code of Ethics of the World Medical Association (Declaration of Helsinki) for experiments involving humans. For buffy coat packs, patients provided informed written consent for sample and data acquisition and the study received full ethical approval from the St. James's Hospital Ethics Review Committee. For fresh venous blood, healthy donors provided informed consent for sample blood acquisition and the study received full ethical approval from the Faculty of Health Sciences Ethics Committee at Trinity College Dublin. Blood samples were pseudonymized to protect the privacy rights of the donors.

2.1.1 Buffers and Cell culture media

Table 1: Ingredients of buffers and cell culture medias

Buffer	**Ingredients**
FACS Buffer	500 ml phosphate buffered saline (PBS) (Cytiva) 2% Foetal bovine serum (FBS) (Sigma-Aldrich, USA), 0.01% sodium azide (Sigma-Aldrich, USA).
FACS Blocking Buffer	50% FACS Buffer 50% FBS
Media	
Complete Roswell Park Memorial Institute (cRPMI) media	500 ml RPMI 1640 (Sigma-Aldrich Gillingham) supplemented with 10% (v/v) FBS (Sigma-Aldrich, USA) 1% penicillin-streptomycin (Lonza, Switzerland)
Minimum essential medium eagle, with EAR (EMEM)	500 ml EMEM M4655 (Sigma-Aldrich Gillingham) supplemented with 10% (v/v) FBS (Sigma-Aldrich, USA) 1% penicillin-streptomycin (Sigma-Aldrich, USA)
DMEM/F-12 1:1 (1X) + 2.50 Mm L-Glutamine, + 15Mm HEPES Buffer	500 ml DMEM 10% (v/v) FBS (Sigma-Aldrich, USA) 1% penicillin-streptomycin (Sigma-Aldrich, USA)

2.1.2 Media Preparation

Roswell Park Memorial Institute 1640 (RPMI 1640) medium (Gibco, UK), Minimum essential medium eagle, with EAR (EMEM) (Sigma), DME/F-12 1:1 (1X) + 2.50 Mm L-Glutamine, + 15Mm HEPES Buffer (Cytiva) were all supplemented with 10% foetal bovine serum (FBS) (Biosera), 1% penicillin/streptomycin (Sigma) and are henceforth referred to as complete RPMI (cRPMI), complete EMEM (cEMEM) and complete DMEM (cDMEM).

2.1.3 Preparation of peripheral blood mononuclear cells from venous blood

Blood was diluted 2:1 in PBS, and subsequently layered onto Ficoll-Hypaque (GE, USA) in a laminar flow hood and centrifuged at 400 x g for 25 min with the brake off. The buffy layer was removed and washed twice in 50 ml of PBS at 800 x g for 10 min. The PBS was discarded and the pellet was vortexed. The pellet was resuspended in 1 ml of cRPMI and cells were counted as per section 2.1.5.

2.1.4 Preparation of peripheral blood mononuclear cells from buffy coat packs)

Blood packs were collected from the Irish Blood Transfusion Service. The blood packs were sprayed with 70% ethanol and were accessed in a laminar flow hood. EDTA (1 ml of 0.5 mM per 50 ml tube) was added to the blood. Subsequently, 5 ml of blood was transferred into a 50 ml tube and diluted 1:7 with PBS . The diluted blood (35 ml) was carefully layered over 15 ml Ficoll in a 50 ml tube. This was centrifuged at 400 x g for 20 min with the brake off. The cloudy white layer containing the PBMC was removed carefully using a transfer pipette and transferred into a fresh 50 ml tube containing sterile PBS. This was centrifuged for 10 min at 1800 rpm. The supernatant was discarded and the pellet was resuspended in 50 ml PBS. This was centrifuged for 10 min at 1200 rpm. Cells were counted as per section 2.1.5.

2.1.5 Cell counting

A sample of the cells obtained was diluted 1 in 10 with trypan blue (Sigma-Aldrich, USA) and 10 µl of this dilution was added to the haemocytometer (Neubauer glass haemocytometer 0.1 mm depth, Bright-Live^{R}). Viable, unstained cells were visualised at 20X magnification using a light microscope and counted in the four corners of the haemocytometer. The number of cells per ml was calculated as follows:

$$Avg.no.of\ cells\ x10^4\ X\ dilution\ factor = no.of\frac{cells}{ml}$$

2.2 Drug Treatments of NK cells with Q8, P3 and P3 phosphate

2.2.1 Assessing the effect of P3 on NK cell viability:

PBMC were counted and plated at 1 x 10^6 cells per ml of cRPMI in a 24 well plate. PBMC were incubated overnight in a humidified atmosphere of 5% CO_2 at 37°C. PBMC were treated with DMSO vehicle control (0.1%) or 1, 10, 100 μM P3 for 24hrs and had subsequent analysis of NK cell viability by flow cytometry.

2.2.2 Assessing the effect of P3 on NK cell phenotype and function:

PBMC were counted and plated at 1 x 10^6 cells per ml of cRPMI in a 24 well plate. PBMC were incubated overnight in a humidified atmosphere of 5% CO_2 at 37°C. PBMC were treated with cDMEM or 0.5 ml T98G cell line supernatants (section 2.3.1) for 24 hrs +/- 10 μM P3. The cells were subsequently analysed for surface expression of activation/cytotoxicity receptors (NKG2D, NKP30, NKP46, CD69), inhibitory receptors (NKG2A, TIGIT, PD-1) and death receptors (TRAIL, FasL), degranulation markers (CD107a) or cytokines (IFN-γ, TNF-α, IL-10) by flow cytometry (section 2.4.2).

2.2.3 Assessing the effect of P3, Q8 and P3 Phosphate on NK cell chemotaxis:

PBMC were counted and plated at 1 x 10^6 cells per ml of cRPMI in a 24 well plate. PBMC were incubated overnight in a humidified atmosphere of 5% CO_2 at 37°C. PBMC were treated with 0.1% DMSO (P3/Q8 vehicle control), 0.1% ethanol (P3 phosphate vehicle control), or 10 μM of Q8, P3 or P3 phosphate for 24 hrs and their migration towards T98G cell line supernatant (section 2.3.1) was subsequently measured (section 2.5).

2.3 Cell culture of the T98G cell line

The T98G GBM cell line was gifted by Dr Maria Valasco, Centro Nacional de Investigaciones Oncológicas, CNIO, Madrid, Spain. T98G is an adherent cell line derived from human glioblastoma multiform from a 61-year-old Caucasian male. This cell line was subject to mycoplasma testing by polymerase chain reaction (PCR) prior to use.

All *in vitro* cell culture was performed using stringent aseptic techniques. All cell culture preparations were undertaken under the laminar flow hood (FASTER) and any equipment used was autoclaved and sprayed with 70% ethanol before use. An antifungal agent (AquaStabil, Julabo) was added in incubators and water baths to minimise the incidence of contamination.

T98G glioblastoma cell lines were cultured in T75 flasks of complete media (cDMEM) and maintained in a humidified atmosphere of 5% CO_2 at 37°C. The media was changed every 2-3 days. When 80-100% confluent, cells were sub-cultured by incubating the T98G cells with 2 ml trypsin- EDTA solution 10X (Sigma) for 5 min at 37ºC. Trypsin was neutralised by the addition of 10 ml of cDMEM. The cell suspension was then collected, centrifuged and the cell pellet was resuspended in 5 ml of cDMEM . Subculture at a ratio of 1:6 was performed by adding 2 ml of cells in media into 10 ml of complete media in a T75 flask.

2.4 Drug treatments of T98G cells with P3, Q8 and P3 Phosphate

For drug treatments, T98G cells were trypsinised when 80% confluent and counted using a haemocytometer. T98G cells were plated at 5,000 cells per well in a 96 well plate and incubated overnight in a humidified atmosphere of 5% CO_2 at 37°C. Following overnight incubation, T98G cell media was replenished and cells were treated with Temozolomide (10 μM, 50 μM, 100 μM) +/-10 μM P3 or +/- 10 μM Q8 or +/- 10 μM P3 Phosphate or +/- 10 μM P3 Acetate. To ascertain the effects of the novel compounds alone, cells were treated with 10 μM P3 alone or +/- 10 μM Q8 alone or +/- 10 μM P3 Phosphate alone or +/- 10 μM P3 Acetate alone for 72 hrs before proceeding with the CCK8 assay. The appropriate controls were also added to the T98G cells for 72 hrs (0.1% DMSO (P3/Q8 vehicle control) or 0.1% ethanol (P3 phosphate vehicle control)) before proceeding with the assay. The supernatants were collected after 72 hrs before performing the CCK8 assay.

For subsequent NKR profiling, T98G cells were seeded into a 24 well plate at a density of 50,000 cells per 500µl of media for the 24 hr treatment and 10,000 cells in 500µl for the 60 hr treatment (24 hr treatment and 36 hr data collection period). T98G cells were incubated overnight after which the media was replaced, and the cells were treated with 10µM of P3) or 0.1% DMSO control for 24 hrs. The supernatant was collected after 24 hrs, and the media was replaced. In the case of the 60-hr time point, the supernatant containing the drug was removed after 24 hrs and the media was replaced. These cells were then subject to a subsequent 36-hr culture. Following either 24 or 60 hrs, cells were stained for flow cytometric analysis as per section 2.6.2.

2.5 Functional assays using T98G cell line

2.5.1 CCK8 assay

T98G cells were plated onto a 96 well plate at 5,000 cells per well and cultured for 24 hrs. Following overnight incubation, T98G cell media was replaced and cells were treated with temozolomide (10 µM, 50 µM, 100 µM) +/-10 µM P3 or +/- 10 µM Q8 or +/- 10 µM P3 Phosphate or +/- 10 µM P3 Acetate or 10 µM P3 alone or +/- 10 µM Q8 alone or +/- 10 µM P3 Phosphate alone or +/- 10 µM P3 Acetate alone for 72 hrs before proceeding with the assay. After 72 hrs, supernatant was removed and 100 µl of fresh media was added to each well. Supernatants were cryopreserved for subsequent ELISA, NK cell functional assays and chemotaxis assays. Five microlitres Cell Counting Kit-8 (CCK-8) (Sigma) per 100 µl culture medium was added directly to the cells. The cells were incubated in a cell culture incubator for 0.5 to 4 hrs at 37°C until the colour turned orange. A calibration curve was created using the data obtained to show number of viable cells.

2.5.2 Enzyme linked Immunosorbent assay (ELISA)

Levels of soluble analytes IL-17, IL-6, TGF-β , MICA, TIMP-1, B7-H6, ULBP3 in cell culture supernatant were measured using ELISA kits according to manufactures protocol (Table 2). 96 well ELISA plates were coated with capture antibody diluted in PBS and left overnight at room temperature (R&D systems) or were already pre-coated (Assay Genie). The coated plates were

washed and before blocked with blocking buffer if specified in protocol (Table 2). The washing step was repeated. Standards and samples were diluted as required in reagent diluent and added to the wells in duplicate before incubation for specified time and at specified temperature in protocol (Table 2). The wash step was repeated and detection antibody diluted in reagent diluent was added before incubation for specified time and at specified temperature in protocol (Table 2). The plate was then washed again, before streptavidin-HRP in reagent diluent was added for specified time and at specified temperature in protocol away from direct light. Substrate solution was added to each well for specified time and at specified temperature in protocol, protected from direct light. At this point, stop solution was added. The optical density in each well was determined using a microplate reader (Labsystem Multiskan) at 490 nm (R&D systems) or 450 nm (Assay Genie). A standard curve was produced using the average absorbance values from sample wells were plotted against the standard curve, and protein concentrations in pg/ml were determined.

Table 2: Buffer solutions and reagents for ELISA

Buffer solutions and reagents	**Ingredients**
2L 10X PBS	160 g NaCl, 4g KCl, 28.8 g Na_2HPO_4, 4.8 g KH_2PO4, dH_20. Ph 7.4
1L 1X TBS	8.8g NaCl, 2.42 g Trisma Base (20 Mm), dH_20. Ph 7.3
2L washing solution	200 ml 10X PBS, dH_20, 1ml Tween
Reagent dilutions- filter sterilize	IL-17, 1L-6, B7-H6, ULBP3 - 1% BSA/PBS= 0.5 g BSA + 50 ml dPBS Put on roller, store at 4 ºC TGF-ß (HUFI00248), MICA/B (AssayGenie: HUFI00015), TIMP-1, (AssayGenie: HUFI00254) as per AssayGenie reagent stock samples
Strep-Hrp	IL-17: 50 µL 1/40 dilution (R&D systems; DY008-840114) IL-1ß: 50 µL 1/40 dilution (Biolegend; 437016) IL-6: stock concentration 81.25 µl of stock + 3168 µl (1/40 dilution) working concentration, 50 µL (R&D systems; DY206) B7-H6: 50 µL 1/40 dilution (R&D systems; DY7144-05) ULBP3 50 µL 1/40 dilution (R&D systems; DY1517-05) TGF-ß: Dilute HRP-Streptavidin conjugate (SABC) with SABC dilution buffer 1:100, 100µl of SABC working solution (AssayGenie: HUFI00248), MICA/B: Dilute HRP-Streptavidin conjugate (SABC) with SABC dilution buffer 1:100, 100µl of SABC working solution (AssayGenie: HUFI00015), TIMP-1: Dilute HRP-Streptavidin conjugate (SABC) with SABC dilution buffer 1:100, 100µl of SABC working solution TIMP-1, (AssayGenie: HUFI00254)
Capture antibody (in dPBS) :	IL-17: stock concentration 480 µg/ml 1/120 dilution 50 µL of this solution(R&D systems, DY008-840113)

	IL-1ß: stock concentration 60µl of capture antibody (200X) + 12 ml 1X diluent, working concentration 50 µl of this solution (Biolegend; 437016) IL-6: stock concentration 1/120 dilution, 27 µl of stock + 3223 µl PBS, 50 µL of this solution was added (R&D systems; DY206) B7-H6: stock concentration 120µg/ml 0.5 ml PBS was added to the capture, working concentration 2µg/ml, 83.3 µl of stock was added to 10 ml PBS, (R&D systems; DY7144-05) ULBP3: stock concentration 240 µg/ml. 0.5ml of PBS added to capture antibody. Working concentration, 2 µg/ml 83.3 µl of stock + 10ml PBS (R&D systems; DY1517-05) TGF-ß: (AssayGenie: HUFI00248), MICA/B (AssayGenie: HUFI00015), TIMP-1(AssayGenie: HUFI00254) all precoated plates
Detection antibody (in RD) :	IL-17: stock concentration 9µg/ml 1/60 dilution: working concentration 50 µL of this solution(R&D systems; DY008-840114) IL-1ß: stock concentration 60 µl of detection antibody (200X) + 12 ml of 1X diluent, working concentration 50µL of this solution (Biolegend; 437016) IL-6: stock concentration 54.1 µl + 3195 µl (1/60 dilution) working concentration, 50µL of this solution was added (R&D systems; DY206) B7-H6: stock concentration 6 µg/1ml of reagent diluent, working concentration 6000 ng/ml, 166 µl of stock + 10 ml reagent diluent. (R&D systems; DY7144-05) ULBP3, stock concentration 6 µl/1ml of reagent diluent, working concentration 6000 ng/ml, 166 µl of stock was added to 10 ml diluent (R&D systems; DY1517-05) TGF-ß: 100 µL dilute 1:100, 1 µL of stock + 99 µL of diluent buffer (AssayGenie: HUFI00248) MICA/B: 100 µL dilute 1:100, 1 µL of stock + 99 µL of diluent buffer (AssayGenie: HUFI00015) TIMP-1: 100 µL dilute 1:100, 1 µL of stock + 99 µL of diluent buffer (AssayGenie: HUFI00254)

Standards (in RD);	IL-17: 70 mg/ml 1/70 dilution (R&D systems; DY008-840115) 50 µL of this solution IL-1ß: 16 ng/ml in 0.2 diluent to make 80 ng/ml stock concentration to give working concentration of 125 pg/ml, perform 1:10 dilution of stock, 10 µl stock + 90 µl 1X diluent then add 15.6µl of this dilution to 984.4 µl 1X diluent. (Biolegend; 437016) IL-6: (2 ng/ml) stock concentration 1/40 dilution, 7.5 µl stock + 292.5 µl diluent working concentration 50 µL of this solution(R&D systems; DY206) B7-H6: 85 ng/ml. 0.5ml of reagent + standard antibody, working concentration 8000 pg/ml, 23.53 µl of stock + 1 ml reagent (R&D systems; DY7144-05) ULBP3: Stock concentration, 110 ng/ml. 0.5 ml of reagent diluent was added to standard. Working concentration 8000 pg/ml. 72.72 µl of stock was added to 1 ml reagent diluent, this was serially diluted (R&D systems; DY1517-05) TGF-ß: 1ml of sample buffer into one standard tube for stock solution, add 100 µl of standard working solution (AssayGenie: HUFI00248) MICA/B: 1ml of sample buffer into one standard tube for stock solution, add 100 µl of standard working solution (AssayGenie: HUFI00015) TIMP-1: 1ml of sample buffer into one standard tube for stock solution, add 100 µl of standard working solution (AssayGenie: HUFI00254)

2.6 Flow cytometry

2.6.1 Extracellular Flow Cytometric Staining

Unstained controls were subject to the same protocols as their stained counterparts, except for the addition of flow cytometry antibodies.

2.6.2 Extracellular (Surface) staining

Cells were transferred in suspension to a FACS tube and centrifuged at 1300 rpm for 5 min in FACS buffer. The supernatant was discarded, and the pellet was resuspended in 1 ml of blocking buffer (50% FACS Buffer and 50% FBS) for 5 min at room temperature. Subsequently the cells were centrifuged at 1300 rpm for 3 min and resuspended in FACS buffer. This washing step was repeated twice. Following washing, cells were resuspended in 100 µl of FACS buffer and antibodies were added as in table 3 and incubated at 4˚C for 30 min

in the dark. Cells were washed twice in FACS buffer and resuspended in 200 µl of FACS buffer for acquisition on the BD FACS CANTO II flow cytometer.

Table 3: Fluorochrome conjugated antibody panels used for extracellular staining of blood and tumour for flow cytometric analysis using the BD FACS CANTO II.

Antibody	Volume (µl)	Manufacturer	Cat No.	Clone	Antibody type
CD56-FITC^{Viobright}	1	Miltenyi Biotec, USA	130-114-552	REA196	Surface
CX3CR1-PE	1	Miltenyi Biotec, USA	130-122-912	REA385	Surface
CD3-APC-Cy7	1	Biolegend, USA	300318	HIT3a	Surface
NKG2D-PerCP/Cyanine5.5	5	Biolegend, USA	320817	1D11	Surface
NKP46-PE/Cyanine7	1	Biolegend, USA	331915	9E2	Surface
NKG2A-APC	2	Miltenyi Biotec, USA	130-114-089	REA110	Surface
NKp30-Brilliant Violet 421	1	Biolegend, USA	325227	P30-15	Surface
CD69-Brilliant Violet 510	1	Biolegend, USA	310935	FN50	Surface
FasL-Brilliant Violet 421	1	Biolegend, USA	306411	NOK-1	Surface
CD62L-Brilliant Violet 510	1	Biolegend, USA	304843	DREG-56	Surface
TIGIT-PerCP/Cyanine5.5	2	Biolegend, USA	372717	A15153G	Surface
PD-1-PE/Cyanine7	5	Biolegend, USA	329917	EH12.2H7	Surface
Zombie Aqua (bv2)	1 of 1/1000 dilution	Biolegend, USA	423101	N/A	Surface
FITC anti-human CD155 (PVR)	1	Biolegend, USA	337627	SKII.4	NKR Ligand
PE-conjugate B7-H6	2.5	R&D, USA	FAB7144P-025	875001	NKR Ligand

PerCP/Cyanine5.5 anti-human HLA-E	2	Biolegend, USA	342609	3D12	NKR Ligand
PE/Cyanine7 anti-human MICA/B	2	Biolegend, USA	320917	6D4	NKR Ligand
FITC anti-human CD95 (Fas)	1	Biolegend, USA	305605	DX2	NKR Ligand
PE anti-human CD262 (TRAIL-R2)	1	Biolegend, USA	307405	DJR2-4(7-8)	NKR Ligand
PerCP/Cyanine5.5 anti-human CD137 (4-1BBL)	2	Biolegend, USA	311517	5F4	NKR Ligand
APC-conjugated ULPB3	2.5	R&D, USA	FAB1517A	166510	NKR Ligand
PE anti-human CD112 (PVRL2)	1	Miltenyi Biotec, USA	130-122-782	REA1195	NKR Ligand
PE/Cyanine7 anti-human CD274 (B7-H6/PD-L1)	1	Biolegend, USA	329717	29E.2A3	NKR Ligand

2.6.3 Flow cytometry acquisition and analysis

Cells were acquired using the FACS CANTO II software (BD, UK). Data was analysed using FlowJo Version 10 software (Treestar Inc, USA). The lymphocyte population was gated on using SSC-A and FSC-A. To ensure there are no doublets, single cells were gated within FSC-H and FSC-A. NK cells were gated as $CD56^{+}CD3^{-}$ cells within this gate *(Figure 12A)*. To distinguish between positive and negative populations, unstained controls were utilised. The T98G cells were gated on using SSC-A and FSC-A. To ensure there are no doublets, single cells were gated within FSC-H and FSC-A *(Figure 12B)*. To compensate for spectral overlap, Compensation beads (Miltenyi Biotec and BD) were used as per manufacturer's instructions on the BD FACS CANTO II.

A)

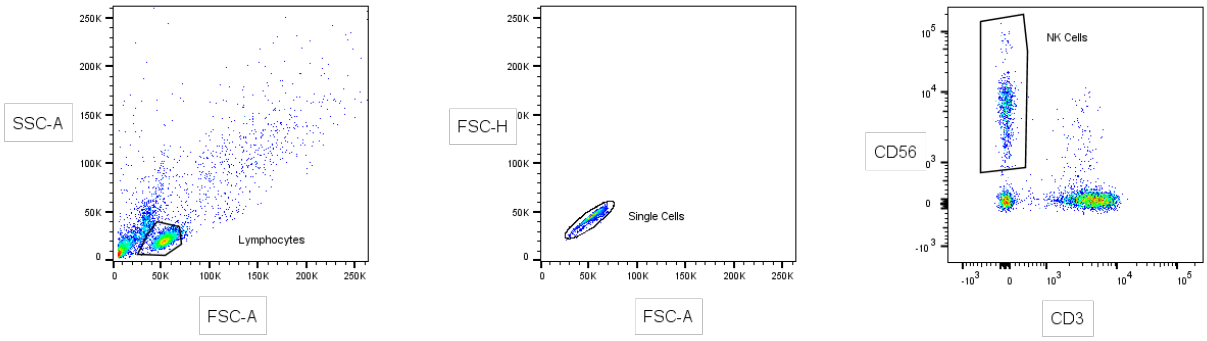

B)

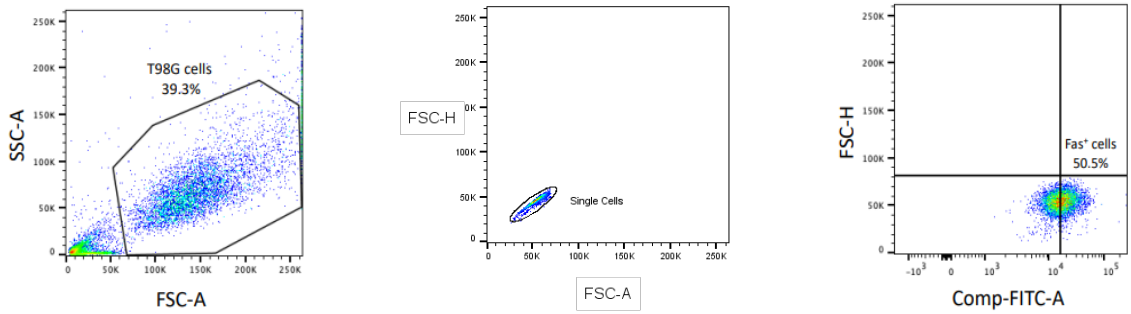

Figure 12: Representative Dot Plot Showing NK Cell and T98G Gating Strategy. A: The lymphocyte population was gated using the SSC-A and FSC-A (left). Following this to remove doublets, single cells were gated on FSC-H and FSC-A (centre). NK cells were gated as $CD56^{+}CD3^{-}$ cells within this gate (right). **B:** T98G cell population was gated on using the SSC-A and FSC-A (left). Following this to remove doublets, single cells were gated on FSC-H and FSC-A (centre). FSC-H and NKR Ligand were used to quantify NKR ligand expression (right).

2.7 NK Cell chemotaxis assay

D1 NK cells DMEM (no FBS)	D2 NK cells DMEM (no FBS)	D3 NK cells DMEM (no FBS)	D1 NK cells DMEM + 20% FBS	D2 NK cells DMEM + 20% FBS	D3 NK cells DMEM + 20% FBS
D1 NK cells GBM	D2 NK cells GBM	D3 NK cells GBM	D1 NK cells GBM Vehicle	D2 NK cells GBM Vehicle	D3 NK cells GBM Vehicle
D1 NK cells GBM +P3	D2 NK cells GBM+P3	D3 NK cells GBM+P3	D1 NK cells GBM + Q8	Untreated D1	Untreated D2
				Untreated D3	

Figure 13: NK cell chemotaxis Plate 1, Untreated NK cell chemotaxis towards drug-treated T98G cells (plus controls). This assay was performed to ascertain the effects of the novel drugs on the chemotactic cues in the GBM Tumour microenvironment.

D1 NK cells + P3 GBM	D2 NK cells + P3 GBM	D3 NK cells + P3 GBM	D1 NK cells + Q8 GBM	D2 NK cells + Q8 GBM	D3 NK cells + Q8 GBM
D1 NK cells + P3PhosVeh GBM	D2 NK cells + P3PhosVeh GBM	D3 NK cells + P3PhosVeh GBM	D1 NK cells + Veh GBM	D2 NK cells + Veh GBM	D3 NK cells + Veh GBM
D1 NK cells + P3Phos GBM	D2 NK cells + P3Phos GBM	D3 NK cells + P3Phos GBM			

Figure 14: NK cell chemotaxis Plate 2, Drug-treated NK cell chemotaxis towards untreated T98G cells. This assay was performed to ascertain the effects of the novel drugs on the migratory capacity of NK cells.

Peripheral blood mononuclear cells (PBMC) from 3 healthy donors were obtained and incubated overnight in RPMI at 1 x 10^6 cells per ml. Supernatants from the vehicle-treated or drug-treated T98G cell cultures were added to the lower chamber of a 5 μm pore Transwell filter system (Corning Inc, Corning, NY, USA) in plate 1 *(Figure 13)* while supernatants from untreated T98G cell cultures were added to the lower chamber of the transwell system in plate 2 *(Figure 14)*. Serum-free DMEM was used as a negative control and DMEM supplemented with 20% FBS was used as a positive control for chemotaxis. PBMC from 3 healthy donors were subsequently added at a density of 0.2 × 10^6 cells/100 μL RPMI to the upper chamber of the transwell system. This system was incubated for 2 hrs at 37 °C, with 5% CO_2. Migrated cells were collected from the lower chamber and stained for flow cytometric analysis with CD56-FITC-Viobright (Miltenyi Biotec) and CD3-APC-Cy7 (Biolegend). CountBright beads (ThermoFisher, Waltham, MA, United States) were used to enumerate the migrated lymphocytes, $CD56^+CD3^-$ NK (Natural Killer) cells and $CD56^-CD3^+$ T cells. Cells were acquired using the CANTO II flow cytometer (BD Biosciences) and analysed using FlowJo v10 software (Tree Star Inc , USA). Absolute numbers were calculated using the following equation.

$$\frac{\text{No. of beads per 5µl}}{\text{Vol of cells acquired}} \times \frac{\text{No. of cells acquired}}{\text{No. of beads acquired}} = \frac{260 \text{ beads} \times \text{No. cells acquired}}{250 \text{ µl}}$$

No. beads acquired

2.8 Statistical Analysis

All data was compiled using Microsoft Excel. Statistical analysis was carried out using graphPad Prism 9.0 software package (GraphPad software, USA). One-way analysis of variance (one-way ANOVA) tested for multiple comparisons used to compare means from 2 or more groups, where a control group was present. Where two treatment groups with equal sample sizes were compared, a paired one-tailed t-test was used. Individual statistical tests are stated in each figure legend. The significance levels were set up at *p< 0.05, **p< 0.01, ***p< 0.001 and ****p< 0.0001.

2.9 Synthesis of P3 Prodrugs

2.9.1 General Experimental Methods

All reagents used for synthesis were commercially available and were used without purification, unless otherwise stated. Before use all glassware and magnetic stirring bars were washed with water and acetone, then dried in oven at 140 ℃ overnight, unless otherwise stated. All anhydrous reactions were performed under an atmosphere of nitrogen. Thin Layer Chromatography analysis (TLC) was achieved using Merck Silica gel 60 TLC aluminium sheets with fluorescent indicator visualising with UV light at 254 nm and 365 nm. Purification of compounds were performed by flash column chromatography using Silica gel from Merck (pore size 60 Å). Nuclear Magnetic Resonance (both ^{1}H and ^{13}C NMR spectra) were recorded on a Bruker Advance Spectrometer which operates at 600 MHz using an internal standard of tetramethylsilane (TMS) and deuterodimethylsulfoxide (DMSO-d_6) as a solvent by Dr. John O'Brien in the School of Chemistry, Trinity College Dublin. All coupling constant values(J) are given in Hz and chemical shift (δ) in ppm. Multiplicities are given using the following abbreviations: Doublet (d), triplet (t), singlet (s), broad singlet (brs), doublet of doublet (dd), multiplet (m), and septet (sept). FTIR analysis were carried out as ATR by using a Perkin Elmer spectrum IR version 10.6.0 with neat samples and frequency of bands were observed in wavenumbers (cm^{-1}). The melting point analysis was carried out using Stuart melting point

|SMP 201| apparatus and microwave assisted synthesis was carried out using CEM Discover microwave synthesiser.

2.9.2 Synthesis of (E)-2-(2-(Pyrazin-2-yl)vinyl)phenyl acetate (P3 Acetate)

2 methylpyrazine (0.46 g, 0.45 mL, 5 mmol) and salicyaldehyde (0.60 g, 0.52 mL, 5 mmol) were added to a stirring solution of acetic anhydride (20 ml). This was placed in the microwave for 5 hrs at 160ºC. The product was a dark brown liquid. The solvent was evaporated in *vacuo* under reduced pressure and the residual solvent was removed under nitrogen to afford a brown/yellow crystalline solid (Yield: 750 mg, 62%). The product was carried forward to step 2 without further purification.

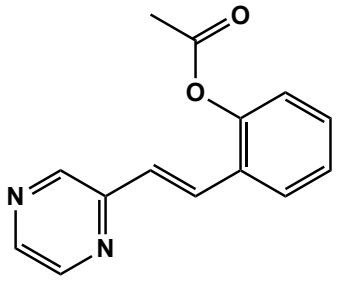

Figure 15: (E)-2-(2-(Pyrazin-2-yl)vinyl)phenyl acetate (P3 Acetate) structure. Chemical Formula: $C_{14}H_{12}N_2O_2$, Molecular weight: 240.26

Rf: 0.5cm (*n*-hexane: ethyl acetate 1:1) (seen under λ 365 and 254nm UV light)

IR (ATR; V_{max}/cm^{-1}) 1758 cm^{-1} (C=O)

^{1}H NMR (600 MHz DMSO-d_6) δ 8.84 (d, 1H, ArH, pyrazine ring), 8.65 (dd, 1H, ArH, Pyrazine ring), 8.52 (d, 1H, ArH, pyrazine ring), 7.93 (dd, 1H, ArH), 7.76 (d, 1H, *J*= 16 Hz), 7.43 (t, 1H, *J*= 7 Hz ArH), 7.41 (d, 1H, *J*= 16 Hz), 7.35 (t, 1H, *J*= 7 Hz ArH), 7.21 (dd, 1H, ArH), 2.38 (s, 3H, CH_3 acetate group)

^{13}C NMR (600 MHz DMSO-d_6) δ 168.5, 150.2, 148.6, 145.24, 144.67, 143.87, 129.15, 128.36, 127.7, 127.4, 126.2 125.6, 123.6, 20.7

2.9.3 Hydrolysis of P3 Acetate to generate P3

P3 acetate (200 mg) was dissolved in a mixture of ethyl acetate/ethanol (1:1 mixture, 40mL). The stirring mixture was refluxed at (100ºC) followed by the addition of NaOH (~2 ml). The reaction was run for 2 hrs. TLC analysis was done to monitor the reaction progress Then, the solvent was removed *in vacuo* and the crude mixture was purified by using flash column chromatography on a gradient of 1:1 to 1:2 (hexane: ethyl acetate) to afford a bright yellow solid (Yield: 90 mg, 15%).

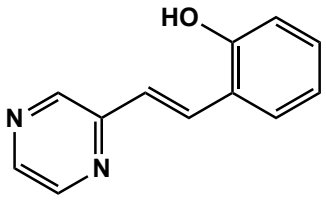

Figure 16: Structure of P3. Chemical Formula $C_{12}H_{10}N_20$, Molecular Weight: 198.23

Rf: 0.35cm (n-hexane: ethyl acetate 1:1) (seen under λ 365 and 254 nm UV light)

Melting point: 207 ℃

IR (ATR; V_{max}/cm $^{-1}$) 3301 cm^{-1} (Broad, OH); absence of C=O peak

^{1}H NMR (600 MHz DMSO-d_6) δ 10.0 (br s, 1H, OH), 8.72 (d, 1H, ArH, Pyrazine ring), 8.60 (dd, 1H, ArH, pyrazine ring), 8.46 (d, 1H, ArH, Pyrazine ring), 8.02 (d, 1H, *J* = 16 Hz), 7.63 (dd, 1H, ArH), 7.37 (d, 1H, *J* = 16Hz), 7.17 (t, 1H, *J*= 7 Hz, ArH), 6.92 (d, 1H, ArH), 6.86 (t, 1H, *J*= 7 Hz, ArH)

^{13}C NMR (600 MHz DMSO-d_6) δ 155.92, 151.22, 144.42, 143.74, 142.68, 129.94, 129.84, 127.49, 123.62, 122.75, 119.35, 116.14

2.9.4 Addition of dibenzylphosphite to Pyrazinib to afford Pyrazinib dibenzylphosphite

Due to timing issues the Pyrazinib dibenzylphosphite was not synthesised or purified, however, the procedure is as follows. Pyrazinib (P3) should be 50 mg minimum (250 mg, 1.16 mmol, 1Eq) was added to a stirring solution of anhydrous Acetonitrile (5 ml) under a nitrogen atmosphere. To aid dissolution it was sonicated for 10 min. The reaction vessel was then placed on ice followed by the dropwise addition of Carbon Tetrachloride (0.4 mL, 3.5 mmol, 3 Eq). the solution was allowed to stir vigorously for 20 min. DMAP (16 mg, 0.125 mmol, 0.1 Eq) and DIPEA (0.45 mL, 2.52mmol, 2 Eq) were then added dissolved in 1ml of acetonitrile *via*

injection (turns from pale yellow to darker yellow) The solution was allowed stir for a further 5 min before the addition of dibenzylphosphite (0.16 mL, 1.8 mmol, 1.4 Eq). (turns back very pale yellow almost clear). The solution was allowed stir on ice for 4hrs and monitored by TLC until a decrease in Rf was observed. The reaction was quenched with saturated K_2SO_4 (5 ml). The reaction was diluted ethyl acetate (5 ml). After phase separation the aqueous layer was retained was then extracted with 3X 20 ml ethyl acetate. The combined organic layers were washed with brine and dried using anhydrous Na_2SO_4. A crude yellow oil should be obtained.

2.9.5 General method: Removal of Benzyls on dibenzyl phosphate derivative

P3 dibenzylphosphite oil (200 mg, 0.5 mmol, 1Eq) was weighed and added to a stirring solution of anhydrous toluene (20 ml), under N_2 and on ice water/methanol trough at -10ºC. Boron tribromide 1M in anhydrous toluene (0.5 ml 0.5 mmol, 1Eq,) was added dropwise to the stirring solution while maintaining a temperature of -10ºC. The reaction was allowed to warm to room temperature before bringing the temperature to 80 ºC. On completion of the debenzylation after two hrs reflux, a yellow participate should be observed. The crude solids were purified using Sephadex gel filtration (Sephadez® G10 medium), through size exclusion chromatography.

3. Results

3.1 Elucidating the effects of P3 and Q8 on T98G cell viability and GBM sensitivity to TMZ

3.1.1 P3 exhibits potential to kill T98G cells

The effects of P3 on GBM cell viability were elucidated using a CCK8 colorimetric assay. T98G cells were treated with 10 μM of P3 for 72 hours and were compared to untreated T98G cells. Our data showed that P3 significantly reduced the percentage of viable T98G cells (Untreated vs. P3-treated (100% vs. 84.09%, p=0.024)*(Figure 17)*.

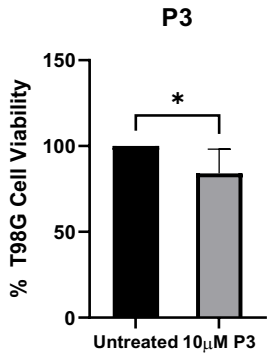

Figure 17: P3 reduces T98G GBM Cell viability. Bar chart showing % cell viability of untreated T98G cells vs T98G cell treated with 10μM of P3 for 72 hours. Cell viability was assessed by CCK8 colorimetric assay. Paired T-test *p < 0.05, n=7

3.1.2 Q8 exhibits potential to kill GBM T98G cells

The effects of Q8 on GBM Cell viability were elucidated using a CCK8 colorimetric assay. T98G cells were treated with 10 μM of Q8 for 72 hours and compared to untreated T98G cells. Our data showed that Q8 did significantly reduce the percentage of viable T98G cells (Untreated vs. Q8-treatment (100% vs. 91.76%, p=0.0085)*(Figure 18).*

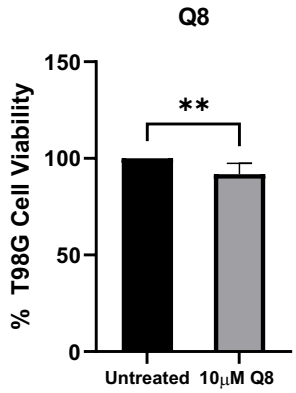

Figure 18: Q8 reduces T98G GBM Cell viability. Bar chart showing % cell viability of untreated T98G cells vs T98G cell treated with 10μM of Q8 for 72 hours. Viability was assessed by CCK8 colorimetric assay. Paired T-test, **p< 0.01, n=7

3.2 Elucidating the effects of P3 and Q8 GBM sensitivity to TMZ

3.2.1 P3 does not sensitize T98G cells to TMZ

The effects of P3 on sensitizing T98G cells to TMZ was elucidated using a CCK8 colorimetric assay. T98G cells were treated with 10, 50, 100 μM of TMZ +/- 10 μM P3 for 72 hours and were compared to untreated T98G cells or the DMSO vehicle control for TMZ. When the vehicle-control treated T98G cells were compared to those treated with 10, 50, 100 μM of TMZ alone there was statistical significance, showing that experimental technique worked and cytotoxic effects of TMZ were achieved (Control vs 10 μM TMZ (100% vs 26.84, p<0.0001), Control vs 50 μM TMZ (100% vs 1.89, p<0.0001), Control vs 100 μM TMZ (100% vs 2.99, p<0.0001)*(Figure 19).* As expected, there was a dose-dependent decrease in cell viability when 10 μM TMZ was compared to 50 μM TMZ (26.84% vs 1.89%, p=0.0011)*(Figure 19)* and when 10 μM TMZ was compared 100 μM TMZ (26.84% vs 2.99%, p=0.0019)*(Figure 19).* Our data showed that while 10 μM P3 alone reduces T98G viability, concurrent treatment with this drug does not significantly sensitize T98G cells to TMZ. There was a decrease in cell viability between 10 μM TMZ + 10 μM P3 vs 50 μM TMZ + 10 μM P3 (20.56% vs 2.76%, p=0.029)*(Figure 19)* and between 10 μM TMZ + 10 μM P3 vs 100 μM TMZ+ 10 μM P3 (20.56% vs 3.35%, p=0.0382)*(Figure 19)*, this is likely due to increasing doses of TMZ as the concentration of P3 remained constant at 10 μM. Significant cytotoxicity observed in response to treatment when combined with TMZ at 10, 50 and 100 μM could have masked any potential effect of P3. Our data demonstrates no TMZ-sensitising effects of P3. Future work will

elucidate whether 24 hour pre-treatment with P3 and/or higher doses of P3 sensitises T98G cells to TMZ treatment.

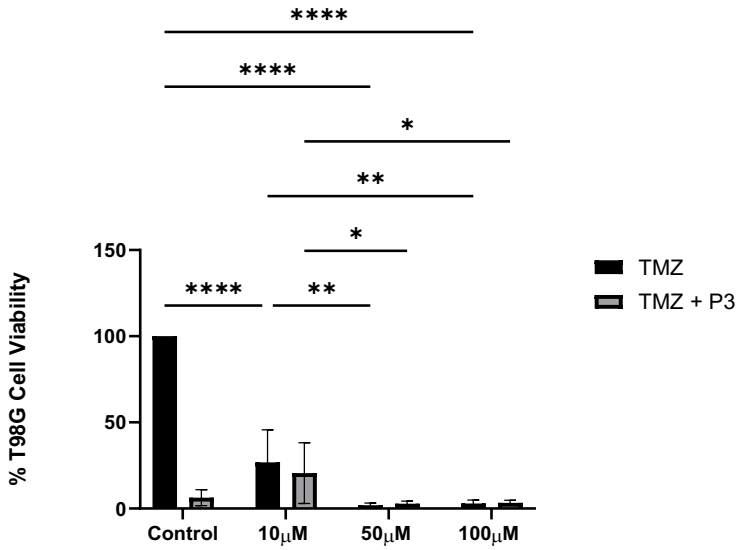

Figure 19: P3 does not sensitize T98G cells to Temozolomide (TMZ). Bar chart showing % cell viability of T98G cells treated with TMZ Vehicle control (Control) or 10 μM, 50 μM or 100 μM TMZ alone (black) vs T98G cells treated with treated with TMZ Vehicle control (Control) or 10 μM, 50 μM or 100 μM TMZ alone TMZ+ 10 μM of P3 for 72 hours. Cell viability was assessed by CCK8 colorimetric assay. 2-way ANOVA *p< 0.05, **p< 0.01, ***p< 0.001 and ****p< 0.0001, n=5

3.2.2 Q8 does not sensitize T98G cells to TMZ

The effects of Q8 on sensitizing T98G cells to TMZ was elucidated using a CCK8 colorimetric assay. T98G cells were treated with 10, 50, 100 μM of TMZ +/- 10 μM Q8 for 72 hours and were compared to untreated T98G cells or the DMSO vehicle control for TMZ. Our data showed that Q8 does not sensitize T98G cells to TMZ. When the untreated T98G cells were compared to 10, 50, 100μM of TMZ alone there was statistical significance (Control vs 10 μM TMZ (100% vs 26.84%, p<0.0001)*(Figure 20),* control vs 50 μM TMZ (100% vs 1.89, p<0.0001)(Figure 14), control vs 100 μM TMZ (100% vs 2.99, p<0.0001)*(Figure 20)*. There was a decrease in cell viability between 10 μM TMZ + 10 μM Q8 vs 50 μM TMZ + 10 μM Q8 (45.37% vs 3.02%, p=0.0010)*(Figure 20)* and between 10 μM TMZ + 10 μM Q8 vs 100 μM TMZ + 10 μM Q8 45.37% vs 4.99%, p=0.0017)*(Figure 20)* but this is likely due to increasing doses of TMZ as the concentration of Q8 remained constant at 10 μM. Due to significant cytotoxicity observed in response to treatment with TMZ at 10, 50 and 100 μM, the concentrations used could have masked any potential effect of Q8. Our data demonstrate no

TMZ-sensitising effects of Q8. Future work will elucidate whether 24 hour pre-treatment with Q8 and/or higher doses of Q8 sensitises T98G cells to TMZ treatment.

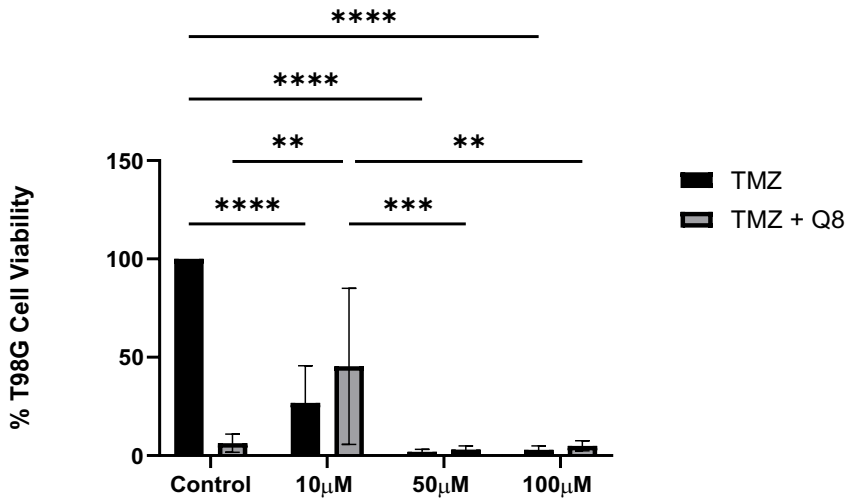

Figure 20: Q8 does not sensitize T98G cells to Temozolomide (TMZ). Bar chart showing % cell viability of T98G cells treated with TMZ Vehicle control (Control) or 10 μM, 50 μM or 100 μM TMZ alone (black) vs T98G cells treated with treated with TMZ Vehicle control (Control) or 10 μM, 50 μM or 100 μM TMZ alone TMZ+ 10 μM of Q8 for 72 hours. Cell viability was assessed by CCK8 colorimetric assay. 2-way ANOVA *p< 0.05, **p< 0.01, ***p< 0.001 and ****p< 0.0001, n=5

3.3 Assessing the ability of P3 to sensitise GBM tumours to NK cell therapies

3.3.1 Treatment with P3 did not alter the expression of NKR activating ligands, ULBP3, MICA/B and B7-H6 present on T98G cells.

The surface expression of NKR activating ligands ULBP3, MICA/B and B7-H6 present on T98G cells were assessed after a 24hr treatment with 10μM of P3. Using flow cytometry, the % frequency and mean fluorescence intensity (MFI) of these NKR ligands were evaluated to ascertain whether the treatment had an effect on NK activation which occurs *via* these ligands. When compared to DMSO vehicle control (VC), treatment with P3 caused a slight increase in the frequency % of T98G cells positive for the NKR ligands ULPB3 (VC vs 10μM P3, 18.826% vs 28.814% p=0.58, *(Figure 21A),* and MICA/B (VC vs 10μM P3, 51.44% vs 60.34%, p=0.34)*(Figure 21B).* However, the % frequency of T98G cells positive for B7-H6 remained unchanged after treatment with P3 (VC vs 10 μM P3, 3.46% vs 3.12% p=0.48)(Figure 15C). No significant changes were observed in the MFI of ULBP3, MICA/B or B7-H6 following P3 treatment *(Figure 21D,E,F).*

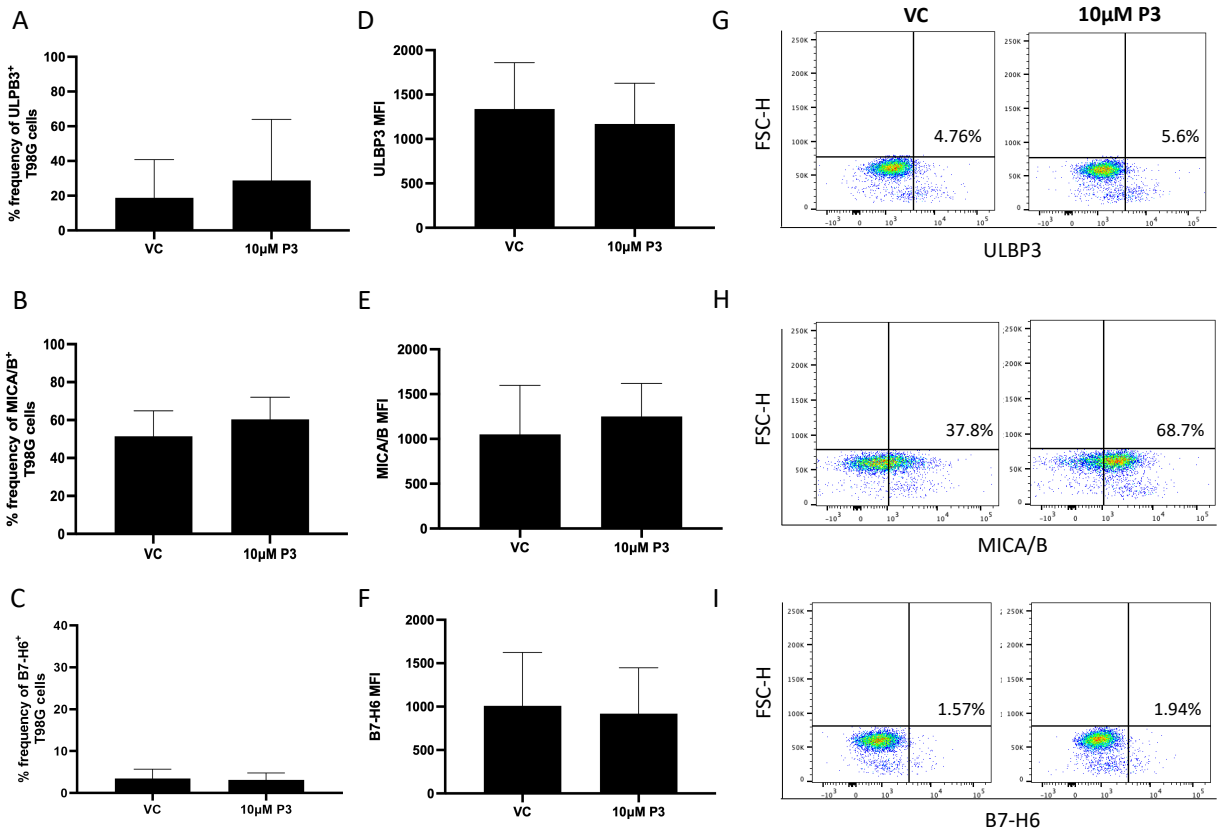

Figure 21: P3 did not change the expression of NKR activating ligands ULBP3, MICA/B and B7-H6 on T98G cells. (Left) Bar chart showing the % frequencies of **(A)** ULBP3$^+$ **(B)** MICA/B$^+$ **(C)** B7-H6$^+$ T98G cells following treatment with DMSO vehicle control (VC) or 10μM of P3 for 24 hours. Bar chart showing the MFI values for **(D)** ULBP3 **(E)** MICA/B **(F)** B7-H6 on T98G cells following treatment with DMSO vehicle control (VC) or 10μM of P3 for 24 hours. **(Right)** Representative dot plots showing **(G)** ULBP3$^+$ **(H)** MICA/B$^+$ **(I)** B7-H6$^+$ T98G cells following treatment with DMSO vehicle control (VC) or 10μM of P3 for 24 hours (n=5), ns by one-way ANOVA. (Experiment carried out in conjunction with MSc Translational Oncology student Jennifer Moran).

3.3.2 P3 did not significantly alter the expression of NKR ligands PVR, PVRL2 and 4-1BBL in T98G cells.

The expression of NKR ligands PVR, PVRL2 and 4-1BBL present on T98G cells were assessed after a 24 hour treatment with 10 μM of P3. Using flow cytometry, the % frequency of these NKR ligands were evaluated. When compared to DMSO vehicle control (VC), treatment with P3 caused a slight increase in the frequency % of T98G cells positive for PVR (VC vs 10 μM P3, 87.4% vs 88.85%, p=0.69)*(Figure 22A)* or 4-1BBL (VC vs 10 μM P3, 45.87% vs 54.82%, p=0.0715)*(Figure 22C)*. The frequency of T98G cells positive for PVRL2 showed a slight decrease after treatment with P3 (VC vs 10 μM P3, 76.7% vs 73.8

p=0.82)*(Figure 22B).* No significant changes were observed in the MFI of PVR, PVRL2 and 4-1BBL following P3 treatment *(Figure 22D,E,F).*

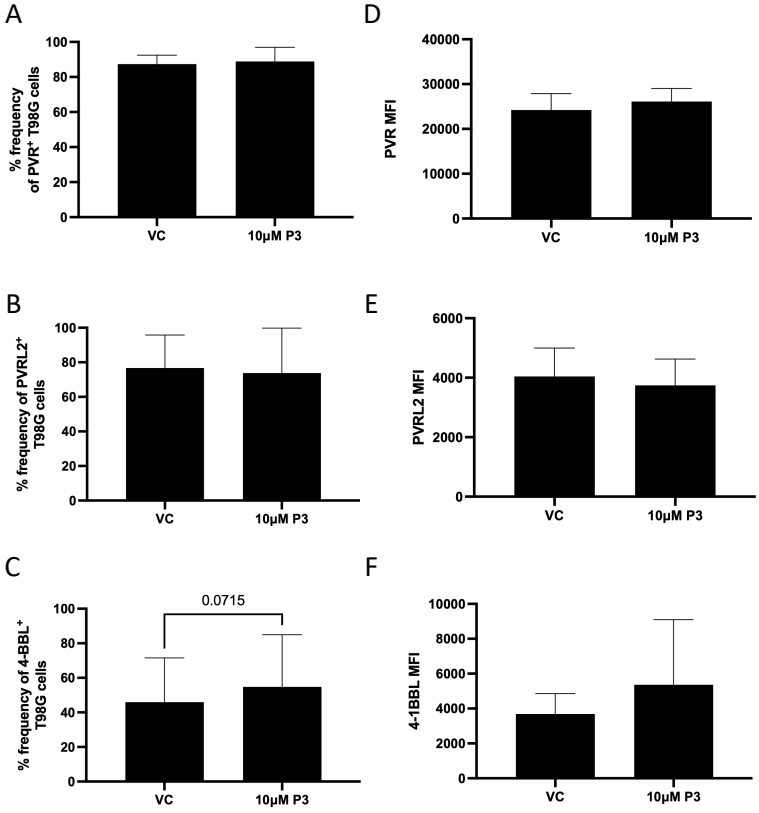

Figure 22: P3 did not change the expression of NKR activating ligands PVR, PVRL2 and 4-1BBL on T98G cells. Bar chart showing the % frequencies of **(A)** PVR **(B)** PVRL2 **(C)** 4-1BBL on T98G cells following treatment with DMSO vehicle control (VC) or 10 μM of P3 for 24 hours. Bar chart showing the MFI values for **(D)** PVR**(E)** PVRL2 **(F)** 4-1BBL on T98G cells following treatment with DMSO vehicle control (VC) or 10 μM of P3 for 24 hours (n=4), ns by one-way ANOVA. (Experiment carried out in conjunction with MSc Translational Oncology student Jennifer Moran)

3.3.3 P3 treatment induced a relative increase in the expression of the death receptor TRAIL-R2 but not Fas in T98G cells.

T98G cells were treated for 24 hours with 10 μM P3 and the expression of death receptors TRAIL-R2 and Fas were analysed by flow cytometry. When compared to DMSO vehicle control (VC), treatment with P3 did not significantly increase the % frequency of TRAIL-R2$^+$ and Fas$^+$ T98G cells. However, the MFI of TRAIL-R2 was significantly increased when T98G cells were treated with P3 suggesting that while the number of cells positive for this death receptor were not increased, the amount on the surface of the glioblastoma cells was significantly enhanced by P3 (VC vs. 10μM P3; 9052.75 vs. 9759; p=0.0497)*(Figure 23).*

There were no significant differences observed between the MFI of death receptor Fas after P3 treatment when compared to the vehicle control.

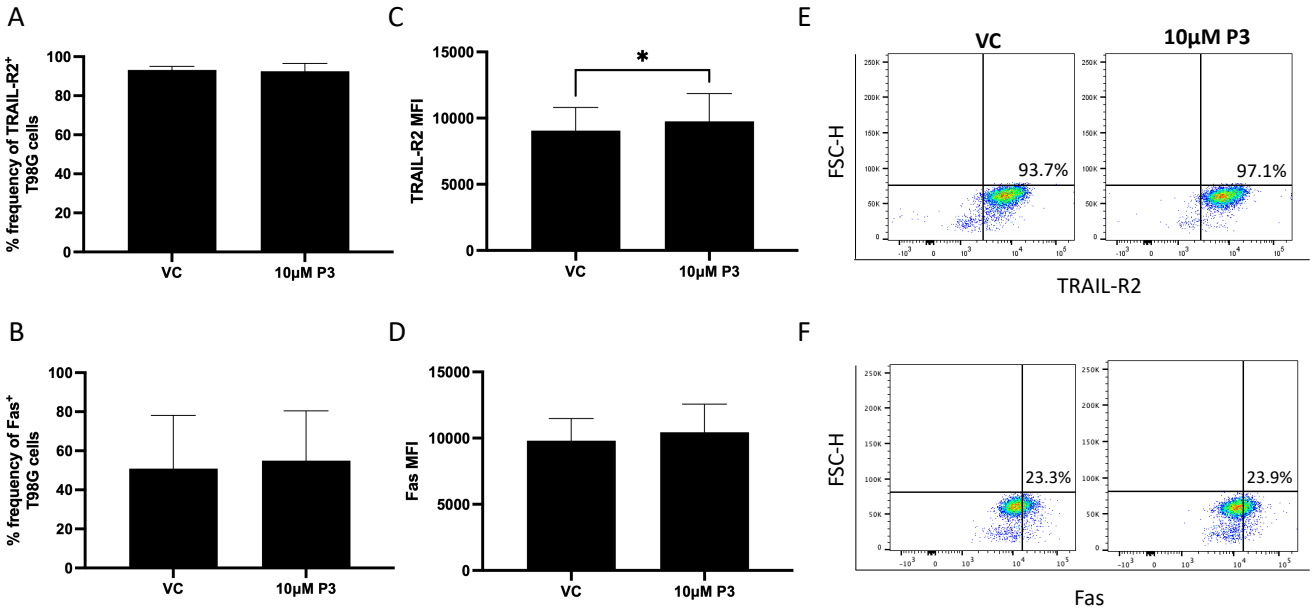

Figure 23: P3 treatment induced a relative increase in the expression of the death receptor TRAIL-R2 but not Fas in T98G cells. (Left) Bar chart showing the % frequencies of **(A)** TRAIL-R2$^+$ (n=4) **(B)** Fas$^+$ T98G cells following treatment with DMSO vehicle control (VC) or 10 μM of P3 for 24 hours. Bar chart showing the MFI values for **(C)** TRAIL-R2 **(D)** Fas on T98G cells. **(Right)** Representative dot plots showing **(E)** TRAIL-R2$^+$ **(F)** Fas$^+$ T98G cells following treatment with DMSO vehicle control (VC) or 10μM of P3 for 24 hours (n=5), *p<0.05 by one-way ANOVA. (Experiment carried out in conjunction with MSc in Translational Oncology student Jennifer Moran).

3.3.4 P3 did not significantly change the expression of the inhibitory ligand HLA-E and the immune checkpoint ligand PD-L1 in T98G cells.

T98G cells were treated with 10 μM of P3 for 24 hours and the expression of inhibitory ligand HLA-E and the immune checkpoint ligand PD-L1 were assessed. There was no significant change in the % frequency of T98G cells that were positive for HLA-E (n=4) and PD-L1 (n=5)*(Figure 24B)* following treatment with P3. There were no significant changes observed in the MFI of HLA-E or PD-L1 when T98G cells were treated with P3 in comparison to the vehicle control treated T98G cells *(Figure 24C,D)*.

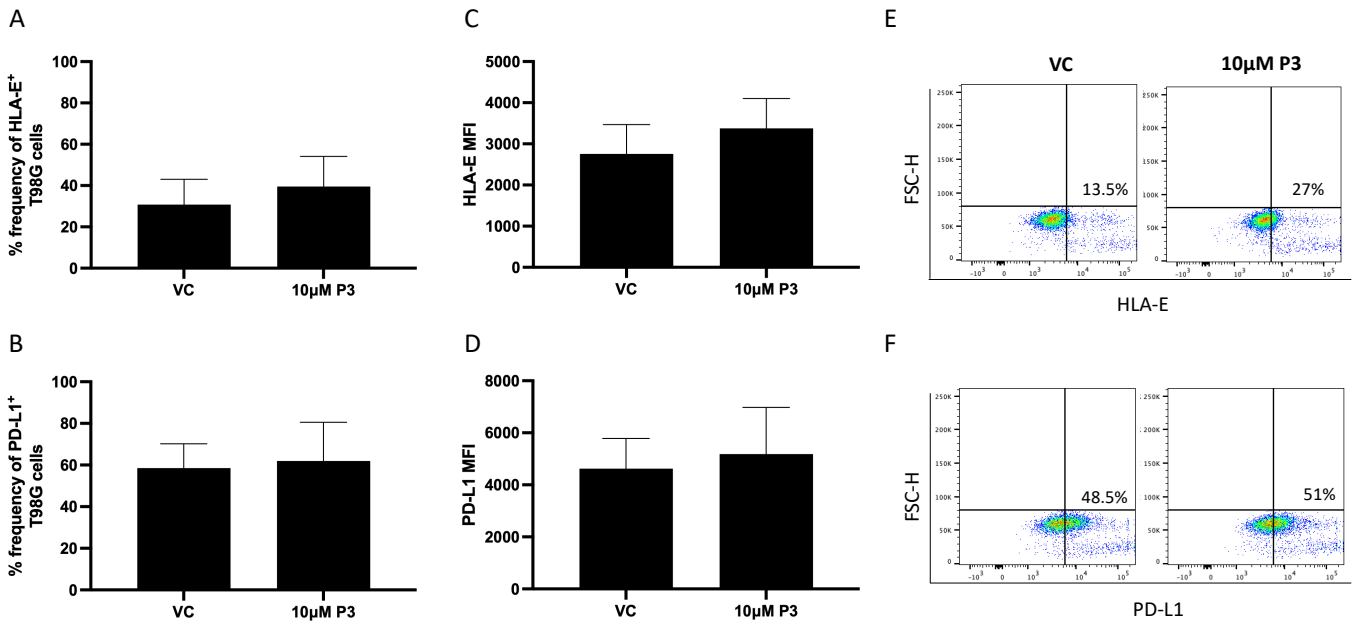

Figure 24: P3 did not significantly change the expression of the inhibitory ligand HLA-E and the immune checkpoint ligand PD-L1 on T98G cells. (Left) Bar chart showing the % frequencies of **(A)** HLA-E$^+$ (n=4) **(B)** PD-L1$^+$ (n=5) on T98G cells following treatment with DMSO vehicle control (VC) or 10 μM of P3 for 24 hours. Bar chart showing the MFI values for **(C)** HLA-E **(D)** PD-L1 on T98G cells. **(Right)** Representative dot plots showing **(E)** HLA-E$^+$ **(F)** PD-L1$^+$ T98G cells following treatment with DMSO vehicle control (VC) or 10μM of P3 for 24 hours (n=5), *p<0.05 by one-way ANOVA. (Experiment carried out in conjunction with MSc in Translational Oncology student Jennifer Moran).

3.3.5 Both P3 and the vehicle control increased the expression of NKR activating ligands MICA/B and B7-H6 when T98G cells were analysed at 60 hours.

When analysed at 60 hours, the frequency % of T98G cells which were positive for ULBP3 and B7-H6 was not altered when treated with 10 μM P3 for 24 hours (24 hours [n=5]; 60 hours [n=3])*(Figure 25A)*. When analysed after 36 hours by flow cytometry there was an increase in the frequency % of T98G cells positive for MICA/B which were treated with P3 for 24 hours (10 μM P3 [24 hours] vs. 10 μM P3 [60 hours]; 60.34% vs. 84.93%; p=0.0323) *(Figure 25B)* however, this increase was also observed in the vehicle control treated cells. In the MFI of ULBP3 there were no significant changes post P3 treatment between the 24 hour and 60 hour time points *(Figure 25D)*.The MFI of MICA/B and B7-H6 was increased with addition of 10 μM P3 at 60 hours (10 μM P3 [24 hours] vs. 10 μM P3 [60 hours]; 1251.6 vs. 2496; p=0.0499)*(Figure 25E)* and (10 μM P3 [24 hours] vs. 10 μM P3 [60 hours]; 918.75 vs. 2465; p=0.0005) *(Figure 25F)* respectively. There was a significant increase in the MFI of B7-H6 at

60 hours by the vehicle control which indicates that DMSO is causing the change in the surface ligand expression, thereby negating the significance of the finding, (VC [24 hours] vs. VC [60 hours]; 1009.5 vs. 2301; p=0.0009) *(Figure 25F)*.

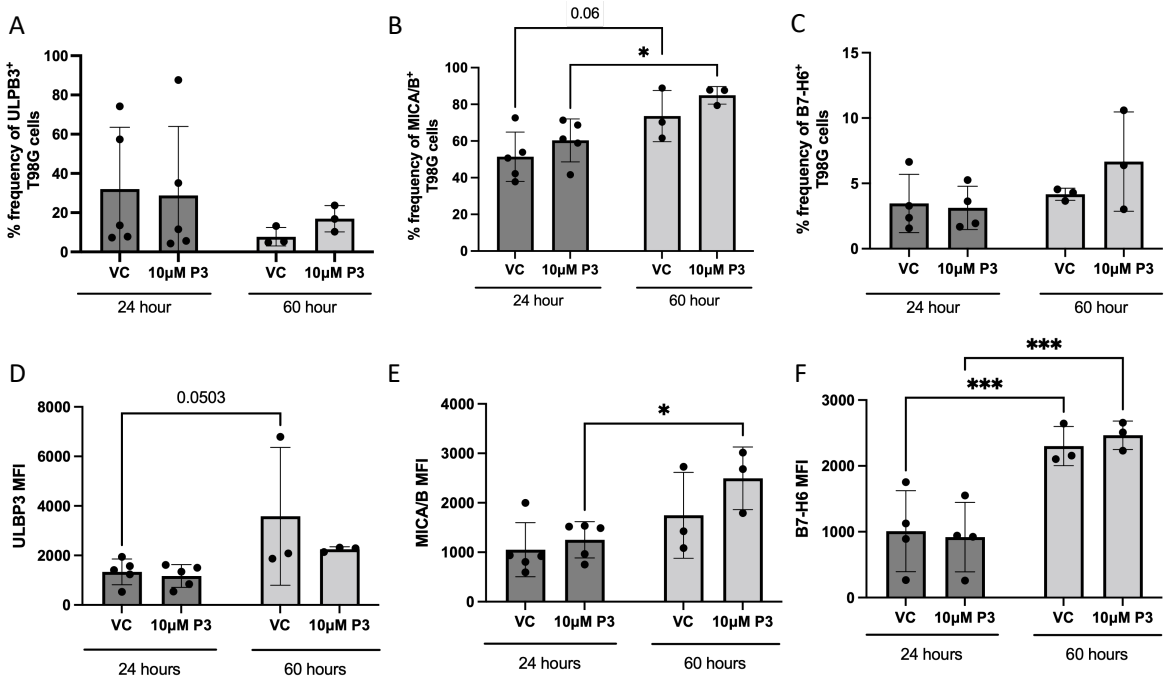

Figure 25: Both P3 and the vehicle control increased the expression of NKR activating ligands MICA/B and B7-H6 when T98G cells were analysed at 60 hours. Data was collected at a 24 (n=5) and 60 hour time point (n=3)**.** Bar chart showing the % of **(A)** ULBP3$^+$ **(B)** MICA/B$^+$ **(C)** B7-H6$^+$ T98G cells. Bar chart showing the MFI values for **(D)** ULBP3 **(E)** MICA/B **(F)** B7-H6 on T98G cells.*p<0.05, ***p<0.001 by one-way ANOVA. (Experiment carried out in conjunction with MSc in Translational Oncology student Jennifer Moran).

3.3.6 P3 did not significantly change the expression of NKR ligands PVR, PVRL2 and 4-1BBL when T98G cells were analysed at 60 hours.

There was no change in the % frequency of T98G cells that were positive for PVR, PVRL2 and 4-1BBL when treated with 10μM P3 for 24 hours and analysed after 60 hours. (24 hours [n=4]; 60 hours [n=3])*(Figure 26A,B,C)*. No significant changes were observed in the MFI values for PVR, PVRL2 and 4-1BBL *(Figure 26D,E,F)*.

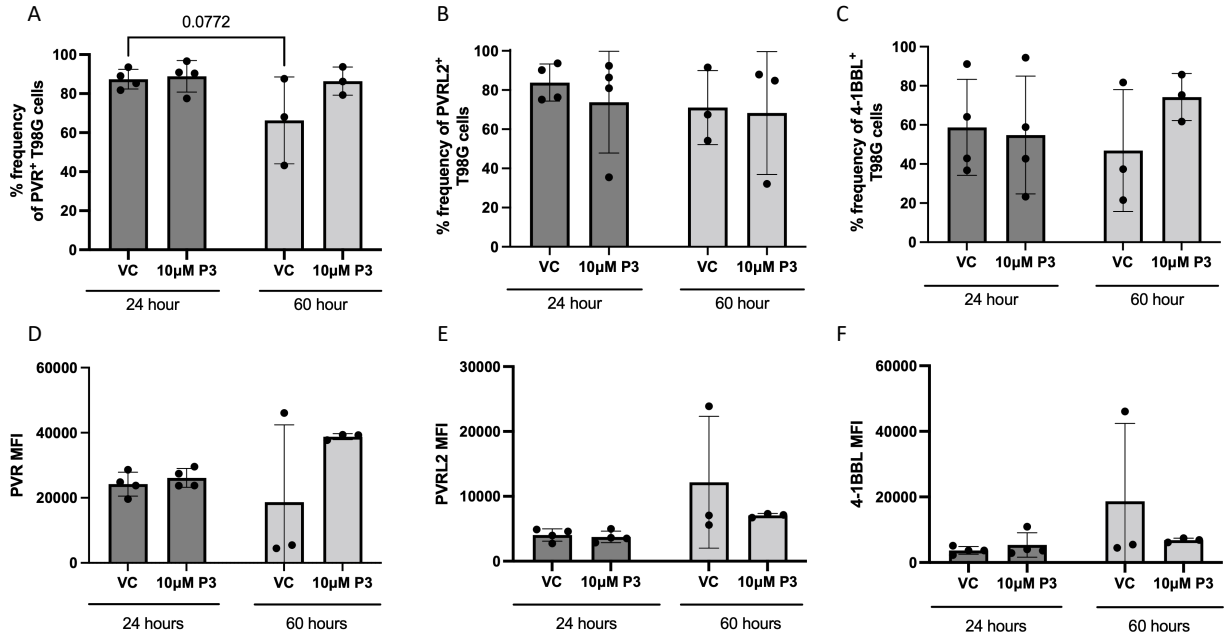

Figure 26*:* P3 did not significantly alter the expression of NKR ligands PVR, PVRL2 and 4-1BBL when T98G cells were analysed at 60 hours. Data was collected at a 24 hours (n=4) and 60 hour time point (n=3). Bar chart showing the % of **(A)** PVR^+ **(B)** $PVRL2^+$ **(C)** 4-1BBL^+ T98G cells. Bar chart showing the MFI values for **(D)** PVR **(E)** PVRL2 **(F)** 4-1BBL on T98G cells.*p<0.05 by one-way ANOVA. (Experiment carried out in conjunction with by MSc in Translational Oncology student Jennifer Moran).

3.3.7 P3 increased the expression of the death receptor TRAIL-R2, the immune checkpoint receptor ligand PD-L1 and the inhibitory ligand HLA-E when T98G cells were analysed at 60 hours.

There was in increase in the % frequency of T98G cells that are positive for TRAIL-R2 when treated with 10 μM P3 for 24 hour and analysed at a 60 hour time point (10 μM P3 [24 hours] vs. 10μM P3 [60 hours]; 95.525% vs. 97.73%; p=0.047)*(Figure 27A).* The frequency % of Fas^+ T98G cells was not altered with P3 treatment between the 24 hour and 60 hour time points *(Figure 27B).* The frequency % of T98G cells that were positive for the immune checkpoint ligand PD-L1 (10 μM P3 [24 hours] vs. 10 μM P3 [60 hours]; 61.94% vs. 92.66%; p=0.0113) *(Figure 27C)* and inhibitory ligand HLA-E (10μM P3 [24 hours] vs. 10μM P3 [60 hours]; 39.55% vs. 75.83%; p=0.0074)*(Figure 27D)* showed an increase subsequent to a 24 hour P3 treatment and analysed by flow cytometry 36 hours later. The frequency % of HLA-E^+ T98G cells (VC [24 hours] vs. VC [60 hours]; 30.825% vs. 61.43%; p=0.0192) and PD-$L1^+$ T98G cells (VC [24 hours] vs. VC [60 hours]; 76.8% vs. 63.36%; p=0.0436) showed to be raised by the vehicle control *(Figure 27).*There was an increase in the MFI of TRAIL-R2 which had been

treated with P3 at 60 hours compared to 24 hours (10 μM P3 [24 hours] vs. 10 μM P3 [60 hours]; 3375.5 vs. 5994.67; p=0.007) *(Figure 27E)*. The MFI of Fas and PD-L1 showed no significant changes subsequent to treatment with P3 at 24 or 60 hour time points. At the 60 hour timepoint the MFI of HLA-E showed an increase following treatment with P3 (10 μM P3 [24 hours] vs. 10 μM P3 [60 hours]; 3375.5 vs. 7321.67; p=0.0019)*(Figure 27H)*. The vehicle control for P3 also induced an increase in MFI of HLA-E (VC [24 hours] vs. VC [60 hours]; 2757.75 vs. 5994.67; p=0.007) *(Figure 27H)*.

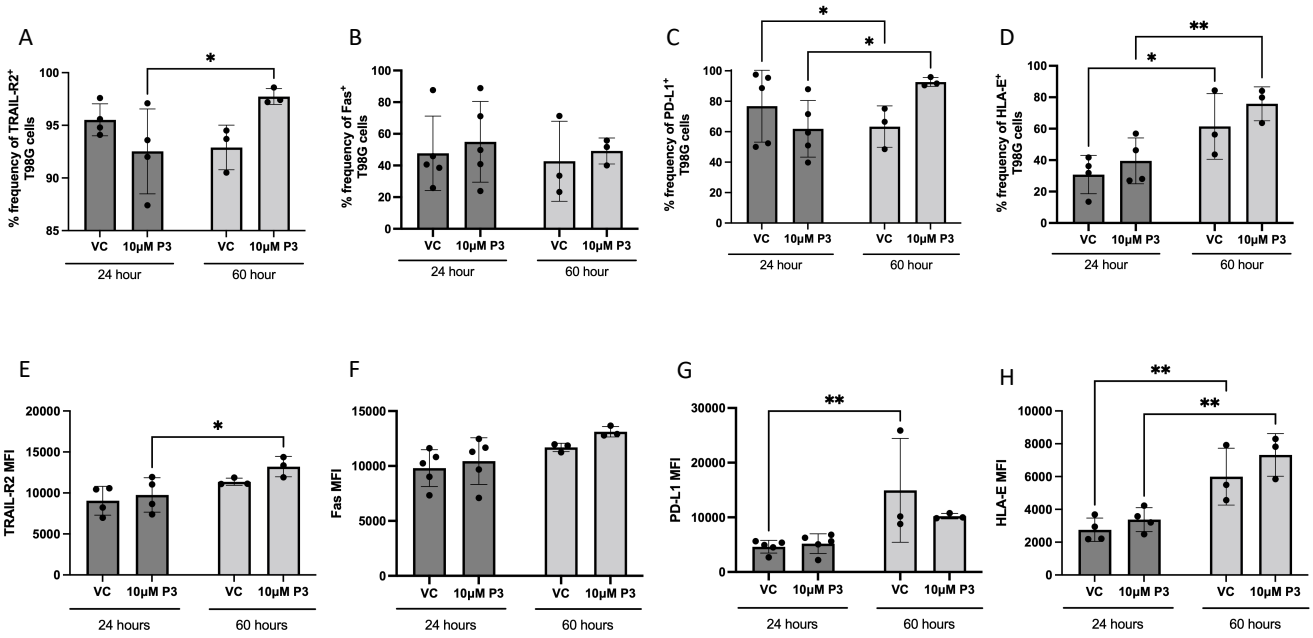

Figure 27: P3 increased the expression of the death receptor TRAIL-R2, the immune checkpoint receptor ligand PD-L1 and the inhibitory ligand HLA-E when T98G cells were analysed at 60 hours. Data was collected at a 24 hour (TRAIL-R2, HLA-E [n=4]; Fas, PD-L1 [n=5]) and 60 hour time point (n=3). Bar chart showing the % of **(A)** TRAIL-R2$^+$ **(B)** Fas$^+$ **(C)** PD-L1$^+$ **(D)** HLA-E$^+$ T98G cells. Bar chart showing the MFI values for **(E)** TRAIL-R2 **(F)** Fas **(G)** PD-L1 **(H)** HLA-E on T98G cells.*p<0.05, **p<0.01 by one-way ANOVA. (Experiment carried out in conjunction with MSc Translational Oncology student Jennifer Moran).

3.4 Elucidating the effects of P3, Q8 on NKR ligand shedding by T98G cells

3.4.1 P3 does not significantly alter NKR ligand B7-H6 shedding by T98G cells

T98G cells were treated with 10 μM P3 for 72 hours and the supernatants were collected and screened by ELISA to determine the effect of P3 on B7-H6 shedding into the GBM tumour microenvironment. Interestingly, P3-treated T98G cell supernatants displayed a substantial but

not significant decrease of 15.7% in B7-H6 levels at the 72 hour time point compared to the untreated cells, however it was not statistically significant (Untreated T98G cells vs 10 μM P3 (39.12 pg/ml vs 23.41 pg/ml, p=0.065)*(Figure 28).* There is a significant increase between the DMSO vehicle control and 10 μM of P3 (VC vs 10 μM P3 (6.25 pg/ml vs 23.4 pg/ml, p=0.0473)*(Figure 28).* There is a significant decrease between untreated and vehicle control suggesting that the vehicle significantly reduced B7-H6 shedding, warranting further investigation (Untreated vs VC (39.12 pg/ml vs 6.25 pg/ml, p=0.0024)*(Figure 28).*

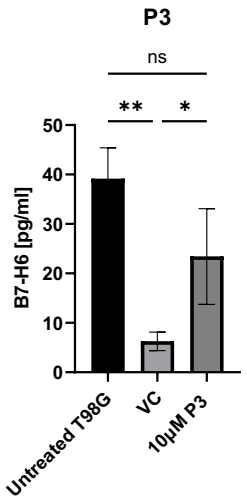

Figure 28: Elucidating the effects of P3 on B7-H6 shedding by T98G cells. Bar chart showing concentration of B7-H6 in (pg/ml) in the supernatants of untreated T98G cells, vehicle control-treated T98G cells (VC, DMSO) and 10 μM P3-treated T98G cells. One-way ANOVA, n=3, ns not significant, p*<0.05, p**<0.01.

3.4.2 Q8 does not significantly alter B7-H6 shedding by T98G cells

T98G cells were treated with 10 μM Q8 for 72 hours and the supernatants were collected and screened by ELISA to determine the effect of Q8 on B7-H6 shedding into the GBM tumour microenvironment. Q8-treated T98G cell supernatants displayed a decrease of 9% in B7-H6 levels at the 72 hour time point compared to the untreated cells, however it was not statistically significant (Untreated T98G cells vs 10 μM Q8 (39.131 pg/ml vs 30.128 pg/ml, p=0.17)*(Figure 29).* There is a significant increase between the DMSO vehicle control and 10 μM of Q8 (VC vs 10 μM P3 (6.25 pg/ml vs 30.128 pg/ml, p=0.0035). There is a significant decrease between untreated and vehicle control suggesting that the vehicle significantly reduced B7-H6 shedding, warranting further investigation (Untreated vs VC (39.131 pg/ml vs 6.25 pg/ml, p=0.0006)*(Figure 29).*

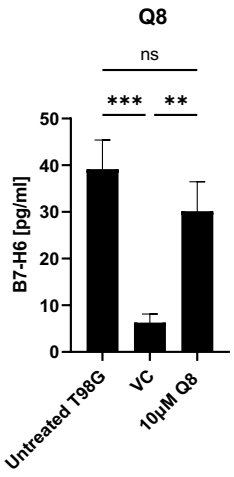

Figure 29: Elucidating the effects of Q8 on B7-H6 shedding by T98G cells . Bar chart showing concentration of B7-H6 in (pg/ml) in the supernatants of untreated T98G cells, vehicle control-treated T98G cells (VC, DMSO) and 10 μM Q8-treated T98G cells.. One-way ANOVA, n=3, p**<0.01, p***<0.001

3.4.3 ULBP3 shedding by GBM cells was below the lowest level of detection

T98G cells were treated with 10 μM P3 or Q8 for 72 hours and the supernatants were collected and screened by ELISA to determine the effect of Q8 or P3 on ULBP3 shedding into the GBM tumour microenvironment (n=3). The ULBP3 levels at the 72 hour time point were too low to detect using an ELISA as they fell below the lowest limit of detection (LLOD) of 125 pg/ml *(Figure 30)*(Table 4). Future studies may warrant more sensitive ELISAs or concentration of supernatants to detect changes in ULBP shedding by T98G cells.

A)

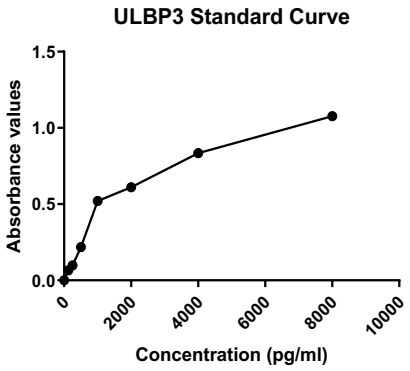

B)

ULBP3 Concentration pg/ml			
Untreated cells	**Vehicle control (DMSO)**	**Q8**	**P3**
-0.028	-0.048	-0.046	-0.055

Figure 30: A) Line graph showing the standard curve of absorbance values vs concentration of ULBP3 shedding by GBM T98G cells. The standard curve ranged from 125 pg/ml – 8000 pg/ml with concentrations in all samples being below the lowest level of detection, 125 pg/ml. **B)** Table 4 showing negative values for ULBP3 concentrations shown in pg/ml in untreated, DMSO-treated, Q8-treated and P3-treated T98G cell supernatants showing values could not be extrapolated from the standard curve because they were below the lowest limit of detection.

3.4.4 MICA/B shedding by GBM cells was below the lowest level of detection

T98G cells were treated with 10 μM P3 or Q8 for 72 hours and the supernatants were collected and screened by ELISA to determine the effect of Q8 or P3 on MICA/B shedding into the GBM tumour microenvironment (n=3). The MICA/B levels at the 72 hour time point were too low to detect by ELISA as the lowest limit of detection (LLOD) was 39.06 pg/ml *(Figure 31)*. Future studies may warrant more sensitive ELISAs or concentration of supernatants to detect changes in MICA/B shedding by T98G cells.

A)

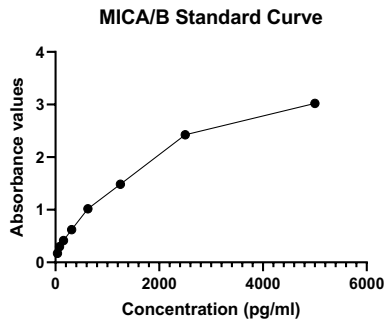

B)

MICA/B Concentration pg/ml				
Untreated cells	**Vehicle control (DMSO)**	**Q8**	**P3 24 hours**	**P3 60 hours**
-480.444	-568.222	-540.444	-533.778	-502.111

Figure 31: A) Line graph showing the standard curve of absorbance values vs concentration of MICA/B shedding by GBM T98G cells. The standard curve ranged from 39.06 pg/ml – 6000 pg/ml with our sample being below the lowest level of detection, 39.06 pg/ml. **B)** Table 5 showing MICA/B concentration pg/ml, samples were below the lowest limit of detection.

3.5 Elucidating the effects of P3 on the GBM inflammatory secretome.

3.5.1 Both Q8 and P3 reduce pro-inflammatory cytokine IL-6 secretion by T98G cells

T98G cells were treated with 10 μM P3 or Q8 for 72 hours and the supernatants were collected and cryopreserved. These supernatants were screened by ELISA to determine the effect of P3/Q8 on IL-6 secretion by T98G cells. P3-treated T98G cells displayed a decrease in IL-6 concentration at the 72 hour time point compared to the untreated cells, however it was close but not statistically significant and may need to be powered as there is some variability (untreated vs 10 μM P3 (2395.2 pg/ml vs 1831.87 pg/ml p=0.0824)*(Figure 32A)*. There was a significant increase between the vehicle control and 10 μM of P3 (VC vs 10 μM P3 (178.5 pg/ml vs 1831.87 pg/ml p <0.0001). There was a significant decrease between untreated and VC (2395.2 pg/ml vs 178.5 pg/ml p <0.0001). Q8-treated T98G cell supernatants displayed a significant decrease in IL-6 concentration at the 72 hour time point compared to the untreated cells (Untreated vs 10 μM Q8 (2395.2 pg/ml vs 1599.87 pg/ml p=0.0136) *(Figure 32B)*. There was a significant increase between the vehicle control and 10 μM of Q8 (VC vs 10 μM Q8 (178.5 pg/ml vs 1599.87 pg/ml p= <0.0001). There was a significant decrease between untreated and VC suggesting that the vehicle significantly reduced IL-6 secretion, warranting further investigation into whether 0.1% DMSO was toxic to the cells or if the concentration added was inaccurate (2395.2 pg/ml vs 178.5 pg/ml p= <0.0001).

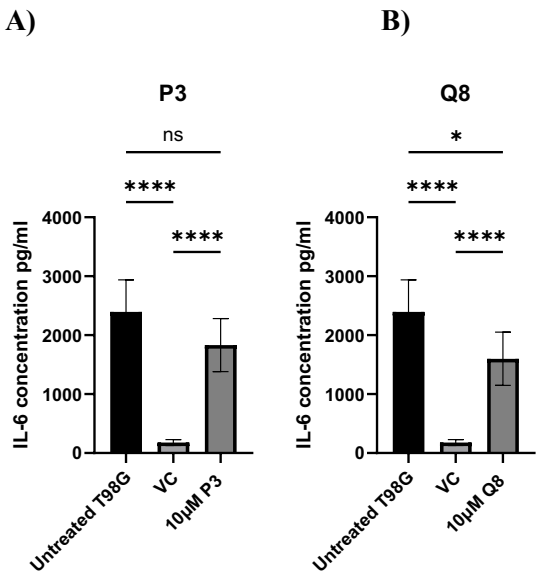

Figure 32: Elucidating the effects of P3 or Q8 on IL-6 shedding by T98G cells. Bar chart showing concentration of IL-6 in (pg/ml) in the supernatants of untreated T98G cells, vehicle control-treated T98G cells (VC, DMSO) and 10 μM **A)** P3-treated or **B**) Q8-treated T98G cells. One-way ANOVA, ns not significant, p*<0.05, p****<0.0001 n=6

3.5.2 IL-17 concentrations in T98G cell supernatants were too low to detect

T98G cells were treated with 10 μM Q8 or P3 for 72 hours and the supernatants were collected. The supernatants were subject to an ELISA to determine the effect of Q8/P3 on IL-17 concentration in the GBM tumour microenvironment (n=3). The IL-17 levels at the 72 hour time point were too low to detect by ELISA *(Figure 33)*.

A)

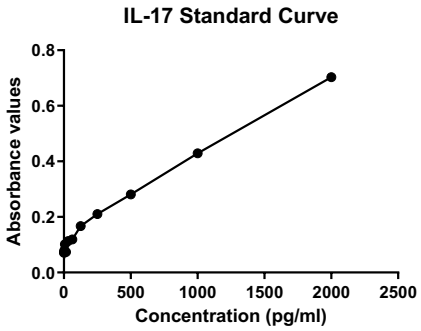

B)

IL-17 Concentration pg/ml			
Untreated cells	**Vehicle control (DMSO)**	**Q8**	**P3**
-94.333	-71	-91	-77.666
-154.333	-141	-141	-137.667

Figure 33: A) Line graph showing the standard curve of absorbance values vs concentration of IL-17 shedding (pg/ml) by GBM T98G cells. The standard curve ranges from 0.12 pg/ml – 2500 pg/ml with our samples being below the lowest level of detection, 0.12 pg/ml. **B)** Table 6 showing IL-17 concentration in pg/ml in untreated and treated samples were below the limit of detection and could not be extrapolated from the curve.

3.5.3 Both Q8 and P3 reduces secretion of the pleiotropic cytokine TGF-ß by T98G cells

T98G cells were treated with 10 µM P3 or Q8 for 72 hours and the supernatants were collected. These supernatants were screened by ELISA to determine the effect of P3 and Q8 on TGF-ß secretion by T98G cells. P3-treated T98G cells displayed a decrease in TGF-ß concentration after 24 hours compared to the untreated cells, however this was not significant (untreated vs 10 µM P3 24 hour, 719 pg/ml vs 258. 16 pg/ml p=0.102)*(Figure 34A)*. There was a significance decrease when P3-treated T98G cell supernatants were compared to untreated cells after 60 hours (untreated vs 10 µM P3 60 hour, 719 pg/ml vs 141.5 pg/ml p=0.039). There was no significance in the decrease between the vehicle control and 10 µM of P3 24 hour or 10 µM of P3 60 hour (VC vs 10 µM P3 24 hour, 106.5 pg/ml vs 258.16 pg/ml p =0.99), (VC vs 10 µM P3 60 hour, 106.5 pg/ml vs 258.16 pg/ml p=0.973). Q8-treated T98G cell supernatants displayed a decrease in TGF-ß concentration at the 72 hour time point compared to the untreated cells this was not significant (untreated vs 10 µM Q8, 719 pg/ml vs 477.3 pg/ml p= 0.33) *(Figure 34B)*. However, there was a significant decrease when Q8-treated T98G cell supernatants were compared to VC (VC vs 10 µM Q8, 106.5 pg/ml vs 477.33 pg/ml p=0.0487). There was also a significant decrease between untreated cells and the vehicle control suggesting again that 0.1% DMSO altered IL-6 production or that this amount was not added (untreated vs VC, 719 pg/ml vs 106.5 pg/ml p=0.0053).

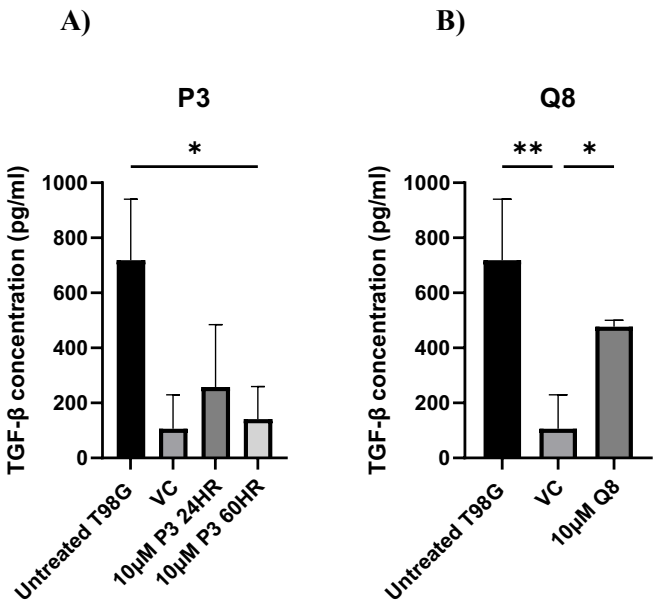

Figure 34: Elucidating the effects of P3 or Q8 on TGF-ß shedding by T98G cells Bar chart showing concentration of TGF-ß in (pg/ml) in the supernatants of untreated T98G cells, vehicle control-treated T98G cells (VC, DMSO) and 10 µM **A)** P3-treated or **B)** Q8-treated T98G cells. One-way ANOVA, ns not significant, p**<0.01, p*<0.05, n=3

3.5.4 Both Q8 and P3 significantly reduces cytokine TIMP-1 in GBM secretome

T98G cells were treated with 10 µM P3 for 24 or 60 hours or with Q8 for 72 hours and the supernatants were collected. These supernatants were screened by ELISA to determine the effect of P3/Q8 on TIMP-1 secretion by T98G cells. 24 hour and 60 hour P3-treated T98G cell supernatants displayed a significant decrease in TIMP-1 concentration at the 60 hour time point compared to the untreated cells, (untreated vs 10 µM P3 24 hours (2137.33 pg/ml vs 1334.83 pg/ml p=0.0001), (untreated vs 10 µM P3 60 hours 2137.33 pg/ml vs 444.41 pg/ml p<0.0001)*(Figure 35A).* There was a significant increase between the vehicle control and 10 µM of P3 24 hours (VC vs 10 µM P3 24 hours (717.16 pg/ml vs 1334.83 pg/ml p=0.0007). There was a significant decrease between untreated and VC (2137.3 pg/ml vs 717.16 pg/ml p <0.0001). There was a significant decrease when 10µM P3 24 hours was compared to 10µM P3 60 hours suggesting that 10µM P3-treated supernatants for 60 hours significantly reduced TIMP-1 shedding, warranting further investigation (10 µM P3 24 hours vs 10µM P3 60 hours (1334.83 pg/ml vs 444.41 pg/ml <0.0001). Q8-treated T98G cell supernatants displayed a significant increase in TIMP-1 concentration at the 72 hour time point compared to the VC (VC vs 10 µM Q8, 717.16 pg/ml vs 2110.67 pg/ml p<0.0001)*(Figure 35B).* There was a

significant decrease between untreated and VC suggesting that the vehicle significantly reduced TIMP-1 shedding, again warranting further investigation into the 0.1% DMSO-treated cells (untreated vs VC, 2137.33 pg/ml vs 717.16 pg/ml p= <0.0001).

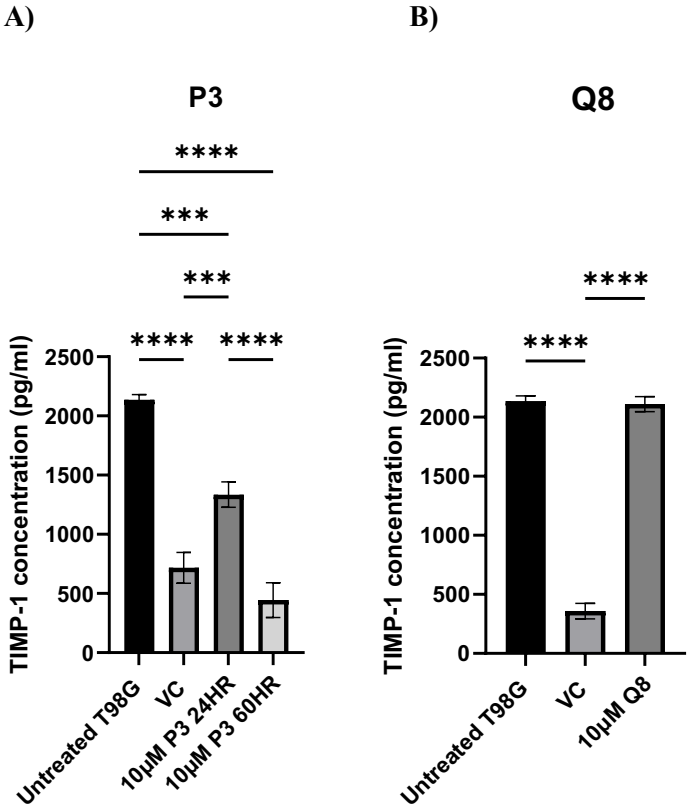

Figure 35: Elucidating the effects of P3 or Q8 on TIMP-1 shedding by T98G cells Bar chart showing concentration of TIMP-1 in (pg/ml) in the supernatants of untreated T98G cells, vehicle control-treated T98G cells (VC, DMSO) and 10 μM **A)** P3-treated or **B)** Q8-treated T98G cells. One-way ANOVA, ns not significant, p****<0.0001, p***<0.001. n=3

3.6 Elucidating the effects of P3 or Q8 on the chemotactic cues in the T98G cell secretome.

3.6.1 Both P3 and Q8 reduce T98G cell-mediated recruitment of NK cells

Since P3 or Q8 showed potential to alter the GBM secretome, the effects of these drugs on the chemotactic pull of T98G cells was assessed. This was achieved by measuring NK cell, T cell and total lymphocyte migration towards supernatant from T98G cells which had been previously treated with P3. NK cell migration towards supernatants from T98G cells treated with 10 µM P3 for 72 hours was slightly but not significantly reduced, compared to that towards supernatants from untreated T98G cells (Untreated vs 10µM P3, 1.85 vs 1.35, p=0.21) *(Figure 36 B)*.The chemotaxis of NK cells toward supernatants from T98G cells previously treated with 10 µM Q8 for 72 hours showed a significant reduction suggesting that Q8 might have negative ramifications for NK cell infiltration of GBM tumours (Untreated vs 10 µM Q8, 1.85 vs 0.92, p=0.045) *(Figure 36 B)*.

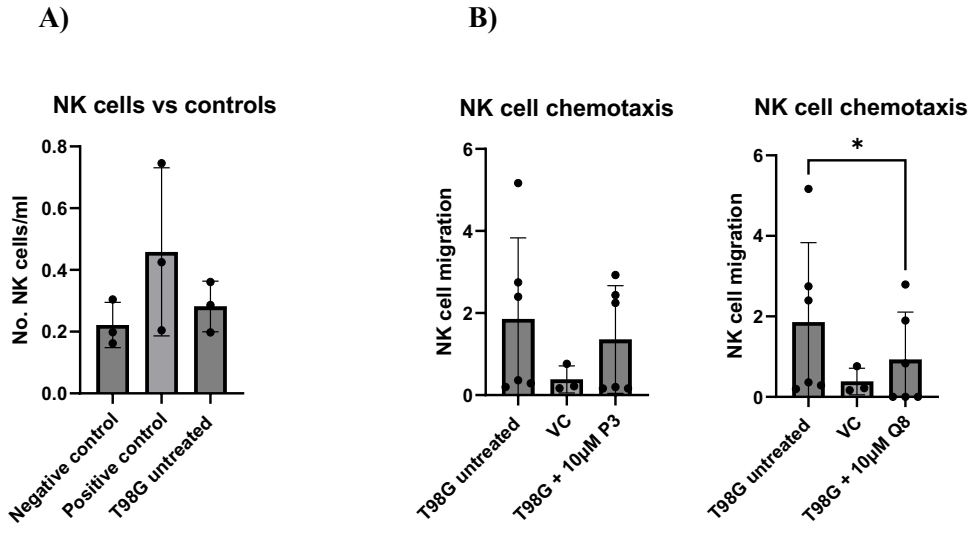

Figure 36: NK Cell chemotaxis, A) NK cell migration from untreated NK cell chemotaxis towards negative control (cDMEM) or positive control (DMEM + 20% FBS), n=3 **B)** NK cell migration from untreated NK cell chemotaxis treated toward GBM T98G cells that were treated with 10 µM of P3/Q8 for 72 hours. Paired T-test n=6, *p < 0.05.

3.6.2 Both P3 and Q8 reduce T98G cell-mediated recruitment of lymphocytes

Lymphocyte migration towards supernatants from T98G cells treated with 10 µM P3 for 72 hours was slightly but not significantly reduced, compared to that towards supernatants from untreated T98G cells (Untreated vs 10µM P3, 0.705 vs 0.46, p=0.35) *(Figure 37 B)*.The chemotaxis of lymphocytes toward supernatants from T98G cells previously treated with 10 µM Q8 for 72 hours showed a reduction, however this was not significant suggesting that Q8 might also have negative consequences for lymphocyte infiltration of GBM tumours (Untreated vs 10 µM Q8, 0.705 vs 0.05, p=0.06) *(Figure 37 B)*.

A) **B)**

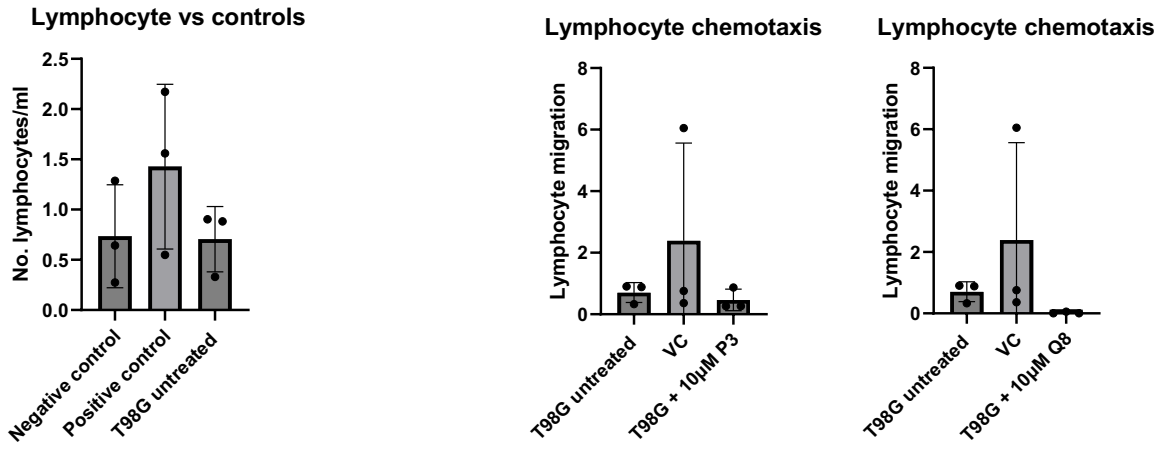

Figure 37: Lymphocyte chemotaxis, A) Lymphocyte migration from untreated lymphocyte cell chemotaxis towards negative control (cDMEM) or positive control (DMEM + 20% FBS), n=3 **B)** Lymphocyte cell migration from untreated lymphocyte cell chemotaxis treated toward GBM T98G cells, treated with 10 µM of P3/Q8 for 72hrs, n=6

3.6.3 Both P3 and Q8 reduce T98G cell-mediated recruitment of T cells

T cell migration towards supernatants from T98G cells treated with 10 µM P3 for 72 hours was slightly but not significantly reduced, compared to that towards supernatants from untreated T98G cells (Untreated vs 10 µM P3, 1.70 vs 1.55, p=0.87)*(Figure 38B)*. The chemotaxis of T cells toward supernatants from T98G cells previously treated with 10 µM Q8 for 72 hours showed a reduction, however this was not significant suggesting that Q8 may have negative effects for lymphocyte infiltration of GBM tumours (Untreated vs 10 µM Q8, 1.70 vs 0.22, p=0.15)*(Figure 38B)*.

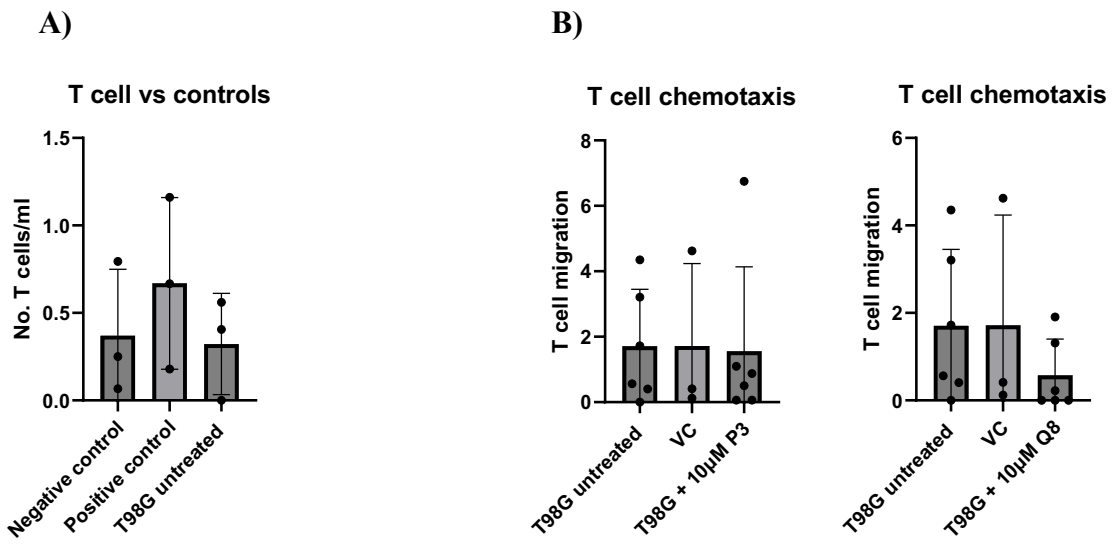

Figure 38: T cell chemotaxis, A) T cell migration from untreated NK cell chemotaxis towards negative control (cDMEM) or positive control (DMEM + 20% FBS), n=3 **B)** T cell migration from untreated T cell chemotaxis treated toward GBM T98G cells that were treated with 10μM of P3/Q8 for 72hrs, n=6

3.7 Elucidating the effects of P3 on NK cell phenotype and function

3.7.1 P3 is toxic at high doses to healthy NK cells.

Blood-derived NK cells were treated with 1, 10 and 100 μM P3 for 24 hours and their viability (ZOMBIE dye) was assessed by flow cytometry. Zombie dye staining showed that P3 is toxic to NK cells at a high dose of 100 μM *(Figure 39)*.

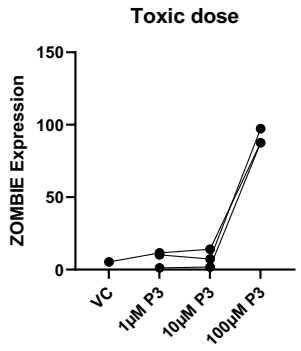

Figure 39: P3 is toxic at high doses to healthy NK cells. Line Graph showing Zombie dye staining in VC, 1,10 and 100 μM P3-treated NK cells. The of viability of NK cells treated 1, 10 and 100 μM of P3 was assessed by zombie dye to determine the toxic dose of P3.

3.7.2 P3 does not elicit immunomodulatory effects on healthy NK cells

Blood-derived NK cells were treated with 1 μM and 10 μM P3 for 24 hours and their surface expression of NKG2D, NKG2A, NKP30, NKP46, CD69, FasL, TRAIL, PD1, TIGIT, and CD62L was assessed by flow cytometry. There was no significance found between the controls and P3-treated cells. The frequencies of NK cells expressing activation receptors CD69, NKP30, NKP46 and NKG2D was not significantly altered by P3 with some variation amongst the human donors and a requirement for more statistical power to account for this *(Figure 40 A)*. Similarly, percentage frequencies of NK cells expressing inhibitory receptors NKG2A, PD-1 and TIGIT and death receptor ligands TRAIL and Fas ligand were not significantly altered by P3 with variation observed between human donors and a need for more statistical power to account for this *(Figure 40 B,C)*.

A) Activating receptors

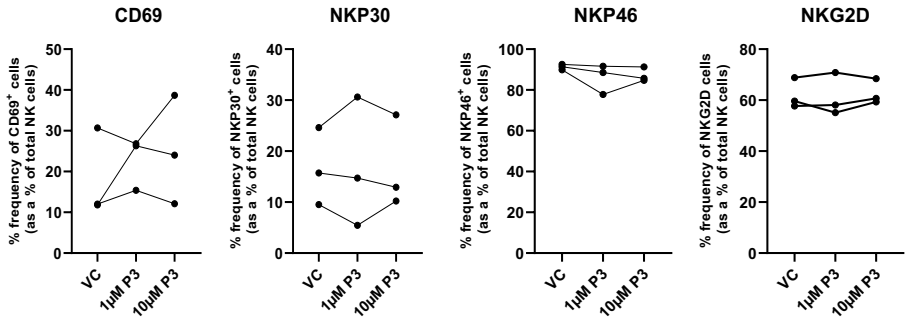

B) Inhibitory receptors

C) Death receptors

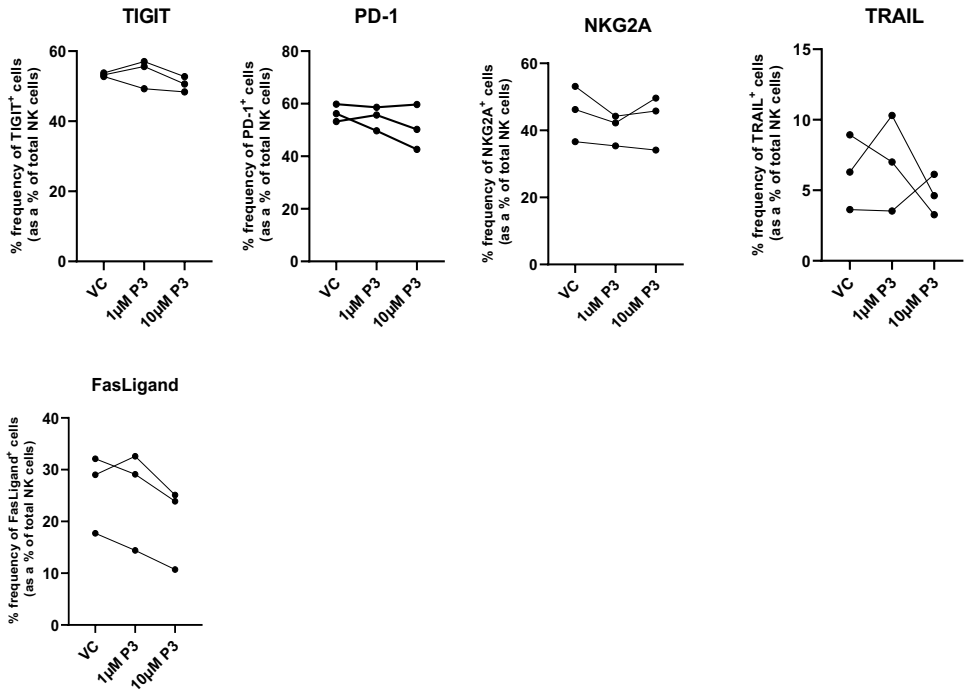

Figure 40: Assessing the immunomodulatory effects of P3 on healthy NK cells. Line graphs showing NK cell expression of **(A)** activation/cytotoxicity receptors (NKG2D, NKP30, NKP46, CD69), **(B)** inhibitory receptors (NKG2A, TIGIT, PD-1) and **(C)** death receptors (TRAIL, FasL) following treatment with vehicle control (DMSO) or 1 and 10 μM of P3.

3.8 Elucidating the effects of P3 on GBM-mediated modulation of NK cell phenotype and function

3.8.1 P3 attenuates T98G cell supernatant-mediated downregulation of NK cell activation receptors NKG2D and CD69, NK cell cytotoxicity receptor NKP30.

Blood-derived NK cells were cultured in T98G cell supernatants +/- 10 μM P3 for 24 hours. NK cell surface expression of NKG2D, NKG2A, NKP30, NKP46, CD69, FasL, TRAIL, PD1, TIGIT, and CD62L was assessed by flow cytometry. The frequencies of NK cells expressing activation receptors CD69, NKP30 and NKG2D were significantly lower following culture in T98G cell supernatants and this was overcome by treatment with P3 *(Figure 41A)*.

A) Activation receptors

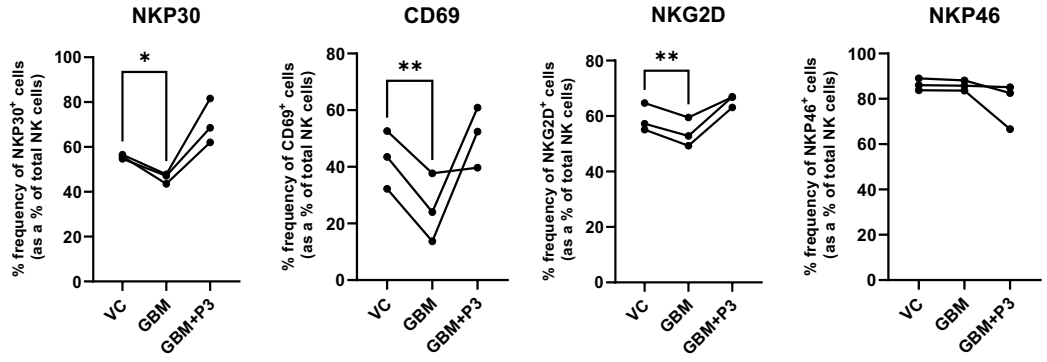

B) Inhibitory receptors

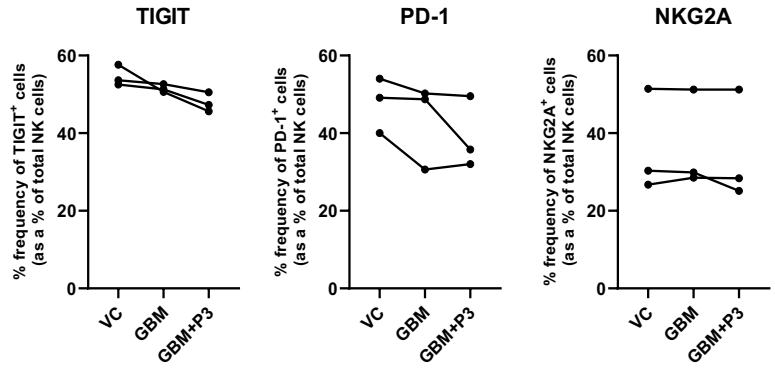

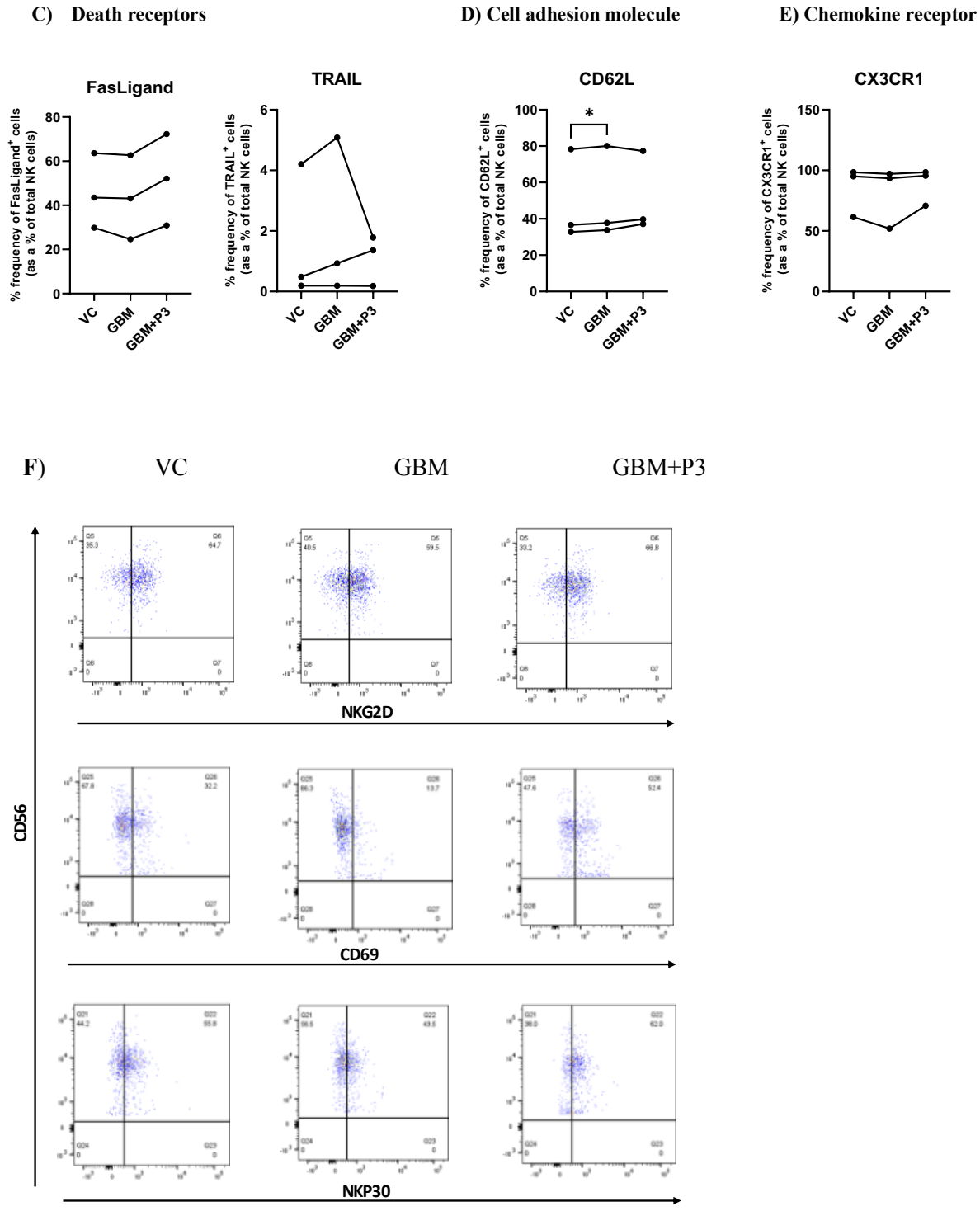

Figure 41: P3 alleviates the negative effects of T98G cell supernatants on NK cell activation phenotype. Line graphs showing NK cell expression of **(A)** activation/cytotoxicity receptors (NKG2D, NKP30, NKP46, CD69), **(B)** inhibitory receptors (NKG2A, TIGIT, PD-1), **(C)** death receptors (TRAIL, FasL), **(D)** Cell adhesion molecule (CD62L) and **(E)** Chemokine receptor (CX3CR1) following treatment with vehicle control (DMSO) or 10 µM of P3. **F)** Representative flow cytometry dot plots of NKG2D, CD69, and NKP30 expression by NK cells following culture in media alone or T98G cell supernatant for 24 hours +/- 10 µM P3. Paired T-test *p<0.05, **p<0.01. n=3

3.8.2 P3 did not significantly alter the expression of activation and maturation markers by NK cells co-cultured with T98G cells.

The previous sections examined the direct effect of P3 on NK cell phenotype and elucidated whether P3 could attenuate NK cell modulation mediated by soluble factors in the T98G cell supernatant. The next steps were taken to investigate whether co-culture with T98G cells impact NK cell phenotype and function and if this was altered by P3. To achieve this, NK cells were co-cultured with untreated T98G cells or P3-treated T98G cells. The expression of different NK cell markers were assessed to determine if treatment with 10 μM of P3 would alter the NK cell phenotype in GBM. CD69, CD57 and CD27 were assessed on the surface of NK cells after a 24 hour treatment with P3 and co-culture with T98G cells. NK cells cultured with untreated T98G cells and NK cells cultured with P3-treated T98G cells showed no significant alteration in the frequency of $CD69^+$ NK cells (n=6)*(Figure 42A).* The frequency of $CD57^+$ NK cells and $CD27^+$ NK cells when cultured with untreated T98G cells or cultured with P3-treated T98G cells were not altered *(Figure 42 B,C).* The MFI of CD69, CD57 and CD27 subsequent to co-culture with P3-treated T98G cells showed no significant changes *(Figure 42 D,E,F).*

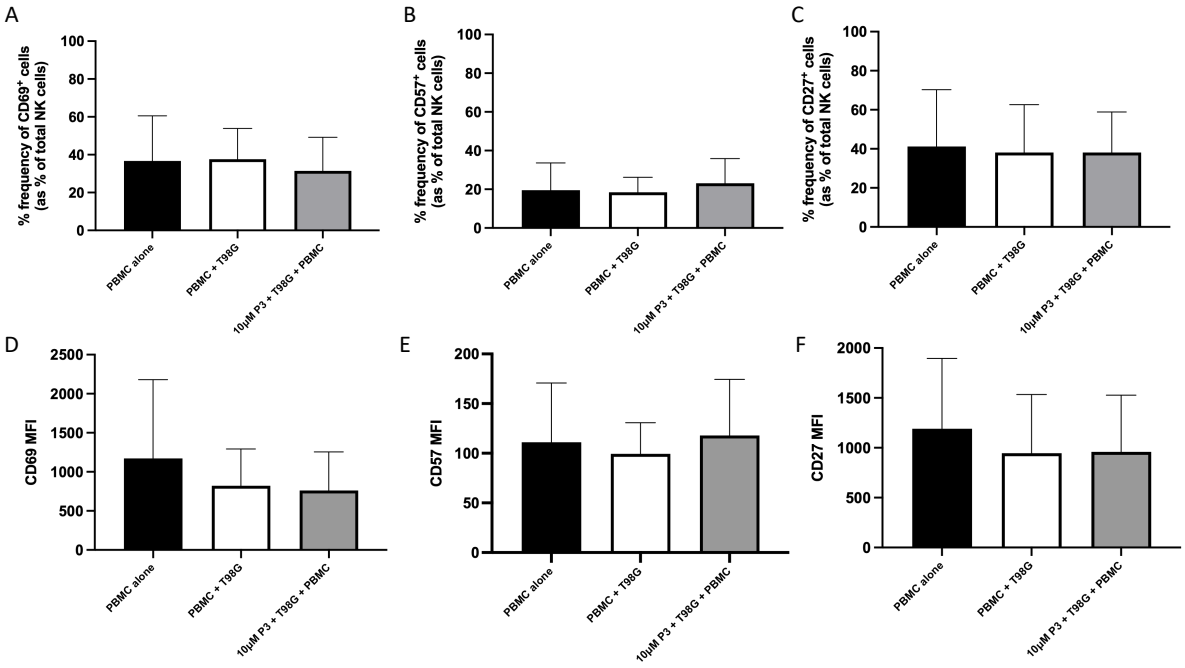

Figure 42: P3 did not significantly alter the expression of activation and maturation markers by NK cells co-cultured with T98G cells. Bar chart showing the frequencies of **(A)** $CD69^+$ **(B)** $CD57^+$ **(C)** $CD27^+$ NK cells as a percentage of total NK cells. Bar chart showing the MFI values for **(D)** CD69 **(E)** CD57 **(F)** CD27 on NK cells (n=6). *$p<0.05$ by one-way ANOVA with post-hoc Dunn's test. (Experiment carried out in conjunction with MSc Translational Oncology student Jennifer Moran).

3.8.3 Co-culture with P3-treated T98G cells significantly reduced the expression of activating receptors NKp30 and NKG2D on NK cells.

To determine the effects of a 24 hour P3 treatment on NK cell function in GBM, NK cells were co-cultured with P3-treated and untreated T98G cells and activated with PMA and Ionomycin. $NKp46^+$ NK cells that had been previously co-cultured with P3-treated T98G cells showed no significant changes (n=6)*(Figure 43A)*. Similarly, $NKp30^+$ NK cells were not significantly altered by co-culture with untreated or P3 treated T98G cells *(Figure 43B)*. However, the frequency % of NK cells positive for NKG2D was decreased by co-culture with P3-treated T98G cells (PBMC alone vs. 10 μM P3+T98G+PBMC; 76.13% vs. 53.11%; p=0.013*)(Figure 43C)*. The MFI of NKp46 following co-culture with untreated and P3-treated T98G cells showed no changes that were significant *(Figure 43D)*. Conversely, the MFI of both NKp30 (PBMC alone vs. 10 μM P3+T98G+PBMC; 1000.33 vs. 405.833; p=0.0102) and NKG2D (PBMC alone vs. 10 μM P3+T98G+PBMC; 989.5 vs. 462.83; p=0.0052) showed significant reduction following co-culture with P3-treated T98G cells *(Figure 43 E,F)*.

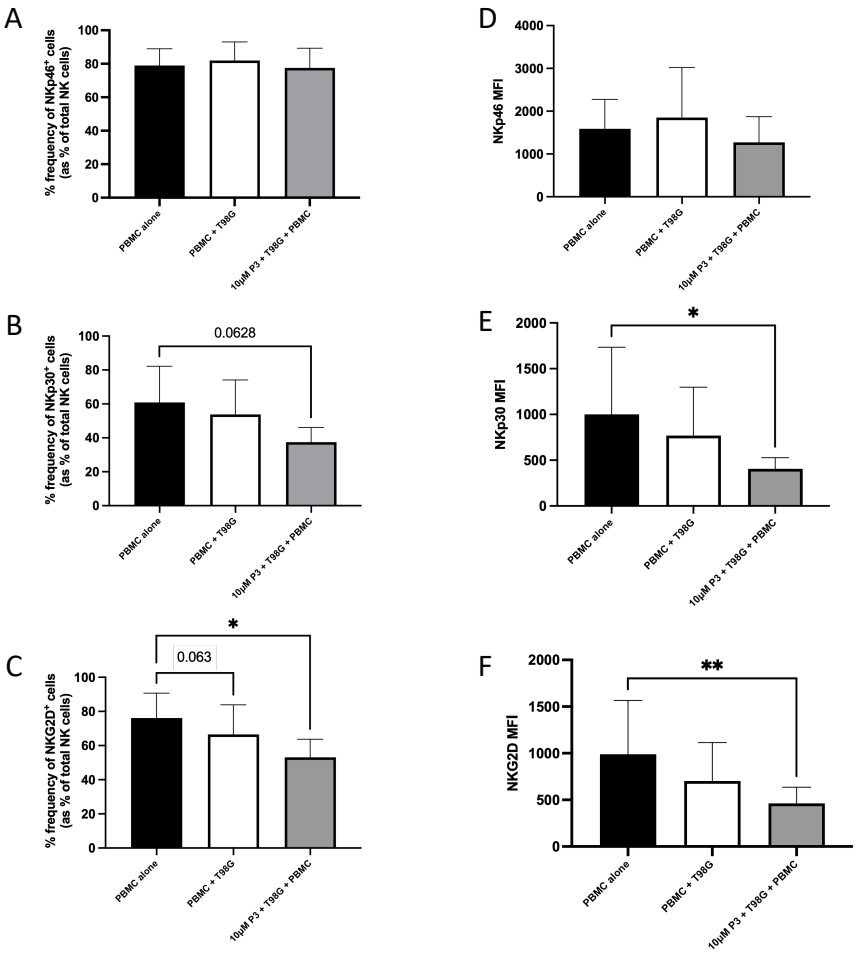

Figure 43: Co-culture with P3-treated T98G cells significantly reduced the expression of activating receptors NKp30 and NKG2D on NK cells. Bar chart showing the frequencies of **(A)** NKp46$^+$ **(B)** NKp30$^+$ **(C)** NKG2D$^+$ NK cells as a percentage of total NK cells. Bar chart showing the MFI values for **(D)** NKp46 **(E)** NKp30 **(F)** NKG2D on NK cells (n=6). *p<0.05, **p<0.01 by one-way ANOVA with post-hoc Dunn's test. (Experiment carried out in conjunction with MSc in Translational Oncology student Jennifer Moran).

3.8.4 Co-culture with T98G cells increased the expression of CD16, a key receptor for ADCC by NK cells and this was not further altered by P3 treatment.

The frequency % of DNAM-1$^+$ NK cells were not altered by co-culture with P3-treated T98G cells (n=6)*(Figure 44A)*. The frequency % of T98G cells positive for CD16 showed a significant increase by co-culture with T98G cells, however it was not further changed by P3 treatment (PBMC alone vs. T98G+PBMC; 79.6% vs. 86.16%; p=0.0429*)(Figure 44B).*The MFI of DNAM-1$^+$ or CD16$^+$ NK cells showed no significant changes *(Figure 44 C,D).*

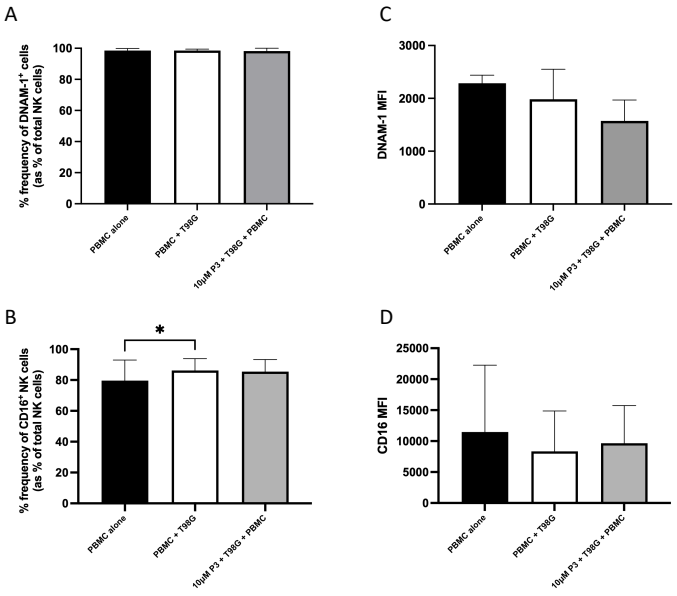

Figure 44: Co culture with T98G cells increased the expression of CD16, a key receptor for ADCC by NK cells and this was not further altered by P3 treatment. Bar chart showing the frequencies of **(A)** DNAM-1^{+} **(B)** CD16^{+} NK cells as a percentage of total NK cells. Bar chart showing the MFI values for **(C)** DNAM-1 **(D)** CD16 on NK cells (n=6). *p<0.05 by one-way ANOVA with post-hoc Dunn's test. (Experiment carried out by MSc in Translational Oncology student Jennifer Moran).

3.8.5 P3 does not alter the expression of death receptor ligands on NK cells co-cultured with T98G cells.

P3-treated T98G cells were co-cultured with NK cells and the data show that treatment with P3 does not cause a significant alteration in the frequency percentage of NK cells positive for FasL or TRAIL. (n=6)*(Figure 45 A,B).* The MFI of FasL or TRAIL on NK cells co-cultured with P3-treated T98G cells exhibited no significant changes *(Figure 45 C,D).*

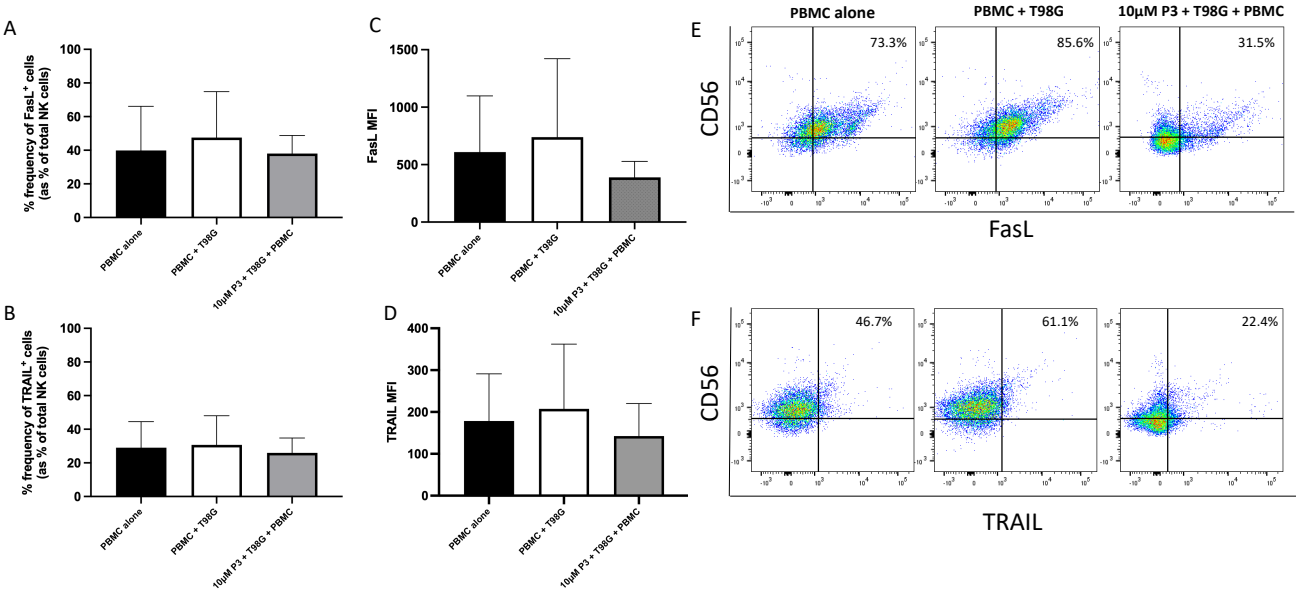

Figure 45: P3 does not alter the expression of death receptor ligands on NK cells co-cultured with T98G cells. (Left) Bar chart showing the frequencies of **(A)** FasL$^+$ **(B)** TRAIL$^+$ NK cells as a percentage of total NK cells. Bar chart showing the MFI values for **(C)** FasL **(D)** TRAIL on NK cells (n=6). **(Right)** Representative dot plots showing **(E)** FasL$^+$ **(F)** TRAIL$^+$ T98G cells. *p<0.05 by one-way ANOVA with post-hoc Dunn's test. (Experiment carried out in conjunction with MSc in Translational Oncology student Jennifer Moran).

3.8.6 P3 significantly reduced the expression of immune checkpoint receptor TIGIT on NK cells co-cultured with T98G cells.

P3-treated NK cells co-cultured with T98G cells compared to NK cells alone did not exhibit significant alterations in the percentage frequency of NKG2A$^+$ NK cells (n=6)*(Figure 46A)*. There was a decrease in the frequency % of TIGIT$^+$ NK cells when NK cells were co-cultured with P3-treated T98G cells compared to co-culture with untreated T98G cells (PBMC+T98G vs. 10 μM P3+T98G+PBMC; 77.48% vs. 70.4% ; p=0.0117)*(Figure 46B)*. The frequency of PD-1$^+$ NK cells was not significantly altered by co-culture with P3-treated T98G cells *(Figure 46C)*. Additionally, the MFI of NKG2A, TIGIT and PD-1 showed no significant reduction by P3 treatment and T98G co-culture *(Figure 46 D-F)*.

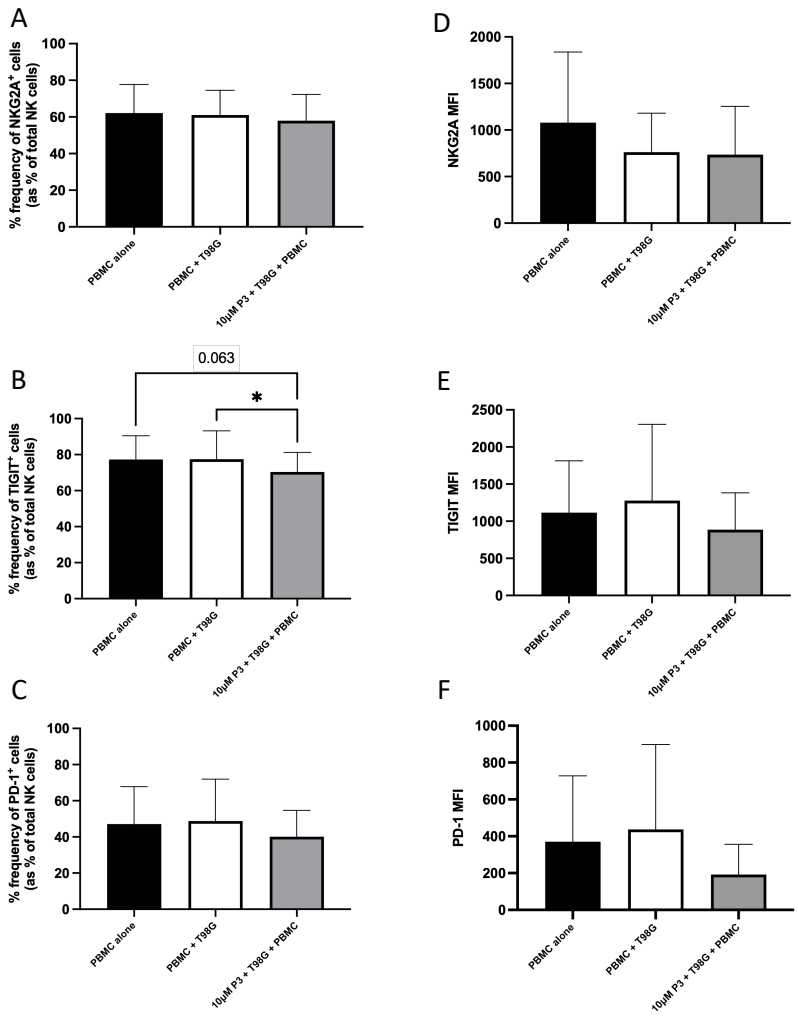

Figure 46: P3 significantly decreased the expression of immune checkpoint receptor TIGIT on NK cells co-cultured with T98G cells. Bar chart showing the frequencies of **(A)** NKG2A$^+$ **(B)** TIGIT$^+$ **(C)** PD-1$^+$ NK cells as a percentage of total NK cells. Bar chart showing the MFI values for **(D)** NKG2A **(E)** TIGIT **(F)** PD-1 on NK cells (n=6). *$p<0.05$ by one-way ANOVA with post-hoc Dunn's test. (Experiment carried out in conjunction with MSc in Translational Oncology student Jennifer Moran).

3.8.7 P3 did not significantly impact the production of inflammatory cytokines by NK cells co-cultured with T98G cells.

P3-treated and untreated T98G cells were co-cultured with NK cells and activated with PMA and Ionomycin to assess the effects of a 24 hour P3 treatment on intracellular NK cell function in Glioblastoma. NK cells co-cultured with P3-treated T98G cells did not exhibit increased frequency percentage of IL-10, IFN-γ or TNF-α when compared to untreated NK cells and NK cells co-cultured with untreated T98G cells (n=6)*(Figure 47 A,B,C).* Following co-culture with P3-treated T98G cells, the MFI of IL-10, IFN-γ and TNF-α showed no significant changes *(Figure 47 D,E,F).*

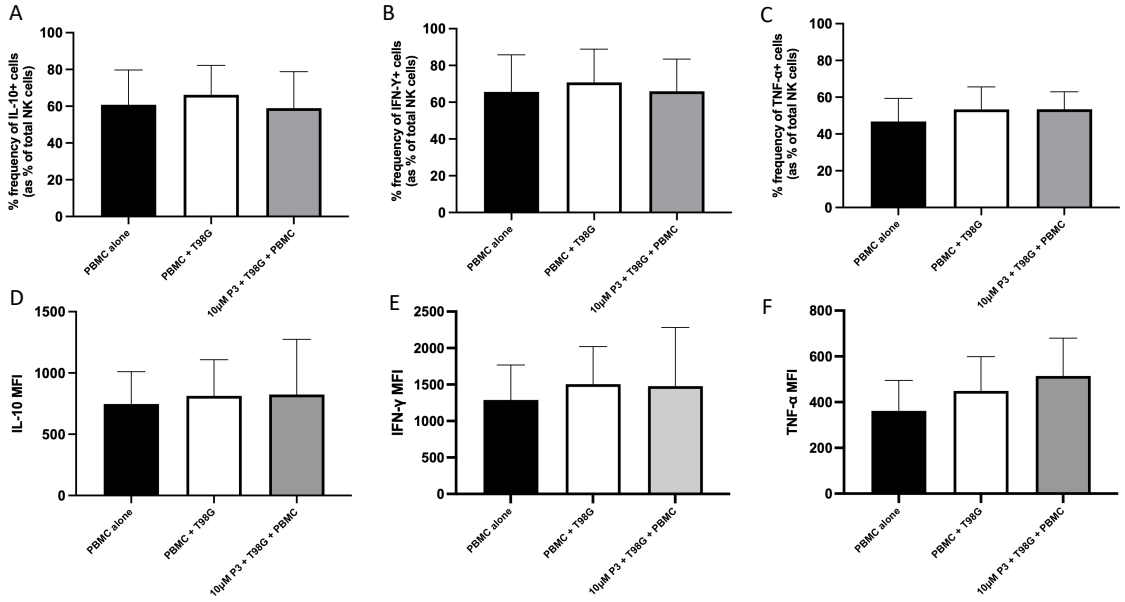

Figure 47: P3 did not significantly change the expression of inflammatory markers on NK cells co-cultured with T98G cells. Bar chart showing the frequencies of **(A)** IL-10^+ **(B)** IFN-γ^+ **(C)** TNF-α^+ NK cells as a percentage of total NK cells. Bar chart showing the MFI values for **(D)** IL-10 **(E)** IFN-γ **(F)** TNF-α^+ on NK cells (n=6). *$p<0.05$ by one-way ANOVA with post-hoc Dunn's test. (Experiment carried out in conjunction with MSc in Translational Oncology student Jennifer Moran).

3.8.8 P3 did not alter the degranulation of NK cells co-cultured with T98G cells.

P3-treated and untreated T98G cells were co-cultured with NK cells and activated with PMA and Ionomycin to elucidate the effects of a 24 hour P3 treatment on intracellular NK cell function in GBM. The frequency % of NK cells which were positive for both CD107a and granzyme B showed no significant alteration by co-culture with P3-treated T98G cells (n=6)*(Figure 48 A,B)*. The MFI of CD107a and granzyme B on NK cells co-cultured with P3-treated T98G cells also remained relatively unaffected when compared to the NK cells co-cultured with untreated T98G cells *(Figure 48 C,D)*.

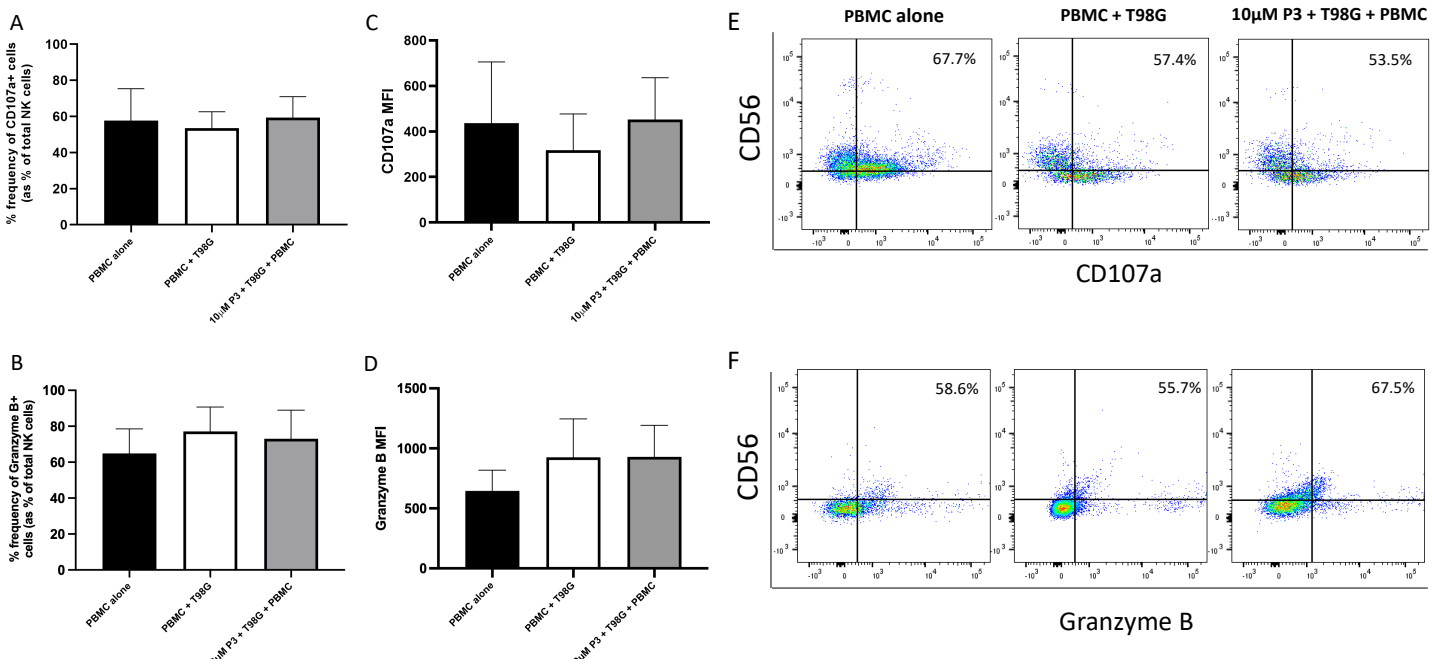

Figure 48: P3 did not alter the degranulation of NK cells co-cultured with T98G cells. (Left) Bar chart showing the frequencies of **(A)** $CD107a^+$ **(B)** granzyme B^+ NK cells as a percentage of total NK cells. Bar chart showing the MFI values for **(C)** CD107a **(D)** granzyme B on NK cells (n=6). **(Right)** Representative dot plots showing **(E)** $CD107a^+$ **(F)** granzyme B^+ NK cells. *$p<0.05$ by one-way ANOVA with post-hoc Dunn's test. (Experiment carried out in conjunction with MSc in Translational Oncology student Jennifer Moran).

3.9 Elucidating the effects of P3 on immune cell chemotaxis

The effects of P3 on the migratory capacity of healthy donor derived PBMC were elucidated. To achieve this lymphocytes, NK cells and T cells were treated with 10 µM of P3 for 72 hours and their migration towards T98G supernatant was examined. There was no statistically significant differences in NK cell, T cell or lymphocyte migration toward T98G cell supernatant, compared to untreated or VC suggesting that P3 does not alter the migratory capacity of key anti-tumour immune cells *(Figure 49)*.

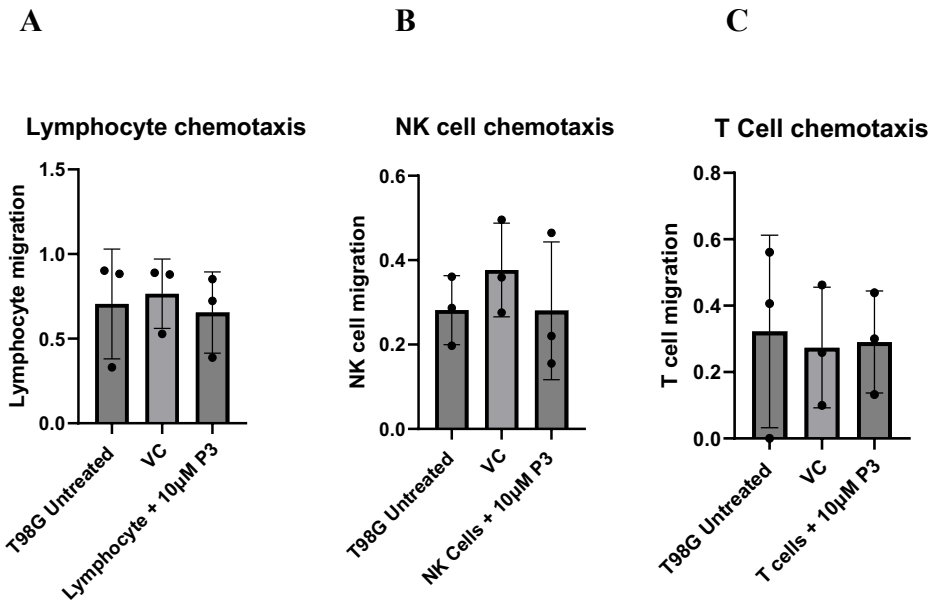

Figure 49: P3 does not affect NK cell migratory capacity towards GBM tumour. A) Lymphocyte cell migration: lymphocyte (treated with 10 µM P3 for 72hrs) chemotaxis towards untreated GBM T98G cells compared to untreated T98G cells and VC (DMSO) **B)** NK cell migration: NK cell (treated with 10 µM P3 for 72hrs) chemotaxis towards untreated GBM T98G cells compared to untreated T98G cells and VC (DMSO). **C)** T cell migration: T cell (treated with 10 µM P3 for 72hrs) chemotaxis towards untreated GBM T98G cells compared to untreated T98G cells and VC (DMSO), Paired T test, ns, n=3

4.0 Developing and testing more soluble candidates of P3 for subsequent clinical application

Novel phosphate prodrugs of P3 were synthesised for improvement of solubility. Their aqueous solubility was determined and their effects on T98G cells were examined for comparison to P3. Using Swissotel the estimated aqueous solubility (ESOL) of the compounds were assessed based directly from their structures. The ESOL value for P3 was -2.62, P3 acetate was -2.72 and P3 Phosphate was -2.04. A solubility class <-2 indicates these compounds moderately soluble and as P3 Phosphate is a pro-drug it has enhanced solubility compared to the parent or intermediate compounds. The final aim of this study was to generate the prodrugs and test their anti-cancer efficacy in GBM in comparison the P3 parent drug.

4.1 Generation of P3 Prodrugs with improved solubility

The molecule Pyrazinib, P3 previously synthesised by Prof. Jacintha O'Sullivan (TCD) has proven anti-cancer potential in OAC [87]. Further testing required in mouse models was hampered by poor P3 solubility. P3 acetate is an intermediate compound of P3 while P3 Phosphate is a P3 prodrug .

Prodrugs are biologically inactive compounds that can be metabolised in the body to produce an active drug. The Prodrug method is alternative way to enhance the aqueous solubility of a parent drug through the attachment to ionizable or polar groups, like amino acids, phosphates or sugar moieties, thereby, increasing the dissolution rate [89]. This approach can be used for parent drugs that have issues associated with solubility and other negative pharmacokinetics [89].

P3 Phosphate (synthesised by Beavan Mcloughlin, PhD student TCD) is a phosphate prodrug and P3 acetate a parent compound intermediate were both synthesised by in the department of Pharmacy and Pharmaceutical Sciences at Trinity College Dublin.

4.2 Perkin condensation reaction of P3

The Perkin condensation reaction is a two-step procedure, the formation of P3 acetate followed by the hydrolysis of P3 acetate to form P3. This type of reaction was used to synthesise P3 with a very long reaction time for P3 (5-6 days) and the very low yield of P3 (15% yield).

We optimised the first step of this reaction to form P3 acetate by using a microwave which reduced the reaction time to 5hrs. The tautomerisation of the pyrazine ring takes place at slower rate than quinoline ring (pK_a of quinoline nitrogen: 4.92 [90]) due to the low basicity of pyrazine nitrogen (pK_a of pyrazine nitrogen: 0.6), contributing to a less stable enamine intermediate. The protonation takes place at N-1 nitrogen atom of pyrazine rather than N-4 nitrogen atom. Furthermore, the tautomerisation process is easily affected by solvent polarity, temperature, and pH [91]. Even though tautomeriastion is not the limiting step and P3 acetate had a good yield (62%), the P3 yield is still reduced which could be due to the hydrolysis or purification step.

The first step in the synthetic route (*Figure 50*) is the reaction of 2-methylpyrazine with 2-hydroxy benzaldehyde mixed with acetic anhydride in the microwave (160 ℃) for 5 hours. This formed the intermediate, P3 acetate which yielded 62% of the crude product (no purification was required). This was followed by the hydrolysis of P3 acetate to form P3. The aim of hydrolysis was to remove the acetate group and to form a hydroxy group (OH) at position 2 of the benzene ring under basic conditions. The hydrolysis reaction was carried out in saturated NaOH solution and mixture of ethanol/ethyl acetate under reflux (100 ℃) for 2-3 days. There was no workup required and the crude mixture was purified by flash column chromatography to give P3 a yellow solid (15% yield). The plausible reaction mechanism for the synthesis of P3 through Perkin condensation involves the activation of C-H (sp^3) bond. 2-Methylpyrazine tautomerised under acid catalytic conditions to generate an intermediate. This intermediate attacks the carbonyl group of the 2-hydroxybenzaldehyde *via* a quasi-cyclic transition state with hydrogen bonding which leads to the formation 2-(1-(pyrazin-2-yl)propan-2-yl)phenol, which suffers dehydration and results in the formation of double bond. Then, the acylation of hydroxy takes place with acetic anhydride at position 2 of the benzene ring at the same time as shown in *(Figure 50).*

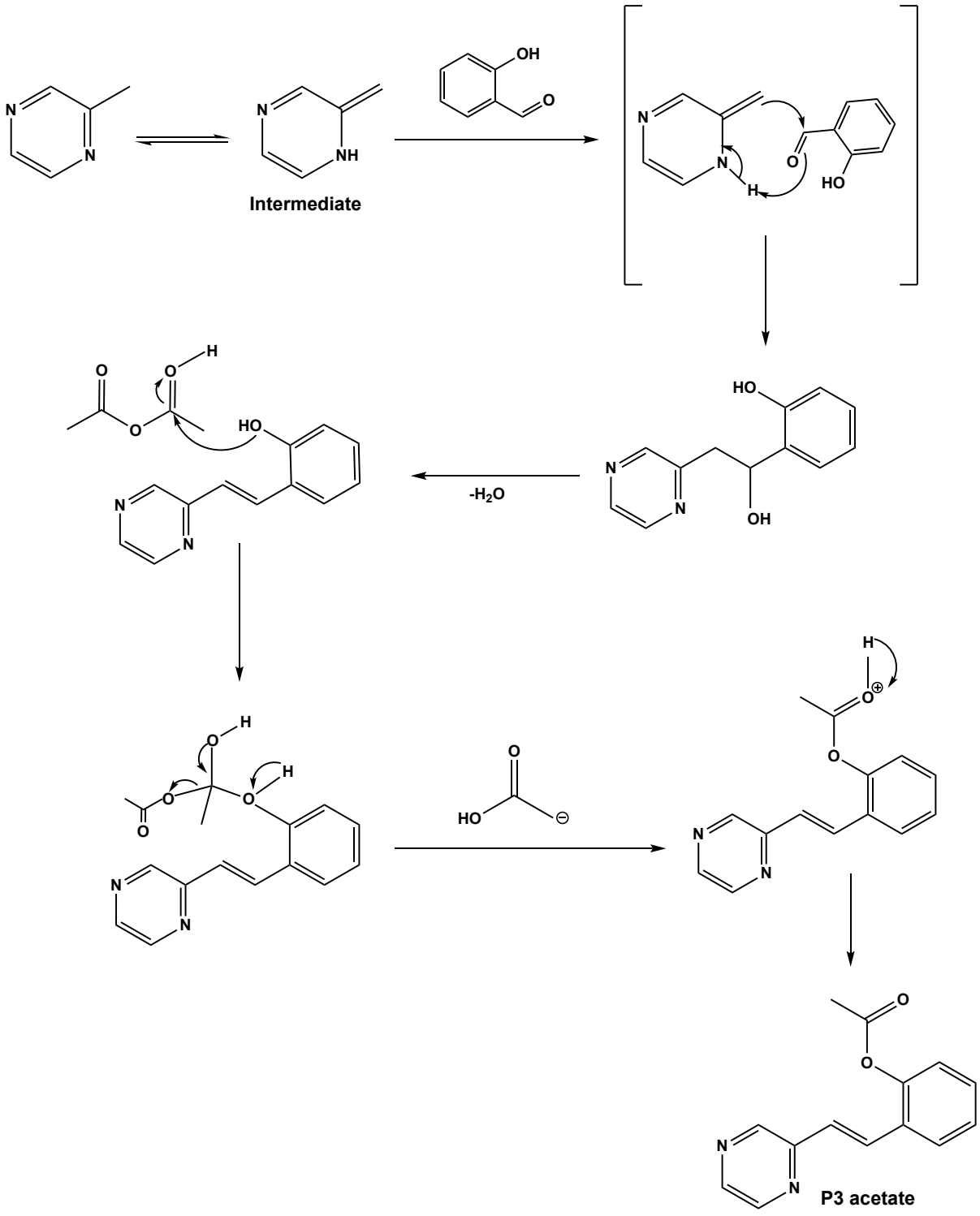

Figure 50: Plausible reaction mechanism for sp^3 functionalisation of 2-methylpyrazine and P3 acetate formation

After acylation step, P3 acetate has been formed which undergoes base catalysed hydrolysis to afford P3 as shown in *(Figure 51)*. The first step of the hydrolysis of P3 acetate involves the nucleophilic attack of the hydroxide ion on the carbon (an electrophile) of the carbonyl group of the acetate which results in the π bond breaking and creates a tetrahedral intermediate. This

tetrahedral intermediate undergoes an elimination, and the loss of the leaving group results in the creation of hydroxy group at position 2 of the benzene ring of the P3.

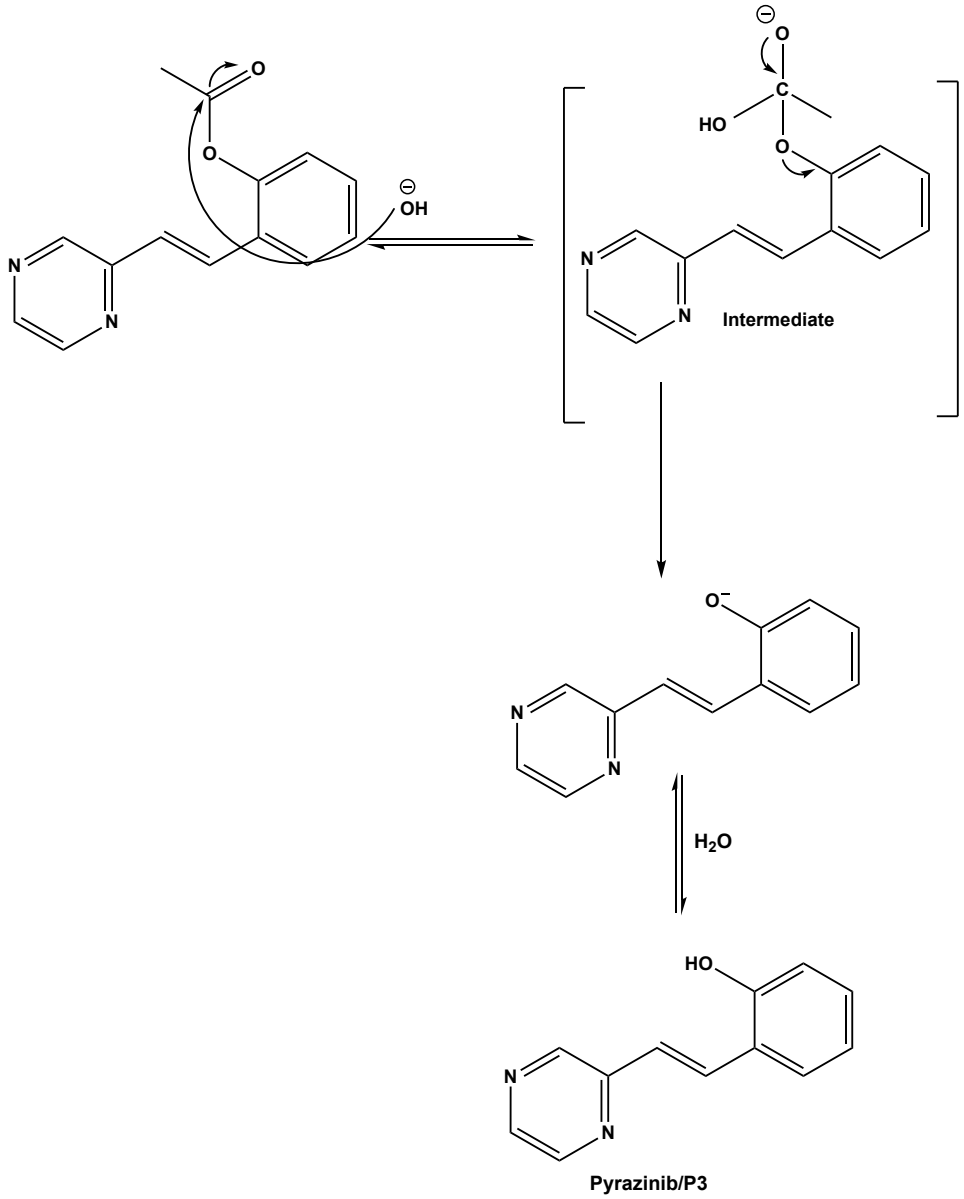

Figure 51:Reaction mechanism of hydrolysis of P3

4.2.1 NMR analysis (^{1}H and ^{13}C) of *(E)-2-(2-(Pyrazin-2-yl)vinyl)phenyl acetate (P3 acetate)*

This section displays the spectral data obtained from the NMR analysis (^{1}H and ^{13}C) of P3 acetate. ^{1}H NMR spectra is shown in *(Figure 52)* and *table 7*. ^{13}C NMR spectra is shown in (F*igure 53)* and *table 8*.

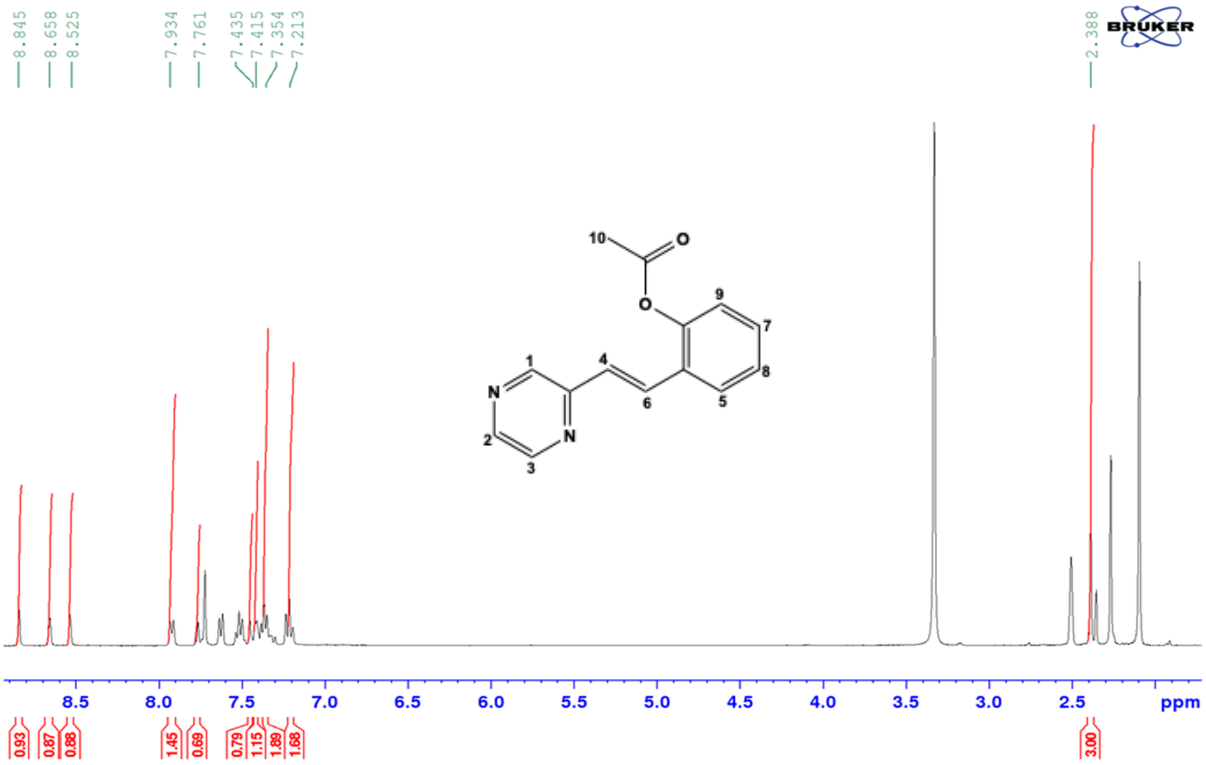

Figure 52: ^{1}H NMR spectra of P3 acetate at 600MHz in DMSO-d_6

Table 7: ^{1}H NMR data obtained from the analysis of P3 acetate at 600 MHz in DMSO-d_6

Chemical shift/δ (ppm)	Integration	Multiplicity	Coupling constant (Hz)	Assignment
8.84	1H	d	2.1	1
8.65	1H	dd	1.4, 4.0	2
8.52	1H	d	2.2	3
7.93	1H	dd	8, 1.2	5
7.76	1H	d	16	6
7.43	1H	t	7	7
7.41	1H	d	16	4
7.35	1H	t	7	8
7.21	1H	dd	8,1.2	9
2.38	3H	s	-	10

Note: DMSO peak at 2.5 ppm

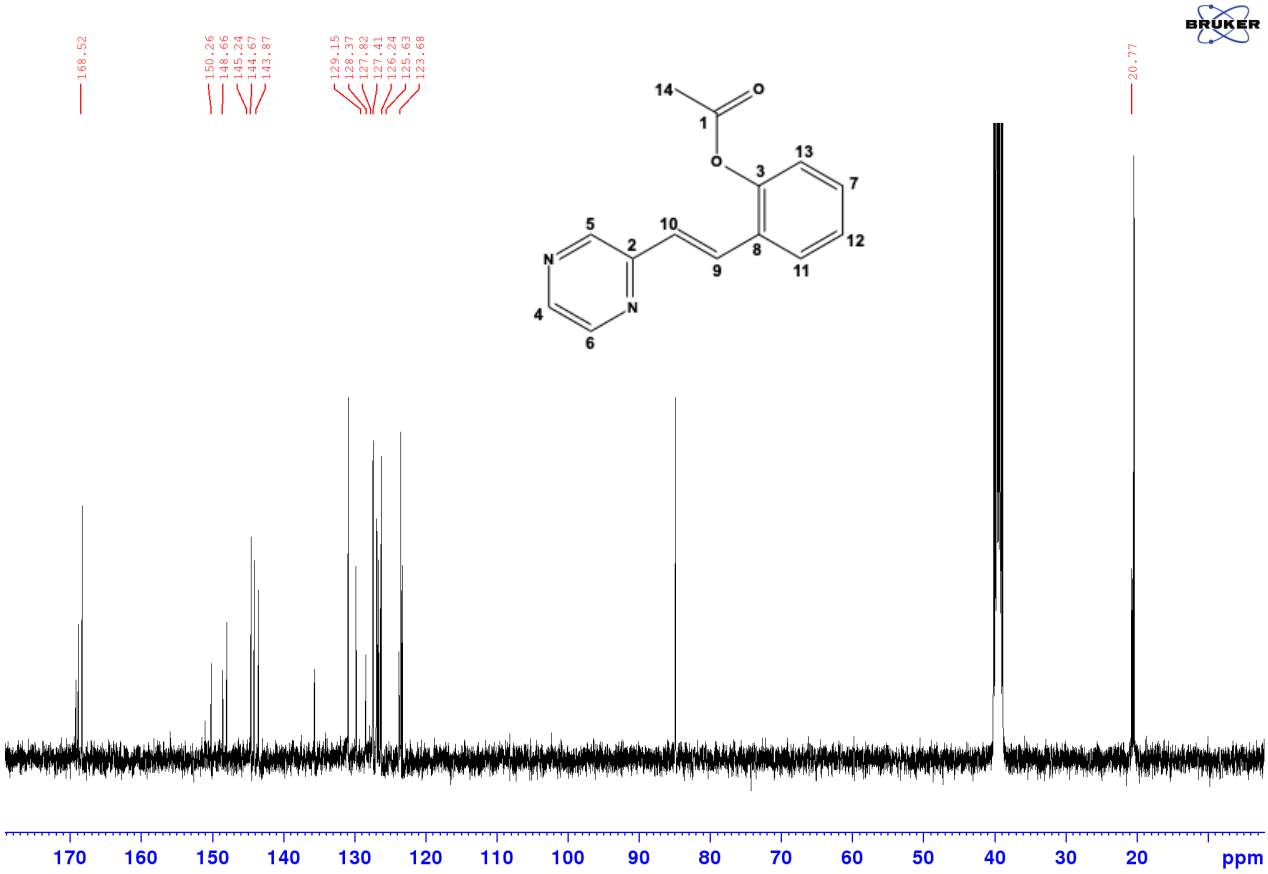

Figure 53: ^{13}C NMR of P3 acetate at 600 MHz in DMSO-d_6

Table 8: ^{13}C NMR data obtained from the analysis of P3 acetate at 600 MHz in DMSO-d_6

Chemical shift/ δ (ppm)	Assignment
168.5	1
150.2	2
148.6	3
145.24	5
144.67	4
143.87	6
129.15	7
128.36	8
127.8	9
127.4	10
126.2	11
125.6	12
123.6	13
20.7	14

4.2.2 NMR analysis (^{1}H and ^{13}C) of *(E)-2-(2-(Pyrazin-2-yl)vinyl)phenol (P3)*

This section displays the spectral data obtained from the NMR analysis (^{1}H and ^{13}C) of P3. ^{1}H NMR spectra is shown in *(Figure 54)* and *table 9.* ^{13}C NMR spectra is shown in *(Figure 55)* and *table 10*.

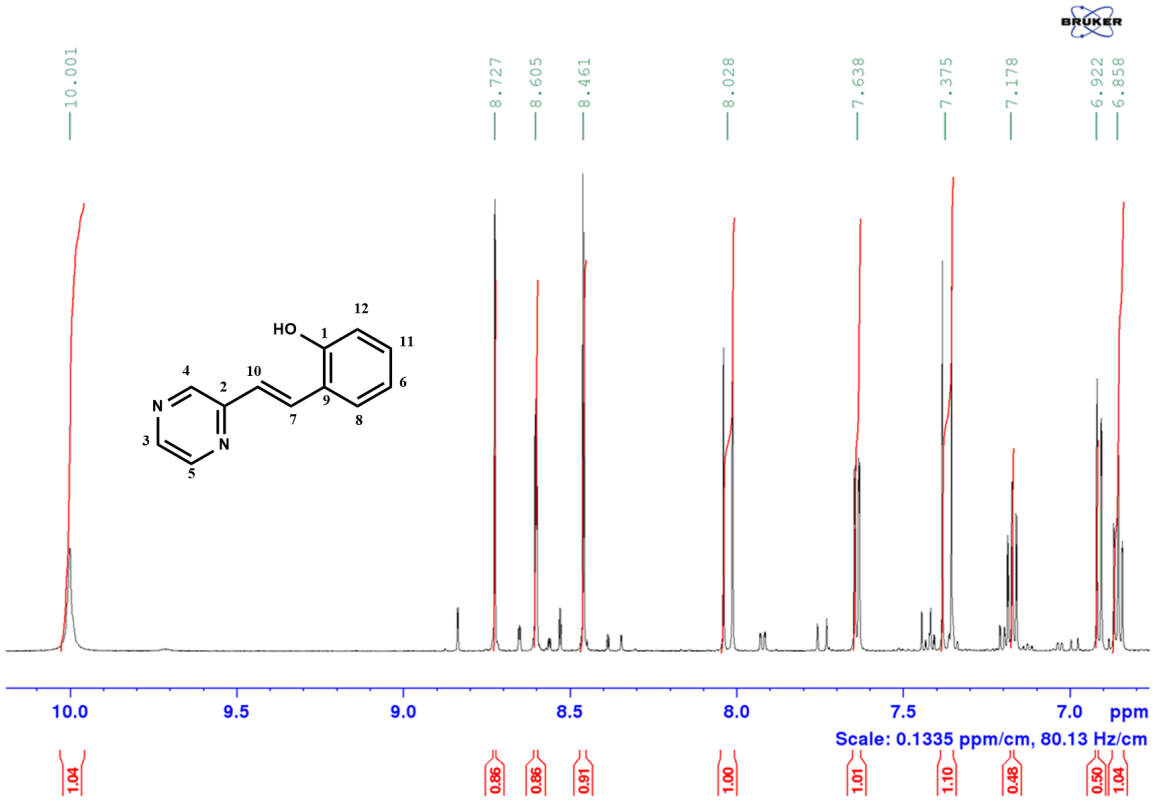

Figure 54: ^{1}H NMR spectra of P3 at 600 MHz in DMSO-d_6

Table 9: ^{1}H NMR data obtained from the analysis of P3 at 600 MHz in DMSO-d_6

Chemical shift/δ (ppm)	Integration	Multiplicity	Coupling constant (Hz)	Assignment
10.0	1H	br, s	-	1
8.72	1H	d	1.4	2
8.60	1H	dd	1.4, 4.0	3
8.46	1H	d	2.4	4
8.02	1H	d	16	5
7.63	1H	dd	8, 1.6	6
7.37	1H	d	16	7
7.17	1H	t	7	8
6.92	1H	d	8	9
6.86	1H	t	7	10

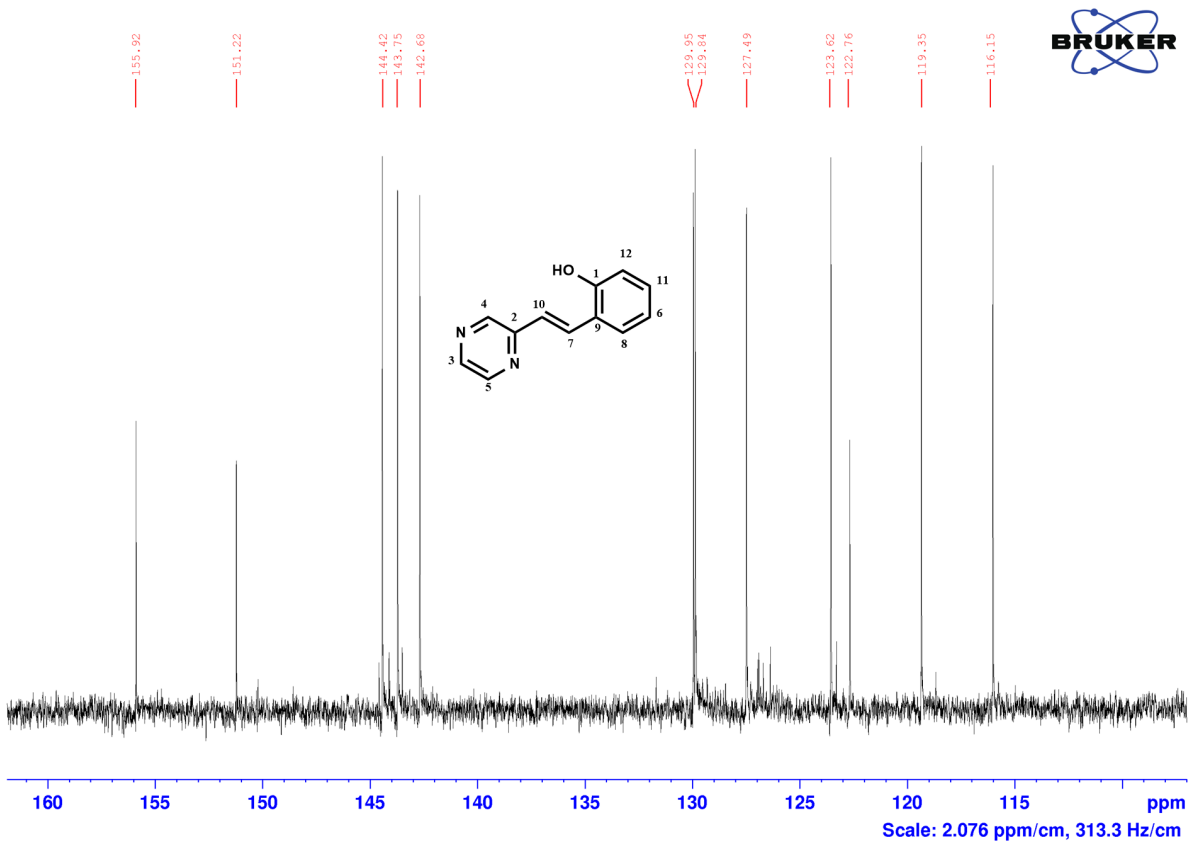

Figure 55: ^{13}C NMR of P3 at 600 MHz in DMSO-d_6

Table 10: ^{13}C NMR data obtained from the analysis of P3 at 600 MHz in DMSO-d_6

Chemical shift/ δ (ppm)	Assignment
155.92	1
151.22	2
144.42	3
143.74	4
142.68	5
129.94	6
129.84	7
127.49	8
123.62	10
122.75	9
119.35	11
116.14	12

4.2.3 Discussion of NMR analysis (^1H and ^{13}C) of P3 acetate and P3

P3 acetate and P3 compounds were fully characterised by ^1H and ^{13}C NMR and all the peaks are assigned. The ^1H spectra of P3 acetate shows three protons that are attributed to the pyrazine ring, they resonate as a doublet at δ 8.84 with a J value of 2 Hz, a doublet of doublet at δ 8.65 and a doublet at δ 8.52 with a J value of 1.7 Hz due to long range coupling *(Figure 56)*. The protons at position 4 and 6 show doublet signals at δ 7.41 and δ 7.76 respectively with a J value of 16 Hz indicating a trans double bond is present in the P3 acetate structure. The other signals in the spectrum are characteristic of the aromatic protons and an acetate group. For example, the peaks at δ 7.93 and δ 7.21 at position 5 and 9 respectively are doublet of doublet signals indicated on (*Figure 56)*. Due to the coupling of two different neighboring protons, both peaks are doublet of doublet with a coupling constant of 8 Hz between H 9 to H 10 and 12 Hz from H 9 to H12. The proton at position 10 is characteristic of the acetate methyl group that is seen at δ 2.38.

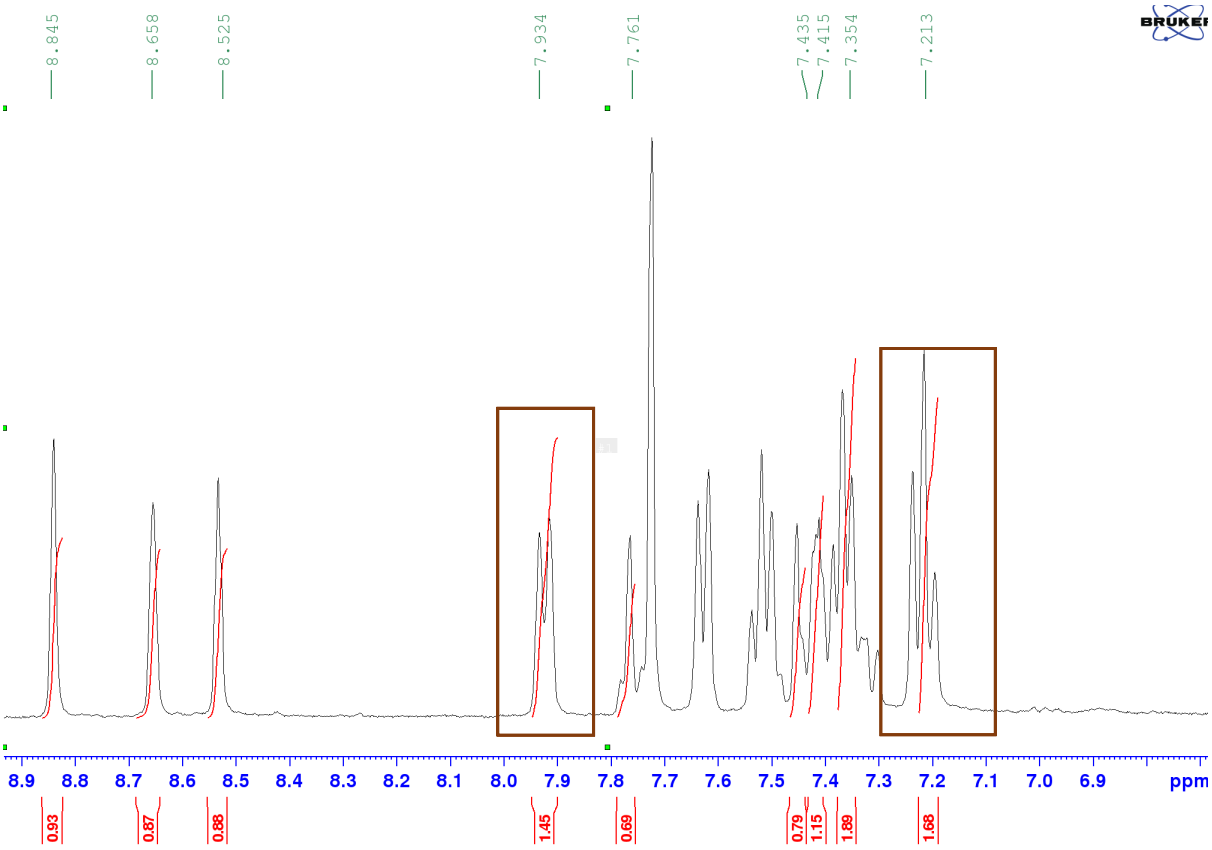

Figure 56: Zoomed version of the aromatic region (from 8.8 to 7.2 ppm, doublet of doublets indicated at 7.20 and 7.92 ppm) of ^{1}H NMR of P3 acetate

In the ^{13}C NMR spectra of P3 acetate *(Figure 53),* the most downfield signal at δ 168.5 is attributed to the carbon at position 1 which represents the carbonyl group of P3 acetate. The three signals δ 150.2 at position 2, δ 144.67 at position 4 and δ 145.24 at position 5 are characteristic of the pyrazine ring carbons. These three signals are downfield as a result of the strong π deficient heteroaromatic system. The chemical shifts at δ 129.125 to δ 125.6 represent the other aromatic carbons. A downfield signal appears at δ 148.6 at position 3 of the P3 Acetate structure which is indicative of the C-O bond between the acetate and benzene ring. The double bond carbons 9 and 11 appeared at δ 127.8 and δ 126.2 and the carbon of methyl group at position 12 appears at δ 20.7.

The ^{1}H spectrum of P3 *(Figure 54),* showed a broad singlet signal at δ 10 which is characteristic of the OH group at position 1. The three protons attributed to the pyrazine ring are like P3 acetate and appear as a doublet at δ 8.72 with a J value of 2 Hz, a doublet of doublets at position 2 at δ 8.60 and a doublet at position 3 at δ 8.46. The downfield shift of the pyrazine ring protons in both ^{1}H and ^{13}C NMR spectrums are due to the π deficient heteroaromatic system. The

double bond protons appear at δ 8.02 and 7.37 with a *J* value of 16 Hz. The only difference between the ^{1}H NMR spectrum of P3 and P3 acetate is that P3 acetate contains an acetate group and P3 contains a OH group. However, due to the presence of OH group, other aromatic proton chemical shifts are slightly changed, for example the proton at position 9 is a doublet at *δ* 6.92 compared to P3 acetate at position 9 is doublet of doublets at *δ* 7.21. This change was observed as the benzene ring is substituted with OH which tends to decrease chemical shift and change the splitting pattern. The ^{13}C NMR spectra of P3 *(Figure 55)* is similar to P3 acetate *(Figure 53)*. However, the absence of carbonyl carbon signal seen at 168.5 ppm in P3 acetate's carbon spectrum indicates the formation of P3 as there is a downfield signal at *δ* 155.92 at position 1 which attributed to the hydroxyl bearing carbon atom.

4.2.4 FTIR analysis of P3 acetate and P3

The IR spectra of P3 acetate showed a characteristic band of ester carbonyl at 1758 cm^{-1} as indicated on (*Figure 57)*. The IR spectra of P3 showed a broad signal of hydroxy (OH) group at 3015 cm^{-1} (*Figure 58*). The absence of the ester carbonyl signal indicated the formation of P3. However, other signals were also identified such as signals for aromatic substituted ring and sp^{2} double bond in both spectra at around 1590 – 1450 cm^{-1} and 1600-1680 cm^{-1} respectively.

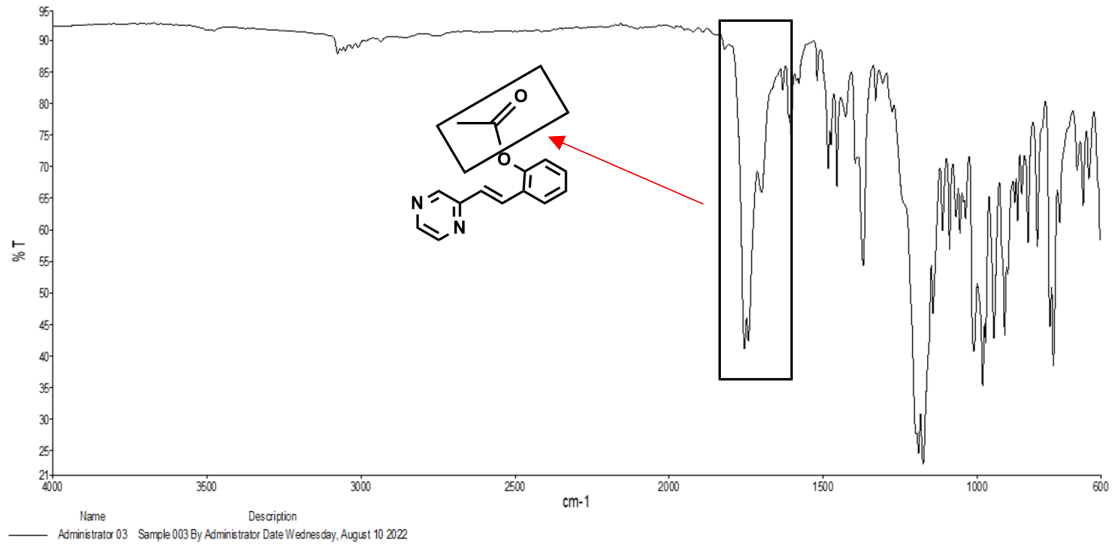

Figure 57: FT-IR analysis of P3 acetate

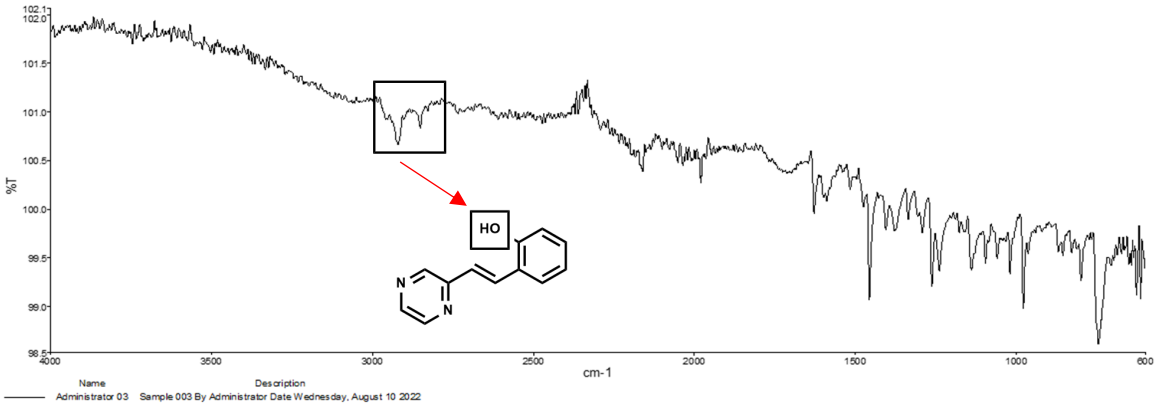

Figure 58: FT-IR analysis of P3

4.3 Elucidating the effects of P3 Phosphate and P3 acetate on T98G cell viability and GBM sensitivity to TMZ

4.3.1 P3 Phosphate exhibits potential to kill T98G cells

The effects of P3 phosphate on GBM Cell viability were elucidated using a CCK8 colorimetric assay. T98G cells were treated with 10μM of P3 phosphate for 72 hours and compared to untreated T98G cells. The graph indicates that 10μM of P3 phosphate significantly reduced the percentage of viable cells by 93.1% when compared to the control (untreated vs 10 μM P3 phosphate, 100% vs 6.45%, p<0.0001*)(Figure 59)*. There was also a significant decrease between VC and 10 μM P3 Phosphate (VC vs 10 μM P3 Phosphate, 95% vs 6.45%, p<0.0001) suggesting that P3 Phosphate is highly toxic to T98G cells at this dose. Future studies will elucidate the effects of increasing doses of P3 Phosphate on T98G viability and proliferation.

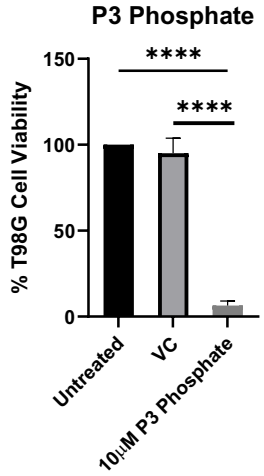

Figure 59: P3 Phosphate reduces T98G GBM Cell viability. Bar chart showing % cell viability of untreated T98G cells vs T98G cell treated with 10 μM of P3 Phosphate or VC (6:4 Ethanol: H_2O) for 72 hours. Cell viability was assessed by CCK8 colorimetric assay. Paired T-test ****p< 0.0001, n=7.

4.3.2 Elucidating the effects of P3 Acetate on GBM Cell viability

The effects of P3 Acetate on GBM Cell viability were elucidated using a CCK8 colorimetric assay. T98G cells were treated with 10 μM of P3 Acetate for 72 hours and compared to untreated T98G cells. In contrast to P3 Phosphate, 10 μM of P3 Acetate caused a significant increase in T98G cell viability compared to control (untreated vs 10 μM P3 Acetate, 100% vs 110.3%, p=0.034, *(Figure 60)*. The potential pro-proliferative effects of P3 acetate on T98G cells warrants further investigation.

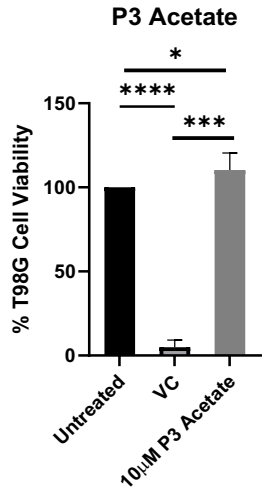

Figure 60: P3 Acetate increased T98G GBM Cell viability. Bar chart showing % cell viability of untreated T98G cells vs T98G cell treated with 10 μM of P3 Phosphate or VC (DMSO) for 72 hours. Cell viability was assessed by CCK8 colorimetric assay. Paired T-test *p< 0.05, n=7.

4.4 Elucidating the effects of P3 phosphate on GBM sensitivity to TMZ

The potential of P3 Phosphate to sensitize T98G cells to TMZ was elucidated using a CCK8 colorimetric assay. T98G cells were treated with 10, 50, 100 μM of TMZ +/- 10 μM P3 Phosphate for 72 hours and were compared to untreated T98G cells or the DMSO vehicle control for TMZ. Our data showed that P3 Phosphate does not sensitize T98G cells to TMZ. When the untreated T98G cells were compared to 10, 50, 100 μM of TMZ alone there was statistical significance showing that the chemotherapeutic agent elicited expected cytotoxic results and demonstrating success of the experimental model (Control vs 10 μM TMZ (100% vs 13.2%, p<0.0001), control vs 50 μM TMZ (100% vs 1.43, p<0.0001), control vs 100 μM TMZ (100% vs 1.78, p<0.0001)*(Figure 61)*. There was also a decrease in cell viability between 10 μM TMZ vs 50 μM TMZ (13.2% vs 1.43%, p<0.0001) and between 10 μM TMZ vs 100 μM TMZ (13.2% vs 1.78%, p<0.0001) *(Figure 61)* showing dose response. As discussed above, P3 alone reduced T98G cell viability. In addition, P3 Phosphate appeared to enhance sensitivity of T98G cells to low dose 10 μM of TMZ but this was not statistically significant and warrants further investigation. Lower doses of TMZ and varying doses of P3 Phosphate will uncover the true TMZ-sensitising effects of this P3 prodrug.

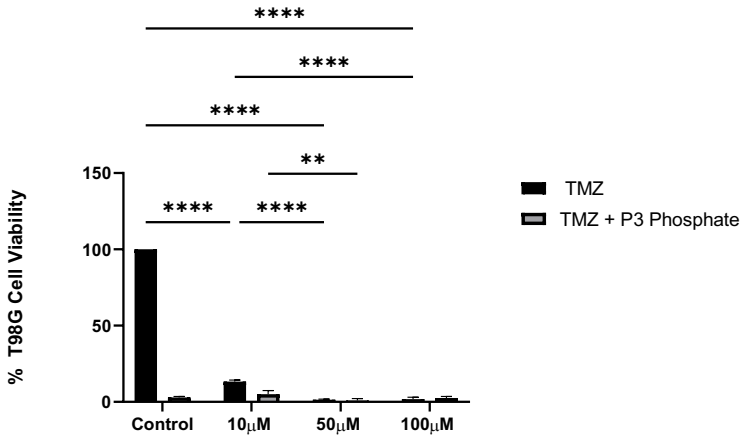

Figure 61: P3 Phosphate does not sensitize T98G cells to Temozolomide (TMZ). Bar chart showing % cell viability of T98G cells treated with TMZ Vehicle control (Control) or 10 μM, 50 μM or 100 μM TMZ alone (black) vs T98G cells treated with treated with TMZ Vehicle control (Control) or 10 μM, 50 μM or 100 μM TMZ alone TMZ+ 10 μM of P3 Phosphate for 72 hours. Cell viability was assessed by CCK8 colorimetric assay. 2-way ANOVA **p< 0.01, ***p< 0.001 and ****p< 0.0001, n=5.

4.5 Elucidating the effects of P3 Phosphate and P3 Acetate on NKR ligand shedding by T98G cells

4.5.1 P3 phosphate significantly attenuates NKR ligand B7-H6 shedding by T98G cells

T98G cells were treated with 10 μM P3 Phosphate for 72 hours and the supernatants were collected and screened by ELISA to determine the effect of P3 Phosphate on B7-H6 shedding into the GBM tumour microenvironment. Interestingly, P3 Phosphate-treated T98G cell supernatants displayed a significant decrease of 18.2% in B7-H6 levels at the 72 hour time point compared to the untreated cells (Untreated T98G cells vs 10 μM P3 Phosphate (39.12% vs 20.97%, p=0.0143)*(Figure 62).* Interestingly, there is a significant decrease between the vehicle control (ethanol:dH_2O,6:4) and 10 μM of P3 Phosphate suggesting that this prodrug may alleviate immunomodulation of NK cells in the GBM tumour microenvironment (VC vs 10μM P3 (46.58% vs 20.97%, p=0.0197)*(Figure 62)*.

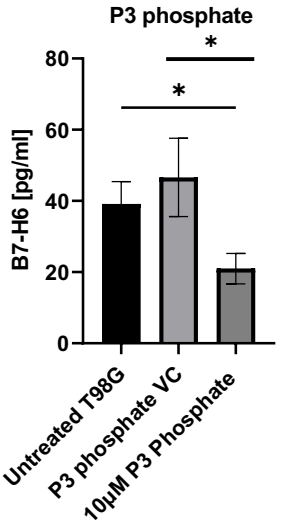

Figure 62: Elucidating the effects of P3 Phosphate on B7-H6 shedding by T98G cells. Bar chart showing concentration of B7-H6 in (pg/ml) in the supernatants of untreated T98G cells, vehicle control-treated T98G cells (VC, ethanol:dH_2O,6:4) and 10 µM P3 Phosphate-treated T98G cells. Unpaired T-test *$p < 0.05$, n=3.

4.5.2 P3 Acetate does not significantly alter NKR ligand B7-H6 shedding by T98G cells

T98G cells were treated with 10 µM P3 Acetate for 72 hours and the supernatants were collected and screened by ELISA to determine the effect of P3 Acetate on B7-H6 shedding into the GBM tumour microenvironment. P3 Acetate-treated T98G cell supernatants showed a substantial decrease of 11.2% in B7-H6 levels at the 72 hour time point compared to the untreated cells, however this was not significant and should be repeated in future studies (Untreated T98G cells vs 10 µM P3 Acetate (39.13% vs 27.93%, p=0.174)*(Figure 63)*. There is a significant increase between the vehicle control (DMSO) and 10 µM of P3 Acetate (VC vs 10µM P3 which is more related to unusual effects of 0.1% DMSO which have been observed in this study (6.25% vs 27.93%, p=0.02) *(Figure 63)*. There is a significant decrease between untreated and vehicle control suggesting that the vehicle decreased B7-H6 shedding, warranting further investigation (Untreated vs VC (39.13% vs 6.25%, p=0.001).

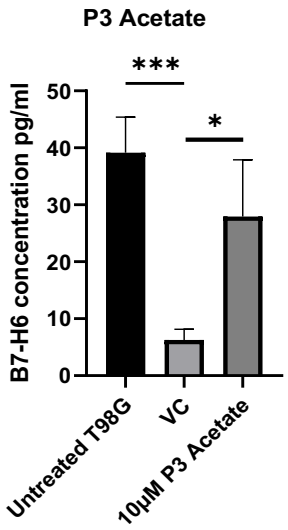

Figure 63: Elucidating the effects of P3 acetate on B7-H6 shedding by T98G cells . Bar chart showing concentration of B7-H6 in (pg/ml) in the supernatants of untreated T98G cells, vehicle control-treated T98G cells (VC, DMSO) and 10 μM P3 Acetate-treated T98G cells. Unpaired T-test *p < 0.05, ***p<0.001, n=3.

4.5.3 ULBP3 shedding by T98G cells was below the lowest level of detection

T98G cells were treated with 10μM P3 Phosphate or P3 Acetate for 72 hours and the supernatants were collected and screened by ELISA to determine the effect of Q8 on ULBP3 shedding into the GBM tumour microenvironment (n=3). The ULBP3 levels at the 72 hour time point were too low to detect using an ELISA as the lowest limit of detection (LLOD) was 125 pg/ml *(Figure 64)*(Table 11). Future studies may warrant more sensitive ELISAs or concentration of supernatants to detect changes in ULBP shedding by T98G cells.

A) **B)**

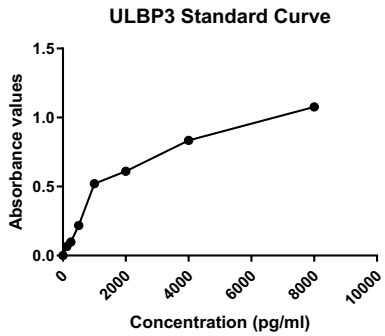

ULBP3 Concentration pg/ml				
Untreated cells	**Vehicle Control (DMSO)**	**P3 phosphate**	**P3 phosphate VC**	**P3 acetate**
-0.028	-0.048	-0.03	52.939	120.291

Figure 64: ULBP3 shedding by GBM T98G cells A) Line graph showing the standard curve of absorbance values vs concentration of ULPB3 shedding by GBM T98G cells. The standard curve ranges from 125 pg/ml-8000pg/ml with our samples being below the lowest level of detection, 0.12 pg/ml. **B)** Table 11: ULBP3 concentration pg/ml, samples were below the limit of detection.

4.5.4 MICA shedding by T98G cells was below the lowest level of detection

T98G cells were treated with 10 μM P3 Phosphate or P3 Acetate for 72 hours and the supernatants were collected and screened by ELISA to determine the effect of P3 on MICA/B shedding into the GBM tumour microenvironment (n=3). The MICA/B levels at the 72 hour time point were too low to detect using an ELISA as the lowest limit of detection (LLOD) was 39.0625 pg/ml *(Figure 65)*(Table 12). Future studies may warrant more sensitive ELISAs or concentration of supernatants to detect changes in ULBP shedding by T98G cells.

A) **B)**

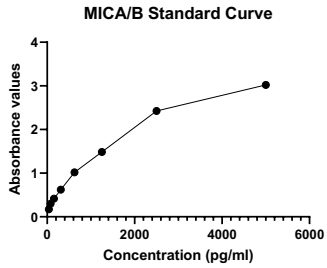

MICA/B Concentration pg/ml				
Untreated cells	**Vehicle Control (DMSO)**	**P3 phosphate**	**P3 phosphate VC**	**P3 acetate**
-480.444	-568.222	-534.889	-527.667	-528.222

Figure 65: MICA/B shedding by GBM T98G cells A) Line graph showing the standard curve of absorbance values vs concentration of MICA/B shedding by GBM T98G cells. The standard curve ranges from 39.0615 pg/ml-6000pg/ml with our samples being below the lowest level of detection, 0.12 pg/ml. **B)** Table 12: MICA/B concentration pg/ml, samples were below the limit of detection.

4.6 Elucidating the effects of P3 Phosphate and P3 Acetate on the GBM inflammatory secretome.

4.6.1 Neither P3 Phosphate nor P3 Acetate alter pro-inflammatory cytokine IL-6 secretion by T98G cells

T98G cells were treated with 10 μM P3 Phosphate or P3 Acetate for 72 hours and the supernatants were collected. These supernatants were screened by ELISA to determine the effect of P3 Phosphate /P3 Acetate on IL-6 concentration in the GBM tumour microenvironment. P3 Phosphate T98G cell supernatants displayed a decrease in IL-6 concentration at the 72 hour time point compared to the untreated cells, however it was close but not yet statistically significant and may need to be powered as there is some variability (untreated vs 10 μM P3 (2395.2 pg/ml vs 1938.2 pg/ml p=0.089)*(Figure 66A)*. There was a decrease between the vehicle control and 10 μM of P3 (VC vs 10 μM P3 (1938.2 pg/ml vs 17.68.2 pg/ml p=0.793) as well as a decrease between untreated and VC (2395.2 pg/ml vs 1938.2 pg/ml p=0.24)*(Figure 66A)*. P3 Acetate-treated T98G cell supernatants displayed a decrease in IL-6 concentration at the 72 hour time point compared to the untreated cells (Untreated vs 10 μM P3 Acetate (2395.2 pg/ml vs 2026.53 pg/ml p=0.38) *(Figure 66B)*. There was a significant increase between the vehicle control and 10 μM of P3 Acetate (VC vs 10 μM Q8 (178.53 pg/ml vs 2026.53 pg/ml p= <0.0001) *(Figure 66B)*. There was a significant decrease between untreated and VC suggesting that the vehicle significantly reduced IL-6 shedding, warranting further investigation (2395.2 pg/ml vs 178.53 pg/ml p= <0.0001).

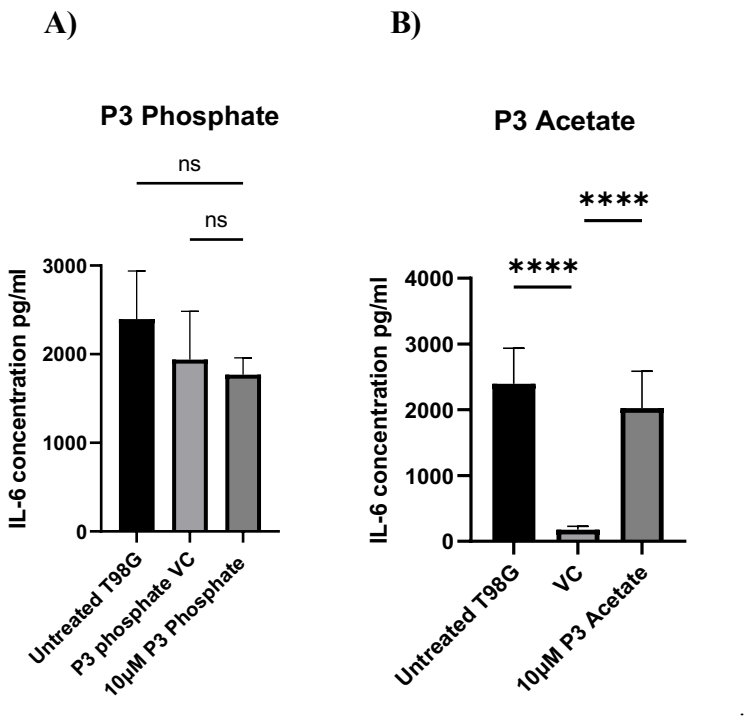

Figure 66: NKR ligand shedding (IL-6) by GBM T98G cells . Bar chart showing concentration of IL-6 in (pg/ml) in the supernatants of untreated T98G cells, vehicle control-treated T98G cells (VC, ethanol:dH_2O,6:4 or DMSO) and 10 μM **A)** P3 Phosphate-treated or **B)** P3 Acetate-treated T98G cells. One-way ANOVA, ns not significant, p****<0.0001 n=6

4.6.2 IL-17 secretion by GBM cells was below the lowest level of detection

T98G cells were treated with 10 μM P3 Phosphate or P3 Acetate for 72 hours and the supernatants were collected. The supernatants were screened by ELISA to determine the effect of P3 Phosphate and P3 acetate on IL-17 concentration in the GBM tumour microenvironment (n=3). The IL-17 levels at the 72 hour time point were too low to detect by ELISA. However, P3 acetate-treated cell supernatants contained detectable IL-17 unlike untreated or vehicle control treated T98G cell supernatants suggesting that this prodrug may increase inflammatory cytokine secretion to detectable levels *(Figure 67)*.

A) **B)**

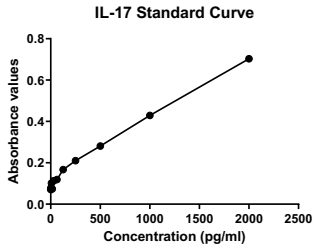

IL-17 Concentration pg/ml				
Untreated cells	**Vehicle control (DMSO)**	**P3 phosphate**	**P3 phosphate control**	**P3 acetate**
-94.333	-71	-77.666	-61	12.333
-154.333	-141	-77.666	-104.333	-117.667

Figure 67: A) Line graph showing the standard curve of absorbance values vs concentration of IL-17 shedding by GBM T98G cells. The standard curve ranges from 0.12 pg/ml-2500pg/ml with our levels being below the lowest level of detection, 0.12 pg/ml. **B)** Table 13 showing IL-17 concentration shown in pg/ml, samples were below the lowest limit of detection and could not be extrapolated from the curve with the exception of P3-acetate-treated T98G cell line supernatants.

4.6.3 Both P3 Phosphate and P3 Acetate significantly reduces secretion of TGF-ß by T98G cells

T98G cells were treated with 10 µM P3 or Q8 for 72 hours and the supernatants were collected. These supernatants were screened using ELISA to determine the effect of P3 Phosphate or P3 Acetate on TGF-ß concentration in the GBM tumour microenvironment. P3 Phosphate-treated T98G cell supernatants displayed a significant decrease in TGF-ß concentration at the 72 hour time point compared to the untreated cells and suggesting that this prodrug might have potential to alleviate TGF-ß-mediated deleterious effects in GBM tumours (untreated vs 10 µM P3 Phosphate, 719 pg/ml vs 407.33 pg/ml p=0.0033)(*Figure 68A)*. P3 Acetate-treated T98G cell supernatants displayed a significant decrease in TGF-ß concentration at the 72 hour time point compared to the VC (10 µM P3 Acetate vs VC, 547.33 pg/ml vs 106.5 pg/ml p=0.027)(*Figure 68B)*. There was a significant decrease between untreated and VC suggesting that the 0.1% DMSO vehicle control significantly reduced TGF-ß shedding, warranting further investigation control (untreated vs VC 719 pg/ml vs 106.5 pg/ml p=0.006).

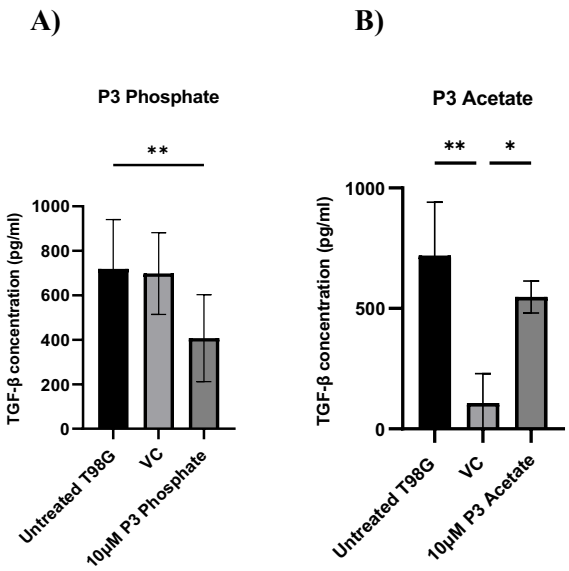

Figure 68: NKR ligand shedding (TGF- ß) by GBM T98G cells . Bar chart showing concentration of TGF-ß in (pg/ml) in the supernatants of untreated T98G cells, vehicle control-treated T98G cells (VC, ethanol:dH_2O,6:4, DMSO) and 10 μM **A)** P3 Phosphate-treated or **B)** P3 Acetate T98G cells. Paired T p**<0.01 and One-way ANOVA, p*<0.05, p**<0.01, n=3

4.6.4 P3 Phosphate significantly reduces TIMP-1 secretion by T98G cells

T98G cells were treated with 10 μM P3 Phosphate or P3 Acetate for 72 hours and the supernatants were collected. These supernatants were subject to an ELISA to determine the effect of P3 Phosphate or P3 Acetate on TIMP-1 concentration in the GBM tumour microenvironment. P3 Phosphate-treated T98G cell supernatants displayed a significant decrease in TIMP-1 concentration at the 72 hour time point compared to the untreated cells (untreated vs 10 μM P3 Phosphate, 2137.33 pg/ml vs 1979.83 pg/ml p=0.0011)(*Figure 69A).*There was a significant decrease between untreated and VC suggesting that the vehicle significantly reduced TIMP1 secretion, warranting further investigation into this control (untreated vs VC 2137.33 pg/ml vs 717.167 pg/ml p=0.006) *(Figure 69B)*.

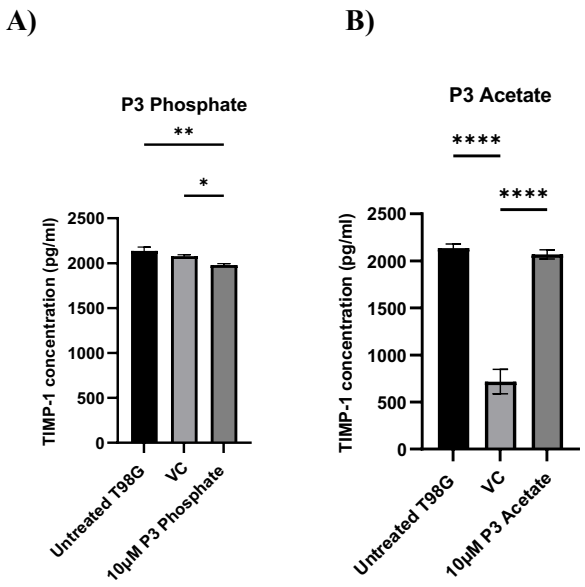

Figure 69: NKR ligand (TIMP-1) shedding by GBM T98G cells . Bar chart showing concentration of TIMP-1 in (pg/ml) in the supernatants of untreated T98G cells, vehicle control-treated T98G cells (VC, ethanol:dH_2O,6:4, DMSO) and 10 µM **A)** P3 Phosphate-treated or **B)** P3 Acetate T98G cells. One-way ANOVA, p*<0.05, p**<0.01, P****<0.0001 n=3

4.7 Elucidating the effects of P3 Phosphate on immune cell chemotaxis

The effects of P3 Phosphate on the migratory capacity of healthy donor-derived PBMC were elucidated. To achieve this, PBMC were treated with 10 µM of P3 Phosphate for 72 hours and their migration towards T98G supernatant was examined. There was a reduction in the migration of P3 Phosphate-treated lymphocytes toward T98G supernatants, compared to VC-treated lymphocytes but was not significant *(Figure 70A).*There was a statistically significant reduction in migration of P3 Phosphate-treated NK cells toward T98G cell supernatant, compared to untreated (Untreated vs 10µM P3 Phosphate, 1.0 vs 0.22, p=0.0043) as well as a statistically significant difference in T cell migration toward T98G cell supernatant, compared to untreated (Untreated vs 10µM P3 Phosphate, 1.0 vs 0.22, p=0.0256). This suggests that P3 Phosphate can alter the migratory capacity of key anti-tumour immune cells *(Figure 70 B,C).*

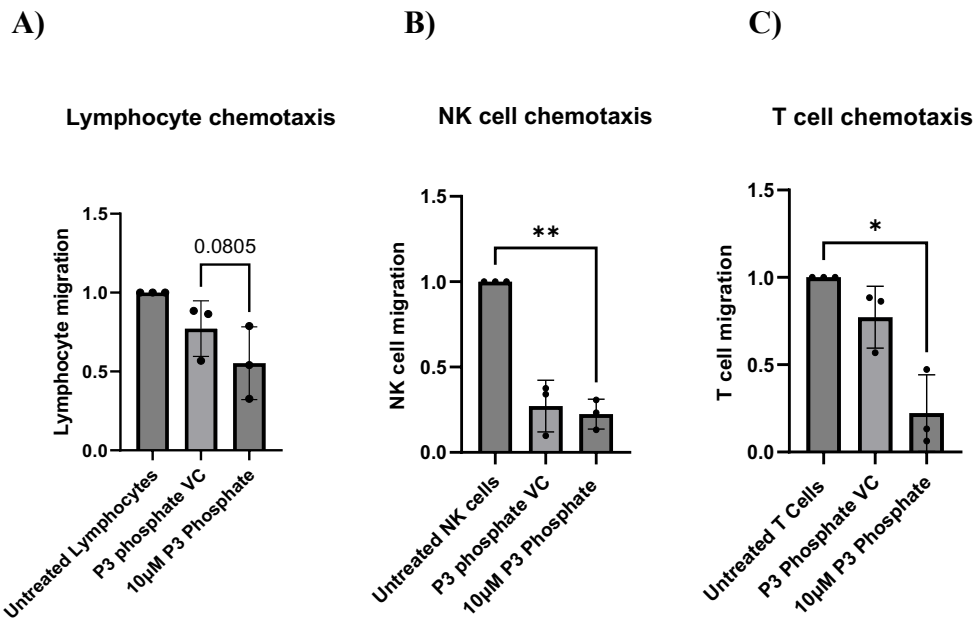

Figure 70: Immune cell chemotaxis, bar charts showing A) Lymphocyte cell migration: lymphocyte (treated with 10 µM P3 Phosphate for 72hrs) chemotaxis towards untreated GBM T98G cells compared to untreated T98G cells and VC (dH_20:ethanol 6:4) **B)** NK cell migration: NK cell (treated with 10 µM P3 Phosphate for 72hrs) chemotaxis towards untreated GBM T98G cells compared to untreated T98G cells and VC (DMSO). **C)** T cell migration: T cell (treated with 10 µM P3 Phosphate for 72hrs) chemotaxis towards untreated GBM T98G cells compared to untreated T98G cells and VC (DMSO), Paired T-test,*<0.05, **p<0.01, n=3.

5.0 Discussion

Glioblastoma multiforme (GBM) is a rapidly growing and aggressive malignant brain tumour. Despite advances in treatment options including surgical resection, radiation, chemotherapy and immunotherapy, most GBMs recur [92]. Current challenges to treating GBM include incomplete surgical resection, extreme genetic heterogeneity of the tumour, the Blood-Brain Barrier barrier (BBB), immune-suppressive microenvironment and treatment resistance [93][94]. Advances in the understanding of the molecular pathology of GBM and related oncogenic pathways signalling pathways, has identified distinct oncogenic pathways, giving hope for more targeted approaches [92]. Here we tested the utility of 2 novel compounds for their anti-cancer efficacy in the T98G cell line.

The efficacy of targeted therapy relies on targeting specific molecular alterations in a tumour or their downstream protein products which maintains malignant cells growth, enhancing tumour invasion and angiogenesis. Alternatively, targeting a pathway that enhances the immune recognition of the GBM cells could enhance tumour killing. Murphy et al., (2016) showed that treatment with 10 μM Q8 in colorectal cancer (CRC) resulted in significant reduction in secretions of important angiogenic mediators like VEGF [83]. Here, we proposed that Q8 could have potential in GBM as anti-angiogenic agents have promising clinical results. [81],[95]. Buckley et al., (2020) demonstrated that pyrazinib (P3) significantly inhibited IL-1β secretion and increased IL-3 and IL-17ß secretion from treatment-naïve biopsies from oesophageal adenocarcinoma (OAC) patients [88]. The ability of pyrazinib (P3) to sensitise OAC tumour cells to radiotherapy and its anti-metabolic utility *via* inhibition of both oxidative phosphorylation and glycolysis is a critical finding and its extended use to other malignancies is a desirable concept [88]. Furthermore, pilot data from Prof. Jacintha O'Sullivan's lab suggest that P3 renders radioresistant OAC tumours as more susceptible to NK cell-mediated responses and might have utility as a NK cell therapy sensitiser. In this study, P3 was tested for its anti-proliferative, anti-inflammatory, and immunomodulatory effects as well as its treatment sensitizing utility in GBM.

5.1 P3 and Q8 slightly but significantly reduced T98G cell viability

This study explored the utility of 2 compounds, P3 and Q8 individually for their anti-cancer efficacy in the GBM cell line T98G. Our data show that T98G cells that were treated with 10 μM of P3 or Q8 for 72 hours have a slight, but significant reduction in their viability when compared to untreated T98G cells. The limited availability of P3 restricted a dose escalation study and further work is required to indicate if varying doses and timepoints elicit greater toxicity in T98G cells.

5.2 P3 and Q8 did not sensitise T98G cells to Temozolomide

Temozolomide (TMZ) is an alkylating agent that is used as standard-of-care in GBM treatment. However, using single agent TMZ, the overall survival of GBM patients is only slightly increased, with most patients being resistant to TMZ treatment [96]. Bevacizumab is a monoclonal antibody that targets VEGF-A, thereby inhibiting its downstream signalling activity by putting stress on the interaction with its VEGF receptor. This approved drug was proven to target tumour angiogenesis in GBM [97]. Studies showed that Bevacizumab alone didn't improve overall survival (OS) or relatively high response rate [98]. However, several clinical trials have been initiated to explore the efficacy of this drug in combination with chemotherapies. Yang et al., (2017) carried out a study demonstrating that when Bevacizumab was combined with chemotherapy it improved progression-free survival compared to bevacizumab or chemotherapy alone [98].

Our study showed that when T98G cells (a GBM cell line with propensity to TMZ resistance [96]) were treated with TMZ alone for 72 hours there was a dose-dependent decrease in cell viability as expected. However, when TMZ was combined with 10 μM P3 or Q8 they did not sensitise the T98G cells to TMZ. Increasing the concentration of these novel drugs in combination with low dose TMZ, might provide more insights into the utility of P3 and Q8 sensitise T98G cells or other cell lines to chemotherapy. In addition, pretreatment with P3 or Q8, rather than concurrent TMZ treatment could increase sensitivity as it would reduce competition between the compounds and inform more about the sequenced timing of these compounds.

5.3 P3 and Q8 reduce IL-6 secretion by T98G cells

Interleukin-6 (IL-6) is a pro-inflammatory cytokine that has a major role in the modulation of immune and inflammatory responses in glioblastoma [99]. The expression levels of this cytokine can be used as a prognostic indicator due to its ability to promote proliferation and block apoptosis that is induced by various chemotherapeutic compounds or reactive oxygen species, thus promoting malignant progression [100], [101]. Liu et al., (2010) showed that IL-6 also promotes cell invasion and migration in U251 and T98G cell lines [99]. Additionally, IL-6 facilitates tumour angiogenesis and invasion, suggesting that this cytokine has the potential to be an anti-invasion target [99]. Our results show that T98G cells treated with either 10 μM P3 or Q8 for 72 hours cause a reduction in IL-6 secretion by T98G cells and future work should evaluate their potential to inhibit angiogenesis and invasion in GBM. GBM cell-derived IL-6 has been shown as a promoter of PDL1-mediated immunosuppression and therefore, its reduction in the GBM tumour microenvironment by P3 and Q8 could augment the anti-tumour immune response [102].

5.4 TGF-ß and TIMP-1 decreased when treated with P3 or Q8

Glioblastomas are highly vascular tumours that are able to secrete several angiogenic factors [103], [104]. Studies have shown that angiogenesis is essential for the proliferation and survival of malignant glioma cells and therefore inhibition of angiogenesis may be effective as an alternative therapeutic strategy [95]. The TGF-ß cytokine and TIMP-1 signalling molecule both promote angiogenesis in GBM. Recently TIMP-1 upregulation was shown to be involved in mechanisms of resistance to anti-VEGF treatment and it is therefore likely to become more important in future glioblastoma research [95]. Whereas, transforming growth factor β1 (*TGFβ1*) mediates angiogenesis through a combination of mechanisms that regulate *VEGF* expression, stimulate endothelial cell proliferation, and regulate expression of proteases implicated in vessel dissolution and migration [105]. Papachristodoulou et al., (2019) showed that targeting TGF-ß expression with two novel phosphorothioate-locked nucleic acid (LNA)-modified antisense oligonucleotide gapmers, ISTH1047 and ISTH0047, which specifically target $TGF\beta_1$ and $TGF\beta_2$ have promising anti-glioma activity *in vitro* and *in vivo* [106]. Our study showed that 10 μM of P3 or Q8 caused significant decreases in both TGF-ß

and TIMP-1 which shows that these novel drugs may have the potential to target pro-angiogenic mediators in T98G cells.

There is little published data on the cellular impact of P3 and its mechanism of action is unknown. For the first time, our data indicate that P3 may have the potential to reduce the secretion of pro-tumourigenic factors in the GBM tumour microenvironment.

5.5 P3 enhanced death receptor expression by T98G cells

NK cells are crucial in the anti-tumour response. This study assessed the impact of P3 on the susceptibility of GBM tumours to NK cells as well as the direct immunomodulatory effect of the drug on NK cell phenotype and function. Pilot data revealed that P3 can increase expression of NK cell receptor (NKR) ligands in the radioresistant oesophageal cancer cell line OE33R and here, we investigated its effect on NKR ligand expression by the T98G cell line.

Apoptosis is a key mechanism that ensures the normal, physiological process of cell number regulation, resulting in the elimination of unnecessary or damaged cells. Cell death pathways are frequently inactivated in human cancers, including glioblastoma, as tumour cells are able to evade programmed cell death leading to further tumour progression and pathogenesis [107]. In the death receptor (extrinsic) pathway, apoptosis can be promoted when death receptor ligands trigger their receptor on the cell surface. Death receptors are part of the tumour necrosis factor (TNF) family of receptors, including Fas and death receptors 4 and 5, also named TRAIL-R1 and TRAIL-R2 [108], with corresponding death receptor ligands, Fas ligand and TNF-related apoptosis-inducing ligand (TRAIL)[109]. Reactivation of programmed cell death represents a promising therapeutic strategy for glioblastoma [107]. Our study showed that T98G cells that were treated with 10 μM P3 exhibited an increase in death receptor surface expression. Confirmation that the loss of cell viability seen previously occurs *via* apoptosis would confirm the biological consequences of such P3-induced TRAIL-R2 expression.

5.6 P3 enhanced activating receptor surface expression by T98G cells and may reduce NKR ligand shedding

Natural killer (NK) cells are key immune effector cells in the anti-tumour response. Through the engagement of several different activating and inhibitory receptors, these cytotoxic lymphocytes are able to recognise transformed cells [110]. Multiple studies have shown that the expression of NK cell activating receptor are frequently decreased during the development and progression of cancers. Our results indicated that culture of NK cells in T98G cell supernatants for 24 hours led to decreased NKG2D, CD69 and NKP30 expression. However, supernatants from T98G cells treated with P3 for 24 hours did not reduce these activating receptors NKG2D, NKp30 and CD69 thus strongly suggesting that P3 prevents GBM-mediated downregulation of NK cell activating receptors.

One way NKG2D is decreased on NK cells is *via* the immune-suppressive cytokine TGF-ß [111],[112]. P3-mediated prevention of NKG2D downregulation in NK cells cultured in T98G supernatant is paralleled by P3-mediated reduction of TGF-ß secretion by T98G cells suggesting that this novel compound has potential to alleviate NK cell modulation in the GBM tumour microenvironment.

The second way in which surface expression of NKR activating receptors by NK cells can be reduced is *via* shedding of their ligands by cancer cells. Many tumours have developed a strategy to evade immunosurveillance and detection by NK cells *via* NKR ligand shedding [110]. This evasion mechanism serves to; A) decrease the amount of NKR ligand at the tumour cell surface, leading to an impaired NK cell recognition and B) decrease the amount of NKR surface expression on the NK cell surface as they are bound to soluble NKR ligands. [113],[114]. Studies have shown that GBM cells release activating receptor NKG2D (i.e., MICA/B and ULBPs) and NKp30 (i.e., B7- H6) ligands through proteolytic cleavage thus, its inhibition could be exploited as an encouraging strategy to preserve the ligands on the surface of cancer cells and to enhance anti-tumour immunity. Interestingly, we also observed that the shedding of NKp30 ligand B7-H6 decreased following a 72 hour treatment with 10 μM P3 suggesting that P3 attenuates NKP30 downregulation by reducing B7-H6 shedding by T98G cells suggesting another mechanism through which this novel compound might alleviate NK cell modulation in the GBM tumour microenvironment.

Interestingly, the immunomodulatory effects and the P3-mediated rescue is only observed when NK cells are cultured in T98G cell supernatant and not when they are co-cultured with

T98G cells suggesting that P3 has a strong effect on the T98G secretome and that T98G cell-derived soluble mediators elicit significant deleterious effects on the immune response

NK cells are the least abundant population of all immune cells that infiltrate the GBM tumour microenvironment. However, despite the quantity of NK cells in the TME being low they still have a potent cytotoxic effect [115]. NK cell migration is a key mechanism to find and kill target cells, this process is driven by the chemokine system which governs immune cell movement or chemotaxis [116]. Therefore, the development of new methods to increase the number of NK cells in GBM tumours could help improve tumour eradication. In our study P3-treated T98G cells recruit less NK cells which could have negative consequences for NK cell therapy and should be investigated further. In contrast, the migratory capacity of NK cells was unaffected by direct P3 treatment.

In summary, we have shown that P3 has no significant immunomodulatory effects on healthy NK cells and has strong potential to attenuate GBM-mediated downregulation of activating receptors on NK cells. This shows that P3 has the potential to be used in patients as it had no overall negative effects on circulating NK cell phenotype and function, and this adds promise for other malignancies such as OAC in which a deeper investigation of the potential off-target effects of systemic P3 is needed to further understand its suitability for combination use with first-line therapies and immunotherapies.

5.7 Potential anti-proliferative utility of P3 Phosphate in GBM

Our final aim generated prodrugs of P3 (P3 Phosphate and P3 Acetate) to improve solubility and uncovered novel data on the antitumour efficacy of these prodrugs in comparison to P3. Our results showed that when T98G cells were treated with 10μM P3 Phosphate or P3 Acetate there was significant reduction in T98G cell viability compared to untreated. P3 phosphate elicited a greater cell death response compared to P3, P3 Acetate and Q8. The attachment of phosphate esters allows for the increased solubility of this prodrug compared to the parent compound, making it easier for pro-drug to enter the cell and this could be a potential indication of the increased in cell death. Alternatively, the different moiety on the molecule may initiate a different mechanism within the cell. When TMZ was combined with 10 μM P3 Phosphate it did not sensitise the T98G cells to TMZ. Further work is required to assess if pretreatment with P3 Phosphate has a more profound effect or treatment with lower dose of TMZ + P3 Phosphate

shows superior results. Future work will examine whether P3 Phosphate at varying concentration and/or prior to TMZ treatment could increase in the cell death response could be seen.

The NKR ligand shedding of NKp30 ligand B7-H6 decreased following a 72 hour treatment with 10 μM P3 Phosphate or P3 Acetate. We also showed significant decreases in both TGF-ß and TIMP-1 which indicates that P3 Phosphate and P3 Acetate may dampen the secretion of pro-angiogenic mediatorses in the GBM tumour microenvironment. Our study showed when T98G cells were treated with P3 phosphate they recruited less total T cells. This could have negative consequences for the anti-tumour immune response if such T cells were found to be Th1 and CD8+ T cells . However, this could be positive if Treg infiltration of GBM tumours was reduced by P3 Phosphate. Further work will elucidate the phenotype of T cells migrating toward T98G cells following P3 treatment. Importantly, the NK cell and total lymphocyte migratory capacity was not significantly affected by direct P3 Phosphate treatment. A deeper investigation of the effects of P3 Phosphate and P3 Acetate on NK cell and T cell viability, phenotype and function is needed to complete the comparison of their biological effects with parent drug P3.

6.0 Conclusion

Our data suggest that Pyrazinib (P3) a small molecule pyrazine compound, the prodrug P3 Phosphate, Intermediate compound P3 Acetate and Q8, an antagonist of cysteinyl leukotriene receptor-1 may have potential to reduce the immunomodulatory effects of GBM tumours. The P3, P3 Phosphate and P3 acetate compounds were synthesized and purified successfully in house. Used individually, we have shown reduction of GBM cell viability and an increase in apoptotic death receptor expression. The drugs have not shown a therapeutic potential in combination with standard GBM chemotherapeutic agent TMZ, at the tested dose of 10 μM. However, pre-treatment and or increased drug concentrations may uncover their utility in combination with TMZ and other therapeutic agents. P3 had no significant immunomodulatory effects on healthy NK cells but could alleviate the inhibitory effects of the GBM secretome on NK cell activating receptor expression. In addition, P3 reduced IL-6 secretion by GBM cells along with pro-tumourigenic factors, TGF-ß and TIMP-1. Interestingly, P3 and P3 Phosphate significantly reduced B7-H6 shedding by T98G cells which indicates their potential to help reduce immunomodulation of NK cells in the GBM TME. Further work is required to fully elucidate the impact of P3 and related compounds on NK cell phenotype and function and its potential in combination with first-line therapies and/or immunotherapies in GBM.

7.0 Future directions

1. Based on this study, higher and varying doses of the individual novel drugs tested, Pyrazinib (P3), the prodrug P3 Phosphate, Intermediate compound P3 acetate and Q8, require further study for their anti-proliferative effects on T98G cells.

2. Combination anti-cancer therapy has huge potential and timing can be crucial. Pre-treatment of T98G cells with our novel drugs may promote their efficacy to sensitise T98G cells to TMZ rather than concurrent treatment and would inform on sequenced timing of combination treatment.

3. This study was carried out on the T98G cell line which has shown chemoresistance in multiple studies. Therefore, an alternative GBM cell line should be examined individually and in combination TMZ. The radio-resistance pathways in GBM are known and therefore the radiosensitivity of T98G cells and other cell lines should be examined following pre-treatment with our novel compounds.

4. The efficacy of our panel of novel drugs should be elucidated under the physiological conditions of the tumour microenvironment e.g., hypoxia, acidosis, nutrient deprivation to more accurately simulate the GBM TME and examine their clinical utility.

5. The reduction of pro-inflammatory mediator IL-6 and pro-tumourigenic mediators TGF-ß and TIMP-1 should be further investigated in terms of the impact of such drug-induced reductions on tumour cell growth and invasion.

6. NK killing assays should be performed to ascertain whether P3 and P3 Phosphate can augment NK cell killing in the GBM tumour microenvironment. Furthermore, the direct phenotypic and functional effects of P3 Phosphate on NK cells should be uncovered.

8.0 Bibliography

[1] I. Golán, L. Rodríguez de la Fuente, and J. Costoya, "NK Cell-Based Glioblastoma Immunotherapy," *Cancers (Basel)*, vol. 10, no. 12, p. 522, Dec. 2018, doi: 10.3390/cancers10120522.

[2] D. W. Donnelly, L. A. Anderson, and A. Gavin, "Cancer Incidence Projections in Northern Ireland to 2040," *Cancer Epidemiology, Biomarkers & Prevention*, vol. 29, no. 7, pp. 1398–1405, Jul. 2020, doi: 10.1158/1055-9965.EPI-20-0098.

[3] S. de Vleeschouwer, Ed., *Glioblastoma*. Codon Publications, 2017. doi: 10.15586/codon.glioblastoma.2017.

[4] K. Eder and B. Kalman, "Molecular Heterogeneity of Glioblastoma and its Clinical Relevance," *Pathology & Oncology Research*, vol. 20, no. 4, pp. 777–787, Oct. 2014, doi: 10.1007/s12253-014-9833-3.

[5] H. Zhao *et al.*, "Recent advances in the use of PI3K inhibitors for glioblastoma multiforme: current preclinical and clinical development," *Mol Cancer*, vol. 16, no. 1, p. 100, Dec. 2017, doi: 10.1186/s12943-017-0670-3.

[6] K. Urbańska, J. Sokołowska, M. Szmidt, and P. Sysa, "Review Glioblastoma multiforme – an overview," *Współczesna Onkologia*, vol. 5, pp. 307–312, 2014, doi: 10.5114/wo.2014.40559.

[7] S. Karcher *et al.*, "Different angiogenic phenotypes in primary and secondary glioblastomas," *Int J Cancer*, vol. 118, no. 9, pp. 2182–2189, May 2006, doi: 10.1002/ijc.21648.

[8] M. G. Castro *et al.*, "Gene Therapy and Targeted Toxins for Glioma," *Curr Gene Ther*, vol. 11, no. 3, pp. 155–180, Jun. 2011, doi: 10.2174/156652311795684722.

[9] J. R. Simpson *et al.*, "Influence of location and extent of surgical resection on survival of patients with glioblastoma multiforme: Results of three consecutive radiation therapy oncology group (RTOG) clinical trials," *International Journal of Radiation Oncology*Biology*Physics*, vol. 26, no. 2, pp. 239–244, May 1993, doi: 10.1016/0360-3016(93)90203-8.

[10] K. L. Kislin, W. S. McDonough, J. M. Eschbacher, B. A. Armstrong, and M. E. Berens, "NHERF-1: Modulator of Glioblastoma Cell Migration and Invasion," *Neoplasia*, vol. 11, no. 4, pp. 377-IN7, Apr. 2009, doi: 10.1593/neo.81572.

[11] R. Stupp *et al.*, "Radiotherapy plus Concomitant and Adjuvant Temozolomide for Glioblastoma," *New England Journal of Medicine*, vol. 352, no. 10, pp. 987–996, Mar. 2005, doi: 10.1056/NEJMoa043330.

[12] M. E. Hegi *et al.*, "*MGMT* Gene Silencing and Benefit from Temozolomide in Glioblastoma," *New England Journal of Medicine*, vol. 352, no. 10, pp. 997–1003, Mar. 2005, doi: 10.1056/NEJMoa043331.

[13] S. Kumari, S. M. Ahsan, J. M. Kumar, A. K. Kondapi, and N. M. Rao, "Overcoming blood brain barrier with a dual purpose Temozolomide loaded Lactoferrin nanoparticles for combating glioma (SERP-17-12433)," *Sci Rep*, vol. 7, no. 1, p. 6602, Dec. 2017, doi: 10.1038/s41598-017-06888-4.

[14] E. C. Filippi-Chiela *et al.*, "Resveratrol abrogates the Temozolomide-induced G2 arrest leading to mitotic catastrophe and reinforces the Temozolomide-induced senescence in glioma cells," *BMC Cancer*, vol. 13, no. 1, p. 147, Dec. 2013, doi: 10.1186/1471-2407-13-147.

[15] J. N. Sarkaria *et al.*, "Mechanisms of Chemoresistance to Alkylating Agents in Malignant Glioma," *Clinical Cancer Research*, vol. 14, no. 10, pp. 2900–2908, May 2008, doi: 10.1158/1078-0432.CCR-07-1719.

[16] X. Qian *et al.*, "Sequence-Dependent Synergistic Inhibition of Human Glioma Cell Lines by Combined Temozolomide and miR-21 Inhibitor Gene Therapy," *Mol Pharm*, vol. 9, no. 9, pp. 2636–2645, Sep. 2012, doi: 10.1021/mp3002039.

[17] S. Y. Lee, "Temozolomide resistance in glioblastoma multiforme," *Genes Dis*, vol. 3, no. 3, pp. 198–210, Sep. 2016, doi: 10.1016/j.gendis.2016.04.007.

[18] N. Singh, A. Miner, L. Hennis, and S. Mittal, "Mechanisms of temozolomide resistance in glioblastoma - a comprehensive review," *Cancer Drug Resistance*, 2020, doi: 10.20517/cdr.2020.79.

[19] J. Feldheim, A. F. Kessler, C. M. Monoranu, R.-I. Ernestus, M. Löhr, and C. Hagemann, "Changes of O6-Methylguanine DNA Methyltransferase (MGMT) Promoter Methylation in Glioblastoma Relapse—A Meta-Analysis Type Literature Review," *Cancers (Basel)*, vol. 11, no. 12, p. 1837, Nov. 2019, doi: 10.3390/cancers11121837.

[20] A. L. Rivera *et al.*, "MGMT promoter methylation is predictive of response to radiotherapy and prognostic in the absence of adjuvant alkylating chemotherapy for glioblastoma," *Neuro Oncol*, vol. 12, no. 2, pp. 116–121, Feb. 2010, doi: 10.1093/neuonc/nop020.

[21] B. K. Hendricks, A. A. Cohen-Gadol, and J. C. Miller, "Novel delivery methods bypassing the blood-brain and blood-tumor barriers," *Neurosurg Focus*, vol. 38, no. 3, p. E10, Mar. 2015, doi: 10.3171/2015.1.FOCUS14767.

[22] G. Koukourakis *et al.*, "Temozolomide with Radiation Therapy in High Grade Brain Gliomas: Pharmaceuticals Considerations and Efficacy;A Review Article," *Molecules*, vol. 14, no. 4, pp. 1561–1577, Apr. 2009, doi: 10.3390/molecules14041561.

[23] M. Fry and A. v. Ferguson, "The sensory circumventricular organs: Brain targets for circulating signals controlling ingestive behavior," *Physiol Behav*, vol. 91, no. 4, pp. 413–423, Jul. 2007, doi: 10.1016/j.physbeh.2007.04.003.

[24] Y. Ramirez, J. Weatherbee, R. Wheelhouse, and A. Ross, "Glioblastoma Multiforme Therapy and Mechanisms of Resistance," *Pharmaceuticals*, vol. 6, no. 12, pp. 1475–1506, Nov. 2013, doi: 10.3390/ph6121475.

[25] S. Tiwary, J. E. Morales, S. C. Kwiatkowski, F. F. Lang, G. Rao, and J. H. McCarty, "Metastatic Brain Tumors Disrupt the Blood-Brain Barrier and Alter Lipid Metabolism by Inhibiting Expression of the Endothelial Cell Fatty Acid Transporter Mfsd2a," *Sci Rep*, vol. 8, no. 1, p. 8267, Dec. 2018, doi: 10.1038/s41598-018-26636-6.

[26] M. W. Pitz, A. Desai, S. A. Grossman, and J. O. Blakeley, "Tissue concentration of systemically administered antineoplastic agents in human brain tumors," *J Neurooncol*, vol. 104, no. 3, pp. 629–638, Sep. 2011, doi: 10.1007/s11060-011-0564-y.

[27] F. Ohka, A. Natsume, and T. Wakabayashi, "Current Trends in Targeted Therapies for Glioblastoma Multiforme," *Neurol Res Int*, vol. 2012, pp. 1–13, 2012, doi: 10.1155/2012/878425.

[28] S. Agnihotri *et al.*, "Glioblastoma, a Brief Review of History, Molecular Genetics, Animal Models and Novel Therapeutic Strategies," *Arch Immunol Ther Exp (Warsz)*, vol. 61, no. 1, pp. 25–41, Feb. 2013, doi: 10.1007/s00005-012-0203-0.

[29] R. Magaña-Maldonado *et al.*, "Immunological Evasion in Glioblastoma," *Biomed Res Int*, vol. 2016, pp. 1–7, 2016, doi: 10.1155/2016/7487313.

[30] A. Gieryng, D. Pszczolkowska, K. A. Walentynowicz, W. D. Rajan, and B. Kaminska, "Immune microenvironment of gliomas," *Laboratory Investigation*, vol. 97, no. 5, pp. 498–518, May 2017, doi: 10.1038/labinvest.2017.19.

[31] R. Uyar, "Glioblastoma microenvironment: The stromal interactions," *Pathol Res Pract*, vol. 232, p. 153813, Apr. 2022, doi: 10.1016/j.prp.2022.153813.

[32] W. Humphries, J. Wei, J. H. Sampson, and A. B. Heimberger, "The Role of Tregs in Glioma-Mediated Immunosuppression: Potential Target for Intervention," *Neurosurg Clin N Am*, vol. 21, no. 1, pp. 125–137, Jan. 2010, doi: 10.1016/j.nec.2009.08.012.

[33] S. F. Hussain, D. Yang, D. Suki, K. Aldape, E. Grimm, and A. B. Heimberger, "The role of human glioma-infiltrating microglia/macrophages in mediating antitumor immune responses1," *Neuro Oncol*, vol. 8, no. 3, pp. 261–279, Jul. 2006, doi: 10.1215/15228517-2006-008.

[34] M. H. Shin, J. Kim, S. A. Lim, J. Kim, S.-J. Kim, and K.-M. Lee, " (Perrin, et al., 2019)*Immune Netw*, vol. 20, no. 2, 2020, doi: 10.4110/in.2020.20.e14.

[35] D. D. Chaplin, "Overview of the immune response," *Journal of Allergy and Clinical Immunology*, vol. 125, no. 2, pp. S3–S23, Feb. 2010, doi: 10.1016/j.jaci.2009.12.980.

[36] S. Paul and G. Lal, "The Molecular Mechanism of Natural Killer Cells Function and Its Importance in Cancer Immunotherapy," *Front Immunol*, vol. 8, Sep. 2017, doi: 10.3389/fimmu.2017.01124.

[37] F. Fasbender and C. Watzl, "Impedance-based analysis of Natural Killer cell stimulation," *Sci Rep*, vol. 8, no. 1, p. 4938, Dec. 2018, doi: 10.1038/s41598-018-23368-5.

[38] L. L. Lanier, “Follow the Leader: NK Cell Receptors for Classical and Nonclassical MHC Class I,” *Cell*, vol. 92, no. 6, pp. 705–707, Mar. 1998, doi: 10.1016/S0092-8674(00)81398-7.

[39] L. L. Lanier, “Up on the tightrope: natural killer cell activation and inhibition,” *Nat Immunol*, vol. 9, no. 5, pp. 495–502, May 2008, doi: 10.1038/ni1581.

[40] M. G. Morvan and L. L. Lanier, “NK cells and cancer: you can teach innate cells new tricks,” *Nat Rev Cancer*, vol. 16, no. 1, pp. 7–19, Jan. 2016, doi: 10.1038/nrc.2015.5.

[41] C. S. Backes, K. S. Friedmann, S. Mang, A. Knörck, M. Hoth, and C. Kummerow, “Natural killer cells induce distinct modes of cancer cell death: Discrimination, quantification, and modulation of apoptosis, necrosis, and mixed forms,” *Journal of Biological Chemistry*, vol. 293, no. 42, pp. 16348–16363, Oct. 2018, doi: 10.1074/jbc.RA118.004549.

[42] M. W. Bennett *et al.*, “The Fas counterattack in vivo: apoptotic depletion of tumor-infiltrating lymphocytes associated with Fas ligand expression by human esophageal carcinoma.,” *J Immunol*, vol. 160, no. 11, pp. 5669–75, Jun. 1998.

[43] T. Burster, F. Gärtner, C. Bulach, A. Zhanapiya, A. Gihring, and U. Knippschild, “Regulation of MHC I Molecules in Glioblastoma Cells and the Sensitizing of NK Cells,” *Pharmaceuticals*, vol. 14, no. 3, p. 236, Mar. 2021, doi: 10.3390/ph14030236.

[44] R. T. Costello *et al.*, “Defective expression and function of natural killer cell–triggering receptors in patients with acute myeloid leukemia,” *Blood*, vol. 99, no. 10, pp. 3661–3667, May 2002, doi: 10.1182/blood.V99.10.3661.

[45] A. Yamauchi, K. Taga, H. Mostowski, and E. Bloom, “Target cell-induced apoptosis of interleukin-2-activated human natural killer cells: roles of cell surface molecules and intracellular events,” *Blood*, vol. 87, no. 12, pp. 5127–5135, Jun. 1996, doi: 10.1182/blood.V87.12.5127.bloodjournal87125127.

[46] M. Dapash, D. Hou, B. Castro, C. Lee-Chang, and M. S. Lesniak, “The Interplay between Glioblastoma and Its Microenvironment,” *Cells*, vol. 10, no. 9, p. 2257, Aug. 2021, doi: 10.3390/cells10092257.

[47] M. Sabry and M. W. Lowdell, “NK Cells and Cancer,” in *Natural Killer Cells*, InTech, 2017. doi: 10.5772/intechopen.69658.

[48] A. Poli *et al.*, “Targeting glioblastoma with NK cells and mAb against NG2/CSPG4 prolongs animal survival,” *Oncotarget*, vol. 4, no. 9, pp. 1527–1546, Sep. 2013, doi: 10.18632/oncotarget.1291.

[49] C. A. Crane, S. J. Han, J. J. Barry, B. J. Ahn, L. L. Lanier, and A. T. Parsa, “TGF- downregulates the activating receptor NKG2D on NK cells and CD8+ T cells in glioma patients,” *Neuro Oncol*, vol. 12, no. 1, pp. 7–13, Jan. 2010, doi: 10.1093/neuonc/nop009.

[50] D. Strepkos, M. Markouli, A. Klonou, C. Piperi, and A. G. Papavassiliou, “Insights in the immunobiology of glioblastoma,” *J Mol Med*, vol. 98, no. 1, pp. 1–10, Jan. 2020, doi: 10.1007/s00109-019-01835-4.

[51] L. Martin-Hijano and B. Sainz, “The Interactions Between Cancer Stem Cells and the Innate Interferon Signaling Pathway,” *Front Immunol*, vol. 11, Mar. 2020, doi: 10.3389/fimmu.2020.00526.

[52] A. K. Kozlowska *et al.*, “Resistance to cytotoxicity and sustained release of interleukin-6 and interleukin-8 in the presence of decreased interferon-γ after differentiation of glioblastoma by human natural killer cells,” *Cancer Immunology, Immunotherapy*, vol. 65, no. 9, pp. 1085–1097, Sep. 2016, doi: 10.1007/s00262-016-1866-x.

[53] C.-Y. Huang, C.-L. Chung, T.-H. Hu, J.-J. Chen, P.-F. Liu, and C.-L. Chen, “Recent progress in TGF-β inhibitors for cancer therapy,” *Biomedicine & Pharmacotherapy*, vol. 134, p. 111046, Feb. 2021, doi: 10.1016/j.biopha.2020.111046.

[54] W. Wick, U. Naumann, and M. Weller, “Transforming Growth Factor-β: A Molecular Target for the Future Therapy of Glioblastoma,” *Curr Pharm Des*, vol. 12, no. 3, pp. 341–349, Jan. 2006, doi: 10.2174/138161206775201901.

[55] B. Qiu *et al.*, “IL-10 and TGF-β2 are overexpressed in tumor spheres cultured from human gliomas,” *Mol Biol Rep*, vol. 38, no. 5, pp. 3585–3591, Jun. 2011, doi: 10.1007/s11033-010-0469-4.

[56] E. Batlle and J. Massagué, “Transforming Growth Factor-β Signaling in Immunity and Cancer,” *Immunity*, vol. 50, no. 4, pp. 924–940, Apr. 2019, doi: 10.1016/j.immuni.2019.03.024.

[57] P. André *et al.*, “Anti-NKG2A mAb Is a Checkpoint Inhibitor that Promotes Anti-tumor Immunity by Unleashing Both T and NK Cells,” *Cell*, vol. 175, no. 7, pp. 1731-1743.e13, Dec. 2018, doi: 10.1016/j.cell.2018.10.014.

[58] C. Alifieris and D. T. Trafalis, “Glioblastoma multiforme: Pathogenesis and treatment,” *Pharmacol Ther*, vol. 152, pp. 63–82, Aug. 2015, doi: 10.1016/j.pharmthera.2015.05.005.

[59] J. Hsu *et al.*, “Contribution of NK cells to immunotherapy mediated by PD-1/PD-L1 blockade,” *Journal of Clinical Investigation*, vol. 128, no. 10, pp. 4654–4668, Sep. 2018, doi: 10.1172/JCI99317.

[60] J. L. Oyer, S. B. Gitto, D. A. Altomare, and A. J. Copik, “PD-L1 blockade enhances anti-tumor efficacy of NK cells,” *Oncoimmunology*, vol. 7, no. 11, p. e1509819, Nov. 2018, doi: 10.1080/2162402X.2018.1509819.

[61] J. Han, C. A. Alvarez-Breckenridge, Q.-E. Wang, and J. Yu, “TGF-β signaling and its targeting for glioma treatment,” *Am J Cancer Res*, vol. 5, no. 3, pp. 945–955, Feb. 2015, [Online]. Available: https://pubmed.ncbi.nlm.nih.gov/26045979

[62] D. A. Wainwright *et al.*, “Durable Therapeutic Efficacy Utilizing Combinatorial Blockade against IDO, CTLA-4, and PD-L1 in Mice with Brain Tumors,” *Clinical Cancer Research*, vol. 20, no. 20, pp. 5290–5301, Oct. 2014, doi: 10.1158/1078-0432.CCR-14-0514.

[63] J. vom Berg *et al.*, "Intratumoral IL-12 combined with CTLA-4 blockade elicits T cell–mediated glioma rejection," *Journal of Experimental Medicine*, vol. 210, no. 13, pp. 2803–2811, Dec. 2013, doi: 10.1084/jem.20130678.

[64] G. Sconocchia *et al.*, "NK cells and T cells cooperate during the clinical course of colorectal cancer," *Oncoimmunology*, vol. 3, no. 8, p. e952197, Aug. 2014, doi: 10.4161/21624011.2014.952197.

[65] C. J. Forlenza *et al.*, "*KIR3DL1* Allelic Polymorphism and HLA-B Epitopes Modulate Response to Anti-GD2 Monoclonal Antibody in Patients With Neuroblastoma," *Journal of Clinical Oncology*, vol. 34, no. 21, pp. 2443–2451, Jul. 2016, doi: 10.1200/JCO.2015.64.9558.

[66] S. Kim *et al.*, "Licensing of natural killer cells by host major histocompatibility complex class I molecules," *Nature*, vol. 436, no. 7051, pp. 709–713, Aug. 2005, doi: 10.1038/nature03847.

[67] V. Varbanova, E. Naumova, and A. Mihaylova, "Killer-cell immunoglobulin-like receptor genes and ligands and their role in hematologic malignancies," *Cancer Immunology, Immunotherapy*, vol. 65, no. 4, pp. 427–440, Apr. 2016, doi: 10.1007/s00262-016-1806-9.

[68] N. T. Joncker and D. H. Raulet, "Regulation of NK cell responsiveness to achieve self-tolerance and maximal responses to diseased target cells," *Immunol Rev*, vol. 224, no. 1, pp. 85–97, Aug. 2008, doi: 10.1111/j.1600-065X.2008.00658.x.

[69] Y. Xu *et al.*, "Killer immunoglobulin-like receptors/human leukocyte antigen class-I, a crucial immune pathway in cancer," *Ann Transl Med*, vol. 8, no. 5, pp. 244–244, Mar. 2020, doi: 10.21037/atm.2020.01.84.

[70] R. D. Schreiber, L. J. Old, and M. J. Smyth, "Cancer Immunoediting: Integrating Immunity's Roles in Cancer Suppression and Promotion," *Science (1979)*, vol. 331, no. 6024, pp. 1565–1570, Mar. 2011, doi: 10.1126/science.1203486.

[71] Y. He, S. Liu, J. Mattei, P. Bunn Jr, C. Zhou, and D. Chan, "The combination of anti-KIR monoclonal antibodies with anti-PD-1/PD-L1 monoclonal antibodies could be a critical breakthrough in overcoming tumor immune escape in NSCLC," *Drug Des Devel Ther*, vol. Volume 12, pp. 981–986, Apr. 2018, doi: 10.2147/DDDT.S163304.

[72] W. Wang *et al.*, "Killer immunoglobulin-like receptor (KIR) and KIR–ligand genotype do not correlate with clinical outcome of renal cell carcinoma patients receiving high-dose IL2," *Cancer Immunology, Immunotherapy*, vol. 65, no. 12, pp. 1523–1532, Dec. 2016, doi: 10.1007/s00262-016-1904-8.

[73] J. M. Venstrom *et al.*, "*KIR* and *HLA* Genotypes Are Associated with Disease Progression and Survival following Autologous Hematopoietic Stem Cell Transplantation for High-Risk Neuroblastoma," *Clinical Cancer Research*, vol. 15, no. 23, pp. 7330–7334, Dec. 2009, doi: 10.1158/1078-0432.CCR-09-1720.

[74] N. Albinger, J. Hartmann, and E. Ullrich, "Current status and perspective of CAR-T and CAR-NK cell therapy trials in Germany," *Gene Ther*, vol. 28, no. 9, pp. 513–527, Sep. 2021, doi: 10.1038/s41434-021-00246-w.

[75] A. J. Hou, L. C. Chen, and Y. Y. Chen, “Navigating CAR-T cells through the solid-tumour microenvironment,” *Nat Rev Drug Discov*, vol. 20, no. 7, pp. 531–550, Jul. 2021, doi: 10.1038/s41573-021-00189-2.

[76] M. v Maus, “Designing CAR T cells for glioblastoma,” *Oncoimmunology*, vol. 4, no. 12, p. e1048956, Dec. 2015, doi: 10.1080/2162402X.2015.1048956.

[77] R. A. Morgan, J. C. Yang, M. Kitano, M. E. Dudley, C. M. Laurencot, and S. A. Rosenberg, “Case Report of a Serious Adverse Event Following the Administration of T Cells Transduced With a Chimeric Antigen Receptor Recognizing ERBB2,” *Molecular Therapy*, vol. 18, no. 4, pp. 843–851, Apr. 2010, doi: 10.1038/mt.2010.24.

[78] J. Fares, Y. Fares, and M. Fares, “Natural killer cells in the brain tumour microenvironment: Defining a new era in neuro-oncology,” *Surg Neuol Int*, pp. 10–43, 2019.

[79] O. Melaiu, V. Lucarini, L. Cifaldi, and D. Fruci, “Influence of the Tumor Microenvironment on NK Cell Function in Solid Tumors,” *Front Immunol*, vol. 10, Jan. 2020, doi: 10.3389/fimmu.2019.03038.

[80] I. Terrén, A. Orrantia, J. Vitallé, O. Zenarruzabeitia, and F. Borrego, “NK Cell Metabolism and Tumor Microenvironment,” *Front Immunol*, vol. 10, Sep. 2019, doi: 10.3389/fimmu.2019.02278.

[81] C. T. Butler *et al.*, “A Quininib Analogue and Cysteinyl Leukotriene Receptor Antagonist Inhibits Vascular Endothelial Growth Factor (VEGF)-independent Angiogenesis and Exerts an Additive Antiangiogenic Response with Bevacizumab,” *Journal of Biological Chemistry*, vol. 292, no. 9, pp. 3552–3567, Mar. 2017, doi: 10.1074/jbc.M116.747766.

[82] C. Magnusson, M. Mezhybovska, E. Lörinc, E. Fernebro, M. Nilbert, and A. Sjölander, “Low expression of CysLT1R and high expression of CysLT2R mediate good prognosis in colorectal cancer,” *Eur J Cancer*, vol. 46, no. 4, pp. 826–835, Mar. 2010, doi: 10.1016/j.ejca.2009.12.022.

[83] A. G. Murphy *et al.*, “Preclinical validation of the small molecule drug quininib as a novel therapeutic for colorectal cancer,” *Sci Rep*, vol. 6, no. 1, p. 34523, Dec. 2016, doi: 10.1038/srep34523.

[84] R. J. Diaz, S. Ali, M. G. Qadir, M. I. de La Fuente, M. E. Ivan, and R. J. Komotar, “The role of bevacizumab in the treatment of glioblastoma,” *J Neurooncol*, vol. 133, no. 3, pp. 455–467, Jul. 2017, doi: 10.1007/s11060-017-2477-x.

[85] P. Piromkraipak *et al.*, “Cysteinyl Leukotriene Receptor Antagonists Inhibit Migration, Invasion, and Expression of MMP-2/9 in Human Glioblastoma,” *Cell Mol Neurobiol*, vol. 38, no. 2, pp. 559–573, Mar. 2018, doi: 10.1007/s10571-017-0507-z.

[86] C. T. Butler *et al.*, “1,4-dihydroxy quininib attenuates growth of colorectal cancer cells and xenografts and regulates the TIE-2 signaling pathway in patient tumours,” *Oncotarget*, vol. 10, no. 38, pp. 3725–3744, Jun. 2019, doi: 10.18632/oncotarget.26966.

[87] A. M. Buckley *et al.*, “Pyrazinib (P3), [(E)-2-(2-Pyrazin-2-yl-vinyl)-phenol], a small molecule pyrazine compound enhances radiosensitivity in oesophageal adenocarcinoma,” *Cancer Lett*, vol. 447, pp. 115–129, Apr. 2019, doi: 10.1016/j.canlet.2019.01.009.

[88] A. M. Buckley *et al.*, “Real-time metabolic profiling of oesophageal tumours reveals an altered metabolic phenotype to different oxygen tensions and to treatment with Pyrazinib,” *Sci Rep*, vol. 10, no. 1, p. 12105, Dec. 2020, doi: 10.1038/s41598-020-68777-7.

[89] R. Karaman, “Prodrugs Design Based on Inter- and Intramolecular Chemical Processes,” *Chem Biol Drug Des*, vol. 82, no. 6, pp. 643–668, Dec. 2013, doi: 10.1111/cbdd.12224.

[90] n. d Davies D, *Aromatic heterocyclic chemistry, United states, Oxford university press, 1st edition* . 1992.

[91] B. S. Vig, K. M. Huttunen, K. Laine, and J. Rautio, “Amino acids as promoieties in prodrug design and development,” *Adv Drug Deliv Rev*, vol. 65, no. 10, pp. 1370–1385, Oct. 2013, doi: 10.1016/j.addr.2012.10.001.

[92] M. Davis, “Glioblastoma: Overview of Disease and Treatment,” *Clin J Oncol Nurs*, vol. 20, no. 5, pp. S2–S8, Oct. 2016, doi: 10.1188/16.CJON.S1.2-8.

[93] W. Wu *et al.*, “Glioblastoma multiforme (GBM): An overview of current therapies and mechanisms of resistance,” *Pharmacol Res*, vol. 171, p. 105780, Sep. 2021, doi: 10.1016/j.phrs.2021.105780.

[94] M. Nakada, S. Nakada, T. Demuth, N. L. Tran, D. B. Hoelzinger, and M. E. Berens, “Molecular targets of glioma invasion,” *Cellular and Molecular Life Sciences*, vol. 64, no. 4, pp. 458–478, Feb. 2007, doi: 10.1007/s00018-007-6342-5.

[95] M. Crocker *et al.*, “Serum angiogenic profile of patients with glioblastoma identifies distinct tumor subtypes and shows that TIMP-1 is a prognostic factor,” *Neuro Oncol*, vol. 13, no. 1, pp. 99–108, Jan. 2011, doi: 10.1093/neuonc/noq170.

[96] L. CHEN, X. LI, L. LIU, B. YU, Y. XUE, and Y. LIU, “Erastin sensitizes glioblastoma cells to temozolomide by restraining xCT and cystathionine-γ-lyase function,” *Oncol Rep*, vol. 33, no. 3, pp. 1465–1474, Mar. 2015, doi: 10.3892/or.2015.3712.

[97] M. Khasraw and A. B. Lassman, “Advances in the Treatment of Malignant Gliomas,” *Curr Oncol Rep*, vol. 12, no. 1, pp. 26–33, Jan. 2010, doi: 10.1007/s11912-009-0077-4.

[98] S.-B. Yang, K.-D. Gao, T. Jiang, S.-J. Cheng, and W.-B. Li, “Bevacizumab combined with chemotherapy for glioblastoma: a meta-analysis of randomized controlled trials,” *Oncotarget*, vol. 8, no. 34, pp. 57337–57344, Aug. 2017, doi: 10.18632/oncotarget.16924.

[99] Q. Liu *et al.*, "IL-6 promotion of glioblastoma cell invasion and angiogenesis in U251 and T98G cell lines," *J Neurooncol*, vol. 100, no. 2, pp. 165–176, Nov. 2010, doi: 10.1007/s11060-010-0158-0.

[100] C.-Y. Chang, M.-C. Li, S.-L. Liao, Y.-L. Huang, C.-C. Shen, and H.-C. Pan, "Prognostic and clinical implication of IL-6 expression in glioblastoma multiforme," *Journal of Clinical Neuroscience*, vol. 12, no. 8, pp. 930–933, Nov. 2005, doi: 10.1016/j.jocn.2004.11.017.

[101] H. Miwa, H. Kanno, S. Munakata, Y. Akano, M. Taniwaki, and K. Aozasa, "Induction of Chromosomal Aberrations and Growth-Transformation of Lymphoblastoid Cell Lines by Inhibition of Reactive Oxygen Species-Induced Apoptosis with Interleukin-6," *Laboratory Investigation*, vol. 80, no. 5, pp. 725–734, May 2000, doi: 10.1038/labinvest.3780076.

[102] J. B. Lamano *et al.*, "Glioblastoma-Derived IL6 Induces Immunosuppressive Peripheral Myeloid Cell PD-L1 and Promotes Tumor Growth," *Clinical Cancer Research*, vol. 25, no. 12, pp. 3643–3657, Jun. 2019, doi: 10.1158/1078-0432.CCR-18-2402.

[103] M. Kirsch, G. Schackert, and P. McL. Black, "Anti-angiogenic Treatment Strategies for Malignant Brain Tumors," *J Neurooncol*, vol. 50, no. 1/2, pp. 149–163, 2000, doi: 10.1023/A:1006487412567.

[104] J. C. Anderson, B. C. McFarland, and C. L. Gladson, "New molecular targets in angiogenic vessels of glioblastoma tumours," *Expert Rev Mol Med*, vol. 10, p. e23, Aug. 2008, doi: 10.1017/S1462399408000768.

[105] J. D. Schulte, M. K. Aghi, and J. W. Taylor, "Anti-angiogenic therapies in the management of glioblastoma," *Chin Clin Oncol*, vol. 10, no. 4, pp. 37–37, Aug. 2021, doi: 10.21037/cco.2020.03.06.

[106] A. Papachristodoulou *et al.*, "Therapeutic Targeting of TGFβ Ligands in Glioblastoma Using Novel Antisense Oligonucleotides Reduces the Growth of Experimental Gliomas," *Clinical Cancer Research*, vol. 25, no. 23, pp. 7189–7201, Dec. 2019, doi: 10.1158/1078-0432.CCR-17-3024.

[107] P. M. Holland, "Death receptor agonist therapies for cancer, which is the right TRAIL?," *Cytokine Growth Factor Rev*, vol. 25, no. 2, pp. 185–193, Apr. 2014, doi: 10.1016/j.cytogfr.2013.12.009.

[108] A. Ashkenazi, "Targeting the extrinsic apoptotic pathway in cancer: lessons learned and future directions," *Journal of Clinical Investigation*, vol. 125, no. 2, pp. 487–489, Feb. 2015, doi: 10.1172/JCI80420.

[109] S. Fulda, "Cell death-based treatment of glioblastoma," *Cell Death Dis*, vol. 9, no. 2, p. 121, Feb. 2018, doi: 10.1038/s41419-017-0021-8.

[110] A. Zingoni *et al.*, "Targeting NKG2D and NKp30 Ligands Shedding to Improve NK Cell-Based Immunotherapy," *Crit Rev Immunol*, vol. 36, no. 6, pp. 445–460, 2016, doi: 10.1615/CritRevImmunol.2017020166.

[111] R. Castriconi *et al.*, "Transforming growth factor β1 inhibits expression of NKp30 and NKG2D receptors: Consequences for the NK-mediated killing of dendritic cells," *Proceedings of the National Academy of Sciences*, vol. 100, no. 7, pp. 4120–4125, Apr. 2003, doi: 10.1073/pnas.0730640100.

[112] F. Ghiringhelli *et al.*, "CD4+CD25+ regulatory T cells inhibit natural killer cell functions in a transforming growth factor–β–dependent manner," *Journal of Experimental Medicine*, vol. 202, no. 8, pp. 1075–1085, Oct. 2005, doi: 10.1084/jem.20051511.

[113] J. Zhang, F. Basher, and J. D. Wu, "NKG2D Ligands in Tumor Immunity: Two Sides of a Coin," *Front Immunol*, vol. 6, Mar. 2015, doi: 10.3389/fimmu.2015.00097.

[114] G. Chitadze, J. Bhat, M. Lettau, O. Janssen, and D. Kabelitz, "Generation of Soluble NKG2D Ligands: Proteolytic Cleavage, Exosome Secretion and Functional Implications," *Scand J Immunol*, vol. 78, no. 2, pp. 120–129, Aug. 2013, doi: 10.1111/sji.12072.

[115] E. M. Levy, M. P. Roberti, and J. Mordoh, "Natural Killer Cells in Human Cancer: From Biological Functions to Clinical Applications," *J Biomed Biotechnol*, vol. 2011, pp. 1–11, 2011, doi: 10.1155/2011/676198.

[116] Y. Xu and S. W. Pang, "Natural killer cell migration control in microchannels by perturbations and topography," *Lab Chip*, vol. 19, no. 14, pp. 2466–2475, 2019, doi: 10.1039/C9LC00356H.